THE LUNAR TIDE IN THE ATMOSPHERE

by

MARVIN A. GELLER

B.S. Massachusetts Institute of Technology

(1964)

SUBMITTED IN PARTIAL FULFILLMENT OF THE

REQUIREMENTS FOR THE DEGREE OF

DOCTOR OF PHILOSOPHY

at the

MASSACHUSETTS INSTITUTE OF TECHNOLOGY

February, 1969

Signature of Author.....

Department of Meteorology, February 7, 1969

Certified by.....

Thesis Supervisor

Accepted by.....

Chairman, Departmental Committee on Graduate Students

THE LUNAR TIDE IN THE ATMOSPHERE

by

Marvin A. Geller

Submitted to the Department of Meteorology on 7 February 1969 in partial fulfillment of the requirement for the degree of Doctor of Philosophy.

ABSTRACT

Previous studies, both observational and theoretical, of the semidiurnal lunar tide in the atmosphere are reviewed. Some of the principal observed characteristics of this tide such as the tidal variation in pressure, temperature, and wind at the surface are discussed. The tidal variation in surface pressure is observed to vary annually in such a manner that the amplitude remains relatively constant throughout the year while the phase lag varies in such a manner that it reaches its maximum values during Northern Hemisphere winter and its minimum values in Northern Hemisphere summer.

The equations of tidal theory with Newtonian Cooling are derived starting with the "primitive equations" of dynamic meteorology. It is shown that the vertical structure of the lunar tide depends on the static stability of the atmosphere. Data on the stability of the atmosphere indicate that seasonal variations in mesospheric temperatures act in the summer months to create an increased "barrier" to wave propagation, in the Schrodinger equation sense.

Calculations without Newtonian Cooling are performed using the empirical atmospheric stability curves. These calculations give results in agreement with the observations, both of annually averaged tidal effects and seasonal variation of these effects. The addition of Newtonian Cooling acts to disturb the agreement in the seasonal variations, but this is not taken to be serious as there are many uncertainties in the Newtonian Cooling

parameter.

Calculations of the vertical energy flux give results in good agreement with the notion of an annually changing "mesospheric barrier".

Finally, simple studies, both numerical and analytic, are performed to make clearer the "barrier" effects.

Thesis Supervisor: Victor P. Starr
Title: Professor of Meteorology

TABLE OF CONTENTS

I. HISTORY OF PROBLEM AND OBSERVATIONS 6

figures for chapter I 17

II. FORMULATION 24

A. Formulation of Equations 27
B. Formulation of Variables 36

III. PROCEDURE 42

A. Gravitational Forcing 42
B. Stability Function 46
C. Newtonian Cooling 51
D. Numerical Procedure 58

figures for chapter III 70

IV. RESULTS AND OBSERVATIONAL AGREEMENT 87

A. Results with No Newtonian Cooling 87
B. Results with Newtonian Cooling 94

figures for chapter IV 98

V. ENERGETICS 124

A. Formulation 124
B. Results 129

figures for chapter V 132

VI. SIMPLE STUDIES 135

A. Numerical 135
B. Analytic 139
(a) Isothermal 139
(b) δ -function barrier 145

figures and tables for chapter VI 150

VII. CONCLUSION 170

A. Discussion of Results 170
B. Suggestions for Further Research 173

Acknowledgements 175

References 176

Biography 179

CHAPTER I

HISTORY OF THE PROBLEM AND OBSERVATIONS

Atmospheric tidal theory is probably the oldest branch of dynamic meteorology. The original workers in this field included such eminent names as Newton (1687), Laplace (1799), Kelvin (1882), and Rayleigh (1890). Since tides have been studied for such a long period of time, there has naturally developed an extensive literature on the subject.

There are several fine review articles that cover both the observational and theoretical aspects of atmospheric tides. Among these are a book by Wilkes (1949), and articles by Chapman (1951), Kertz (1957), and Siebert (1961). All of these references include discussions of the atmospheric lunar tide. Matsushita (1967) has written a more specialized article on "Lunar Tides in the Ionosphere" that reviews observations of lunar tidal variations in ionospheric and neutral atmospheric parameters.

In this section the author will give a brief review of lunar tidal theory and observations. Certain observations will also be cited for later comparison with the author's theoretical results.

The most familiar of all the tides are the sea tides. These are observed to be a twice daily rise and fall of the ocean level

with the time of high tide being associated with the moon's motion. The physical understanding of these tides goes back to Newton (1687) and his hypothesis of a universal inverse square "gravitational" attraction between all material bodies.

The moon is in an equilibrium orbit about the earth with the earth's gravitational force upon the moon supplying the required centripetal acceleration. Thus, at the earth's center, $GL/r_o^2 = \omega^2 r_o$, where G denotes the gravitational constant, L is the mass of the moon, r_o is distance between the centers of the earth and moon, and ω is the orbital angular velocity of the moon.

Considering the spherical shape of the earth, it is easy to see that on the hemisphere nearer the moon the gravitational force is larger while the centripetal acceleration is smaller than their values at the earth's center. This causes an unbalanced distribution of forces directed moonwards. On the hemisphere further from the moon this type of imbalance gives rise to a net force directed away from the moon. Particles free to move, like those of the sea water, will move under the influence of this force distribution. The sea surface will then tend to become spheroidal, with its long axis along the line joining the centers of the moon and earth.

The sun's gravitation also causes a similar semidiurnal tide. The lunar tidal action is 2.4 times as great as the solar action so that the moon chiefly governs the sea tides; however, at different epochs in the month the sun acts to add to or reduce the lunar tide.

The above discussion describes the "equilibrium tide";that is to say, since there has been no mention of the earth's rotation, this "equilibrium tide" is a static phenomenon. Laplace (1799) recognized the importance of incorporating the effects of the earth's rotation into any reasonable theory of the tides. He carried out an analysis of ocean tides approximating the situation by an ocean of uniform depth covering the entire earth. His results are not really applicable to the actual ocean tides since the complex ocean-continent topography of the earth is ignored.

Newton and Laplace both realized that the atmosphere must also react to tidal forcing. In fact, the lack of lateral boundaries makes the atmosphere a more suitable subject for Laplace's idealized tidal theory. Although his theory was formulated for incompressible sea water, Laplace demonstrated that the theory could be easily applied to compressible air so long as the atmosphere was of isothermal structure with pressure changes occurring under isothermal conditions.

Observations of surface pressure variations indicate that, unlike the oceans, the largest tides in the atmosphere are with solar periods. This has been shown to be a consequence of the large thermal forcing of the atmosphere with the solar tidal periods. The lunar tide in the atmosphere, in spite of its small magnitude, has been observed sufficiently to warrant attempts at modelling the observed tide. The history and results of these observations will now be reviewed.

The mercury barometer was invented by Torricelli at about the time of Newton's birth. It soon became known, by the use of this instrument, that barometric variations were of a quite different nature in the tropics than at temperate latitudes. The surface pressure in the tropics usually varies regularly with a range of a couple of millimeters mercury with solar semidiurnal frequency[1]. In temperate latitudes, the barometric readings vary in an apparently irregular fashion with amplitudes on the order of a centimeter mercury. This midlatitude behavior is now known to be due to the passage of migratory cyclones and anticyclones (usually accompanied by low and high pressure centers respectively).

Laplace's theory predicted a "direct" lunar tidal variation of the barometer with a range of about half a millimeter in the

---

1. This regular small-amplitude pressure variation in the tropics is only disturbed by the passage of hurricanes.

tropics. Since he had no access to suitable tropical data, he attempted to detect a lunar tidal variation in barometric readings at Paris. He failed to get a significant result since his data was not for a sufficiently long period to detect such a small regular variation imbedded in such large irregular variations. Many other 19th century investigators also failed to find evidence of the atmospheric lunar tide at midlatitudes. During the middle of the nineteenth century, however, this lunar tide had been determined at such tropical stations as St. Helena, Singapore, and Batavia.

Finally in 1918 Chapman succeeded in detecting the lunar tidal variation in surface pressure at Greenwich. He succeeded in this effort by only considering data on days where the barometric range did not exceed 0.1 inch. In this way, random errors were reduced sufficiently to reliably determine the lunar tidal variation in surface pressure at a nontropical station.

Since this time, many investigations of lunar tidal effects in the surface atmosphere have been undertaken, using the basic methods of Chapman, so that the lunar variations of such parameters as wind and temperature are now at least partially known.

Observations of the vertical structure of the lunar tide in the atmosphere are very poorly known. It might be possible to get such observations by using tropical radiosonde data that has been collected over a long period. To the author's knowledge, this has

not been tried.

There is some knowledge of the vertical structure of the lunar tide that can be gained by ionospheric methods. As mentioned earlier, Matsushita (1967) has written an extensive article reviewing the variation of ionospheric parameters with the lunar period.

Some observations pertaining to the lunar tide in the atmosphere will now be given. In these observations the local lunar semidiurnal tide, L_2, has been represented by the formula,

$$L_2 = \ell_2 \sin(2\theta + \gamma) \qquad \text{I-1}$$

where ℓ_2 is the amplitude, γ is the phase, and θ denotes time reckoned in angle at the rate 360° per one half lunar day. L_2 has a maximum at

$$\theta_{max} = \frac{(90^\circ - \gamma)}{2} \qquad \text{I-2}$$

or at

$$t_{max} = \frac{1}{30}\theta_{max} \quad \text{(in hours).} \qquad \text{I-3}$$

A popular mode of display is the harmonic dial representation that pictures the amplitude as radial distance and the phase as time on a clock's face. Thus figure I-1 would be analogous to formula I-1.

Figures I-2 and I-3 are taken from Chapman (1951) and picture the worldwide distribution of the lunar tidal variation of surface pressure. It is seen from these figures that this lunar tide has a reasonable asymmetry that seems to be associated with the continent-ocean structure; however, certain features of this tide seem to hold throughout. In figure I-2 most arrows point to the northeast which, referring back to figure I-1, implies a phase lag in the surface pressure variation of about one-half hour. In figure I-3, it is obvious that the amplitude of this surface pressure variation decreases poleward. These same features are seen more clearly in figure I-4 which is also taken from Chapman (1951).

This figure shows the amplitude and phase of the zonally-averaged surface pressure variations plotted as a function of latitude. Here again there is seen a decrease in amplitude away from the equator and a phase lag at nearly all latitudes. Figure I-4 also shows the observed annual dependence of amplitude and phase. There is seen a very small annual variation in the amplitude curves with the largest amplitudes in northern hemisphere summer and smallest in northern hemisphere winter. This annual variation in amplitude is a small effect, with amplitudes at the equator being approximately .065 mm. in May-Aug. and

.055 mm in Nov.-Feb. The annual variation in phase is seen to be more significant with a larger phase lag in northern hemisphere winter than summer. The phase lags at the equator are seen to be approximately 1/3 hours in May-Aug. and 1 1/3 hours in Nov.-Feb.

The observed lunar semidiurnal variation in surface temperature at Batavia (7^{o}S, 107^{o}E) is shown in figure I-5 (also taken from Chapman (1951)). This observed temperature variation has an amplitude of approximately 0.008^{o} C with a phase lag of around 2/3 hours. The temperature variation is approximately what one would get from the pressure variation assuming the density variations to be adiabatic.

Figure I-6 (taken from Chapman (1951)) shows the observed lunar tidal variation of the surface wind at Mauritius (20^{o}S, 55^{o}E). The variation of the eastward component is shown to have an amplitude of about 1 cm sec^{-1} with a phase lag of approximately 7 2/3 hours while the northward component's variation has an amplitude around 1.2 cm sec^{-1} with a phase lag of around 3 hours.

There have been previous attempts at modelling the observations of the lunar semidiurnal tide. Three of these will be reviewed. These are the investigations of Wilkes (1949), Sawada (1954, 1956), and Siebert (1961).

Wilkes (1949) carried out his work at a time when the solar semidiurnal tide was thought to be gravitationally forced and vastly amplified through resonance. His upper boundary condition, that of an isothermal atmosphere at 190°K, served to trap all energy as would be crucial to any resonance theory. His calculations predicted a lunar tide in surface pressure with the amplitude equal to that of the equilibrium tide ($\approx 2.8 \times 10^{-2}$ mb.) with zero phase lag[1]. In passing it should be said that Wilkes correctly recognized that the temperature structure of the atmosphere would act as a "barrier" to wave propagation in the mesosphere, but because of a lack of upper atmospheric observations and the supposed need of the "resonance theory", Wilkes used an improper upper boundary condition in his theory of the lunar tide.

Sawada (1954, 1956) in a series of two papers carried out a very nice investigation of the lunar tide in the atmosphere with the goal of determining the atmospheric temperature structure. He reasoned that a good guess for the temperature structure could be obtained by finding the temperature profile for which the lunar tide agreed most closely with observations. Sawada used a correct upper boundary condition in assuming the vertical energy flux to be directed upwards at infinity. His temperature profiles

1. With the upper boundary condition acting to trap all energy the phase lag must be either 0° or 180° as will be shown later.

were comprised of straight line segments connected to form a continuous temperature structure. He obtained best agreement with lunar tide observations (amplitude -1.42×10^{-2} mb, phase lag $-\approx 1/6$ hours at the equator) with the temperature profile that is pictured in figure I-7. This temperature profile does compare quite well with the features of the mean atmosphere. Sawada's work did suffer from one fault that will become clearer later. The tidal equations depend on the atmospheric stability in a way that the shape of the stability curve with height is crucial. Discontinuities in the slope of the temperature (as in figure I-7) might introduce spurious effects into the calculations.

Finally Siebert (1961) performed a theoretical calculation of the lunar tide. Like Wilkes, his upper boundary condition caused the tidal energy to be trapped. With this erroneous upper boundary condition, he found good agreement in amplitude between his theory and observations but contrary to observations found a zero phase lag. Siebert attributed this error in the phase to be due to the neglect of surface friction. It is the author's view that the observed phase lag in the lunar variations of surface pressure is due to the upward energy flux and not to surface friction as suggested by Siebert.

It is hoped that the observed features of the lunar tide in the upper atmosphere will become better known in the immediate fu-

ture through such radio methods as meteor winds. Radio methods were first used in the study of the lunar tide in 1939 when Appleton and Weeks discovered an oscillation in the height of the E-layer over Cambridge, England with a lunar semidiurnal period. This oscillation had an amplitude of .93 km. and a phase lag of 11.25 hours. This result is questioned in Matsushita's review on the basis that the observations of the E-layer also included E_s - layers (sporadic E). When E_s is excluded from such a study, the observations of lunar oscillations of the E-layer show an uncertain result.

In Matsushita's review, lunar variations of absorption parameters and "winds" are shown for the D-region ($\approx$ 60 km), the E-region ($\approx$100 km.), and the F-region ($\approx$ 300 km.). These results are difficult to relate to neutral motions in the atmosphere though. Perhaps the situation will be clearer in the future.

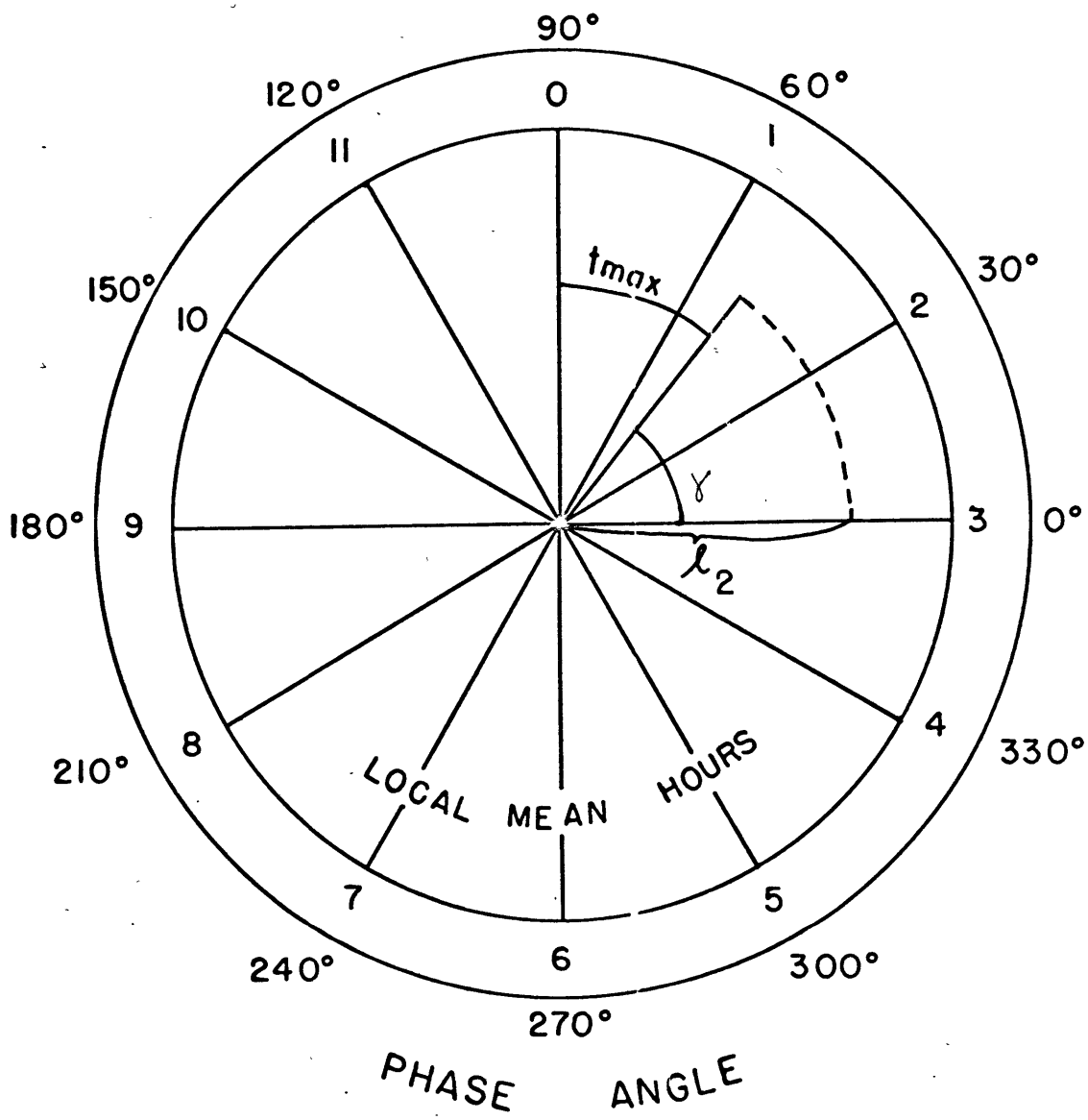

Figure I-1 Harmonic Dial Representation

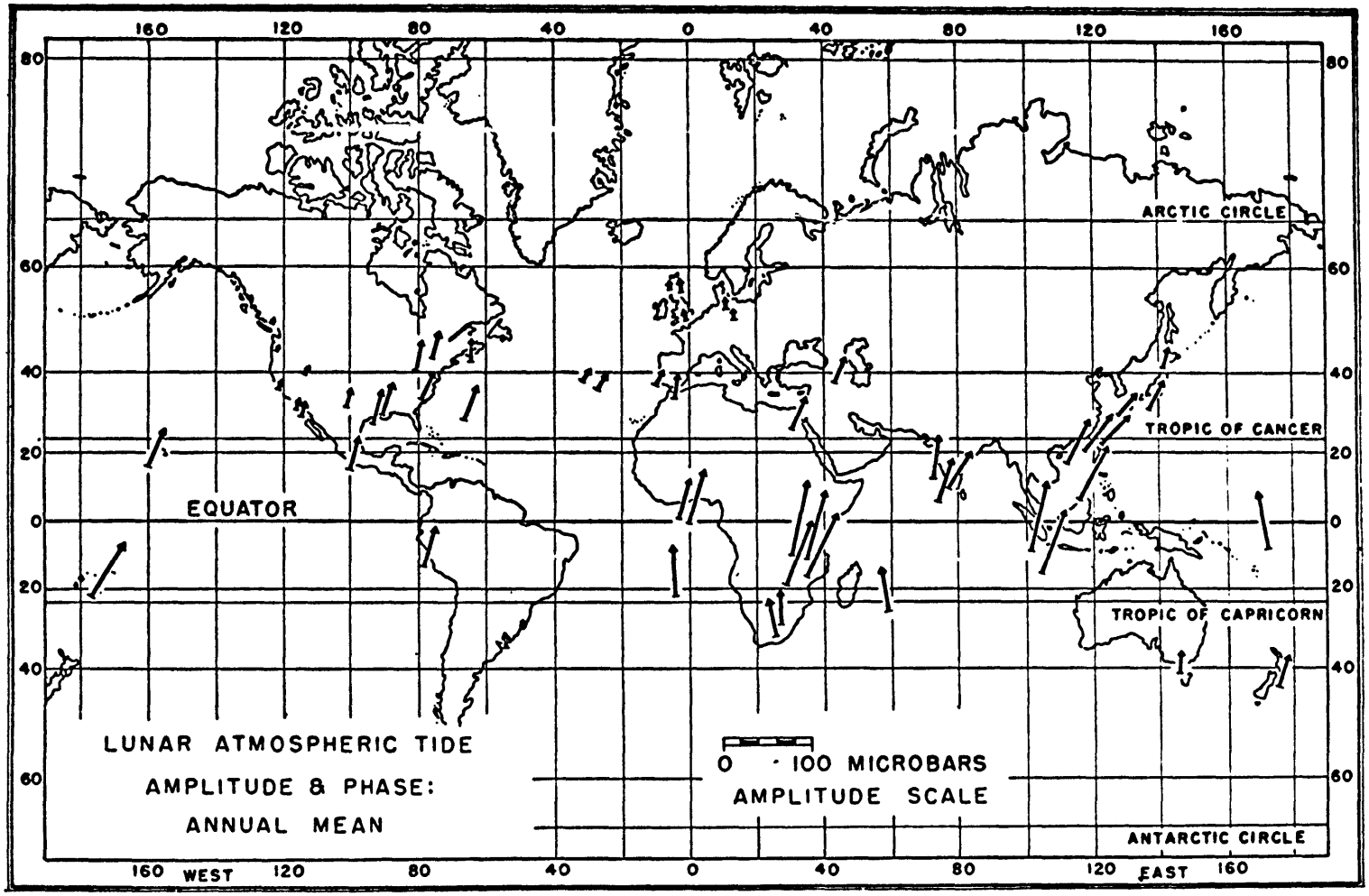

Figure I-2

Geographical distribution of the annual mean lunar semidiurnal air tide L_2 in barometric pressure, indicated by dial vectors, each referring to the place at the mid-point of the arrow, whose length gives the amplitude l_2 on the scale shown, and whose direction gives the time of high air tide, as shown on a local mean lunar clock.

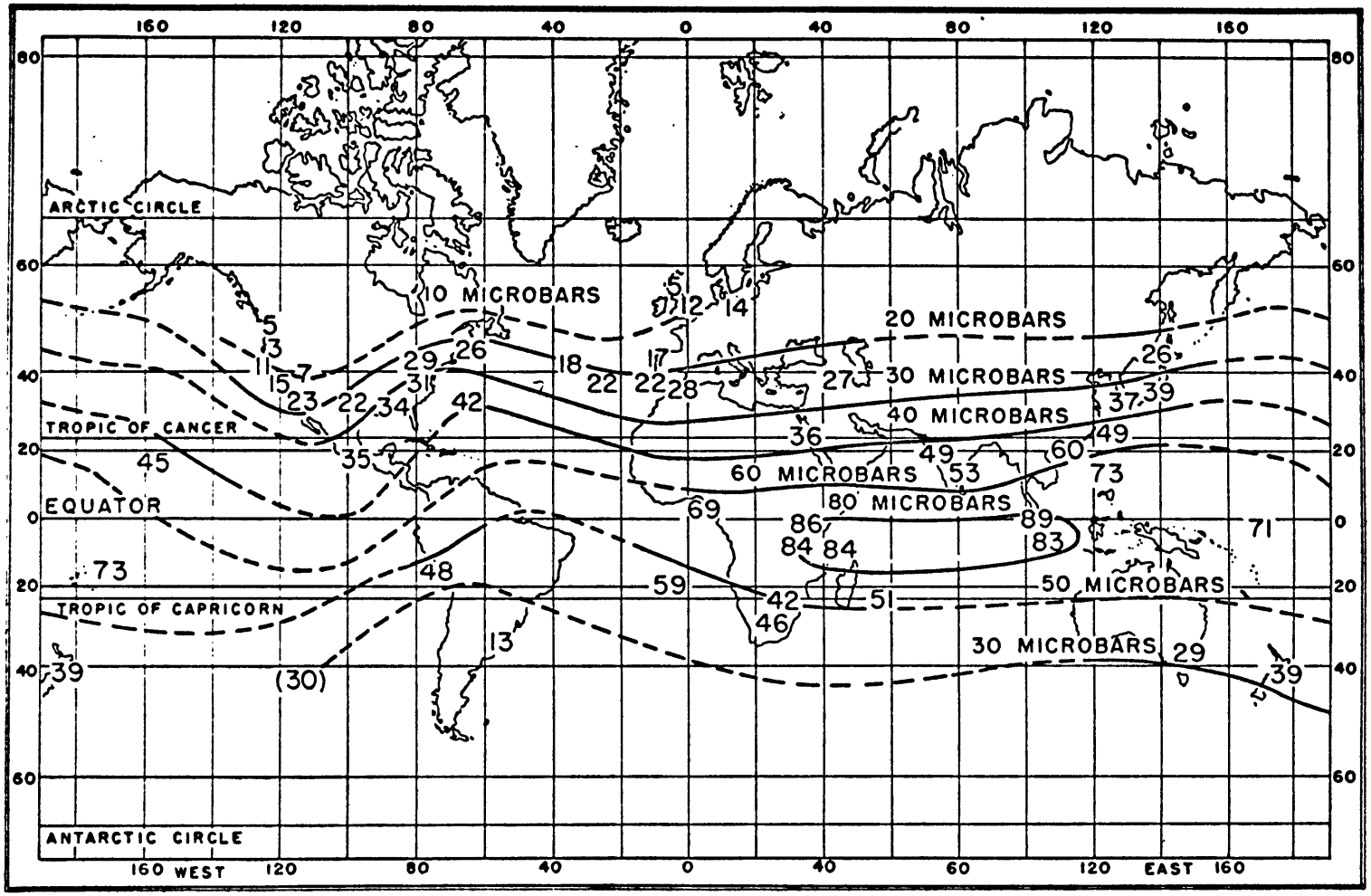

Figure I-3

Tentative lines (broken where only weakly determined) of equal amplitude l_2 (in microbars) of the annual mean lunar semidiurnal air tide L_2 in barometric pressure. The numbers (other than those, 10, 20, . . . , 80, followed by the word "microbar," which show the value of l_2 for each line) show local values of l_2.

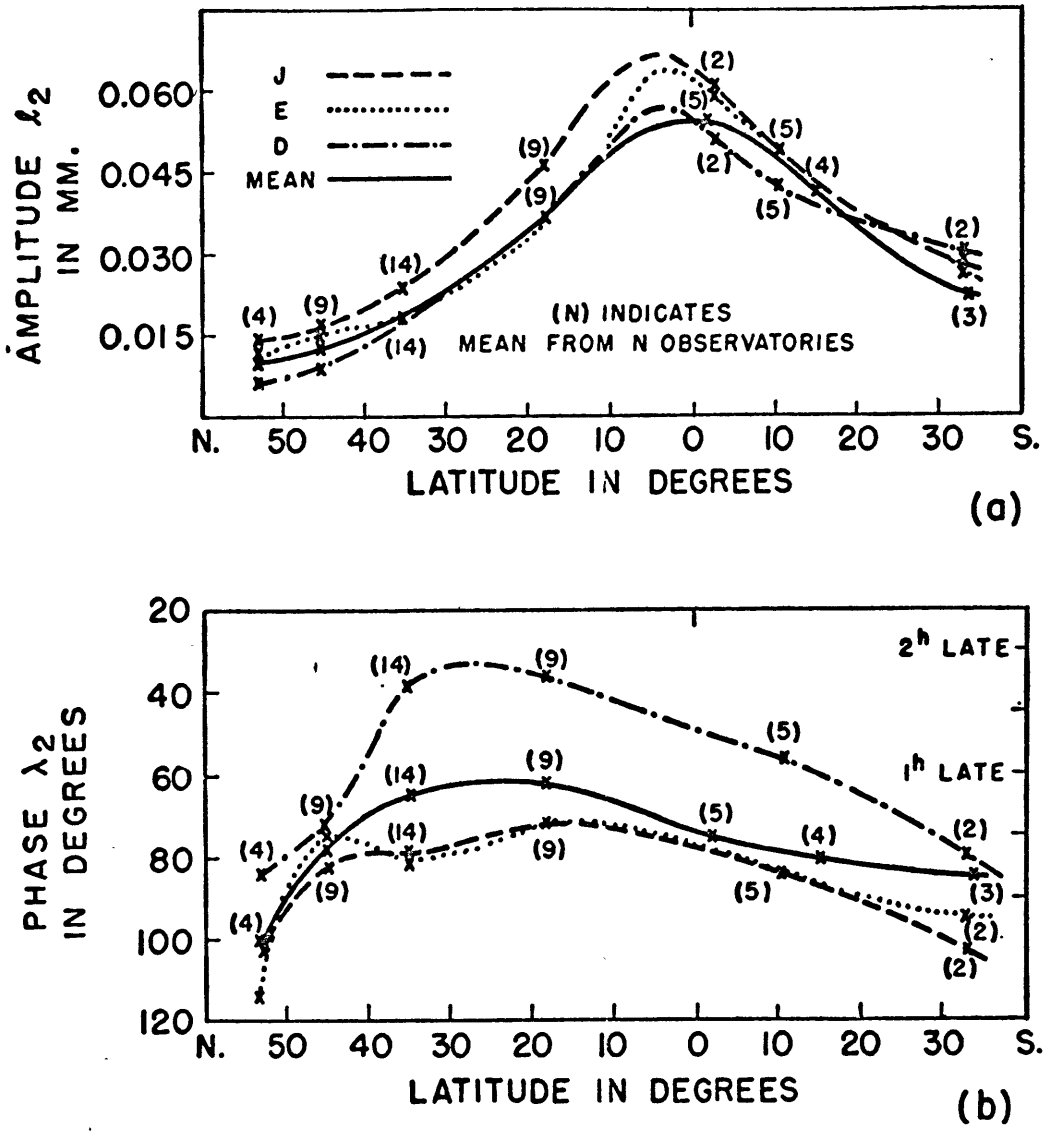

Curves showing the average dependence on latitude of the amplitude l_2 (Fig. 9*a*, above) and phase λ_2 (Fig. 9*b*, below) of the lunar semidiurnal air tide in barometric pressure, for the mean of the year and for groups of months *J* (May to August), *D* (November to February), and *E* (March, April, September, October). The curves are drawn through (or near to) points (×) each giving the mean l_2 or λ_2 for a group of stations (the number of stations is indicated beside each point) within a moderate range of latitude.

Figure I-4

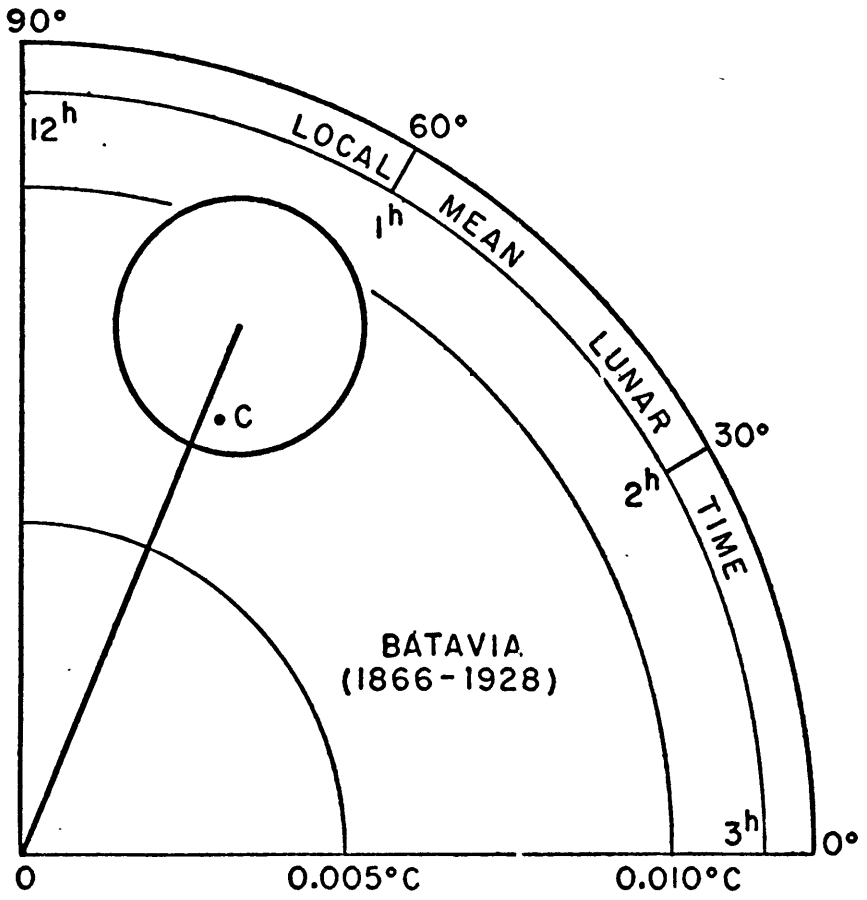

Harmonic dial specifying (with probable-error circle) the lunar semidiurnal tidal variation of *air temperature* at Batavia. The point *C* represents the variation calculated from the lunar semidiurnal variation of *barometric pressure* at Batavia, on the assumption that the density variations are adiabatic.

Figure I-5

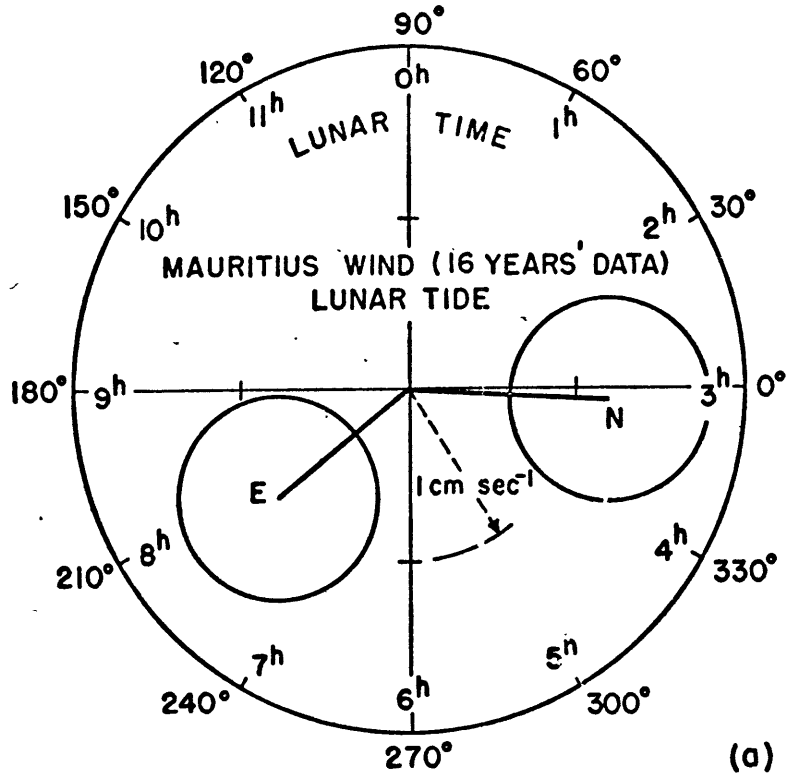

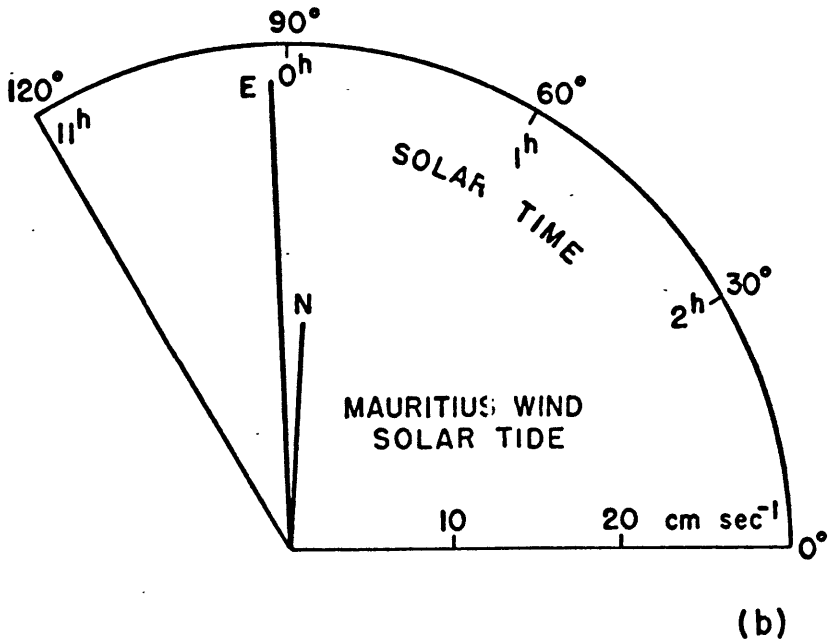

(*a*) Harmonic dial (with probable-error circles) for the annual mean *lunar* semidiurnal variations in the northward and eastward components of wind velocity at Mauritius, from about 16 years' bihourly data. (*b*) Harmonic dial for the corresponding annual mean *solar* semidiurnal variations. Note the tenfold scale difference between the two diagrams.

Figure I-6

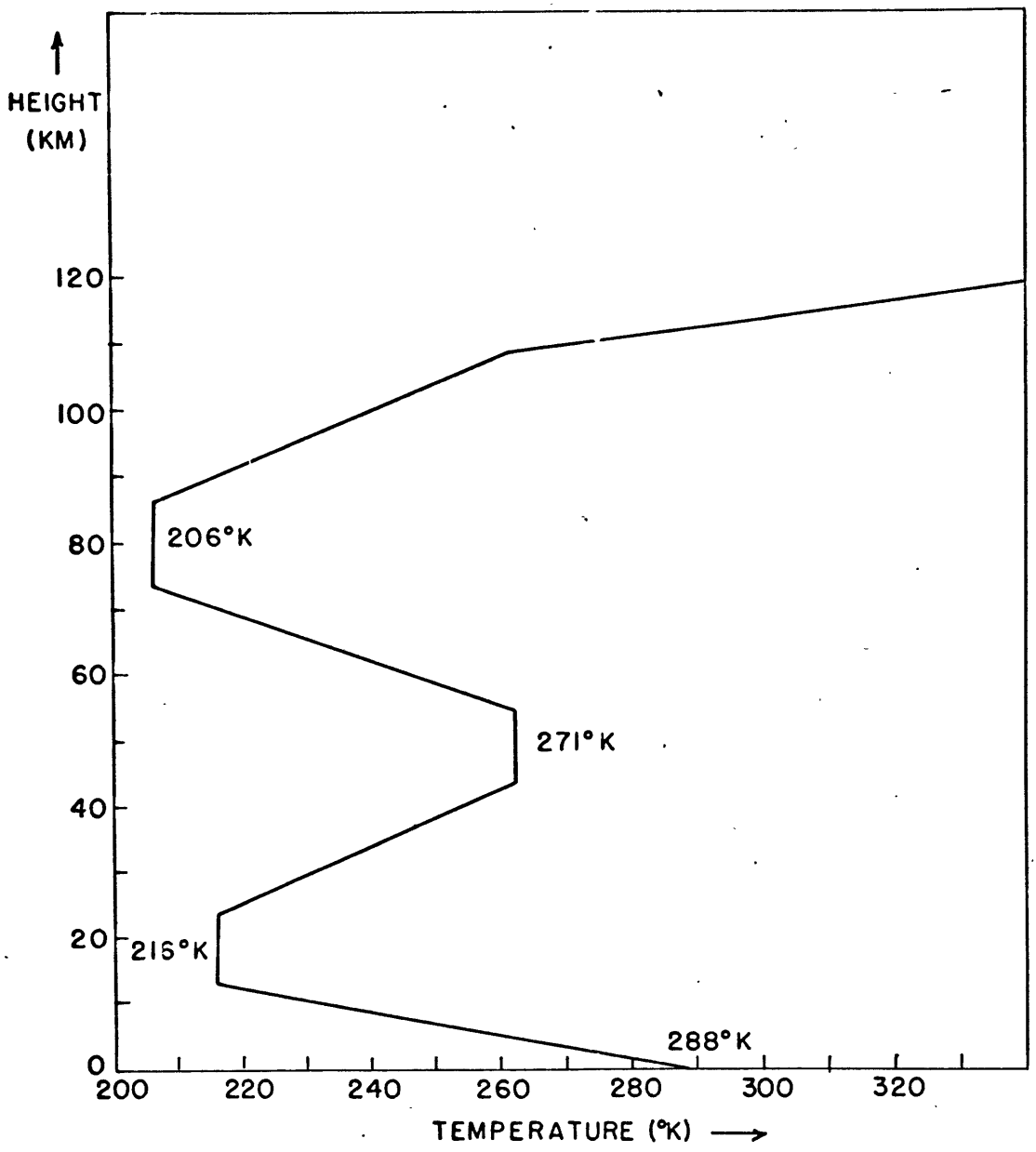

Figure I-7 Sawada's Best Temperature Profile

CHAPTER II

FORMULATION

List of Symbols:

$\overline{(\,)}$ = spherical average of $(\,)$

$(\,)'$ = tidal perturbation of $(\,)$

T = temperature

p = pressure

ρ = density

t = time

g = acceleration due to gravity (= 980.6 cm sec^{-2})

R = gas constant for air

H = atmospheric scale height $(= RT/g)$

p_o = surface pressure (= 1000 mb)

J = solar heating term

χ = three-dimensional velocity divergence

c_p = specific heat of air at constant pressure

c_v = specific heat of air at constant volume

$\varkappa = R/c_p$

$\gamma = c_p/c_v$

u = eastward wind velocity

v = northward wind velocity

φ = latitude

λ = longitude

Ω = rotational frequency of the earth

a = radius of the earth

h = geopotential height

F_λ, F_θ = dissipative forces in eastward and northward directions

z = $\ln(p_0/p)$

χ = altitude

w = $\frac{dz}{dt}$

$\frac{d}{dt}$ = total derivative

Q = diabatic term

N = Brunt Vaisala frequency

α_0 = Newtonian Cooling coefficient

μ = $\sin\theta$

ν = frequency of tide

m = wavenumber of tide

F = Hough operator

γ^m_n = eigenvalue of Hough function

H^m_n = Hough function

S = stability function

$(\,)^m_n$ = coefficient of H^m_n in expansion of $(\,)$

w = vertical velocity

$\Phi^{(T)}$ = tidal potential

ϕ = geopotential $(= gh + \phi^{(T)})$

Ω^m_n = coefficient of H^m_n expansion of $\phi^{(T)}$

Section A: Formulation of Equations

Traditionally, tidal theory has been quite inaccessible to the general meteorological community. This has been due to the use of specialized notation and the resulting difficulty in deriving the main equations of atmospheric tidal theory.

These troubles are actually quite simple to surmount if one starts with the proper meteorological variables instead of the specialized tidal variables. The tidal theorist uses as his vertical coordinate $z = \int_0^z \frac{dz}{H(z)}$ ($H(z) = RT(z)/g$ is the scale height). It can be easily seen that $z = -\ln(p/p_0)$. The tidal theorist formulates his basic equations in terms of $\chi = \frac{\gamma J(z)}{g H(z)}$ as the dependent variable (χ is the three-dimensional divergence of the tidal wind field and J is the heating term in the thermodynamic equation).

It will now be shown that the dependent variable of tidal theory is proportional to the vertical velocity in log-pressure coordinates. From the 1 st Law of Thermodynamics it follows that

$$\frac{1}{c_p T} J = -\frac{1}{\rho}\frac{d\rho}{dt} + \frac{1}{\gamma}\frac{1}{P}\frac{dp}{dt} \qquad \text{II A-1}$$

The continuity equation can be written as

$$\frac{1}{\rho}\frac{d\rho}{dt} = -\chi \qquad \text{IIA-2}$$

Hence defining $W = -\frac{1}{\rho}\frac{d\rho}{dt}$, it follows that

$$w = \gamma\chi - \frac{\gamma\mathcal{H}J}{gH} \qquad \text{IIA-3}$$

Thus motivated, the "primitive equations" of dynamic meteorology will be used to derive the tidal equations[1]. These equations are as follows:

$$\frac{du}{dt} - \frac{uv}{a}\tan\varphi - (2\Omega\sin\varphi)v + \frac{g}{a\cos\varphi}\frac{\partial h}{\partial\lambda} = F_\lambda \qquad \text{IIA-4}$$

$$\frac{dv}{dt} + \frac{u^2}{a}\tan\varphi + (2\Omega\sin\varphi)u + \frac{g}{a}\frac{\partial h}{\partial\varphi} = F_\varphi \qquad \text{IIA-5}$$

$$\frac{1}{a\cos\varphi}\frac{\partial u}{\partial\lambda} + \frac{1}{a\cos\varphi}\frac{\partial}{\partial\varphi}(v\cos\varphi) + \frac{\partial w}{\partial z} - w = 0 \qquad \text{IIA-6}$$

$$\frac{dT}{dt} + \mathcal{H}wT = \frac{Q}{c_p} \qquad \text{IIA-7}$$

$$\frac{\partial h}{\partial z} = \frac{RT}{g} \qquad \text{IIA-8}$$

---

1. The derivation given here is essentially the same as that given in Dickinson and Geller (1968).

The preceding equations apply to all hydrostatic motions in the atmosphere. The following assumptions will now be made in order to deal with the specific case of tidal motions.

(1) The undisturbed atmosphere is at rest relative to the earth.

(2) The perturbations due to the atmospheric tides are so small that terms of second-order in the tidal variables can be neglected leading to a linear theory of tides.

(3) The temperature of the undisturbed atmosphere is uniform in the horizontal directions but varies with height.

(4) The effects of viscosity and turbulence will be ignored.

(5) The vertical component of the gravitational tidal forcing can be neglected.

(6) Electromagnetic effects will be ignored.

Other assumptions have implicitly been made in writing equations (4)-(8). These are as follows:

(1) The atmosphere is in hydrostatic equilibrium.

(2) A spherical earth has been assumed.

(3) The atmosphere is assumed to be of uniform composition.

(4) The variations of gravity with height can be neglected.

Before proceeding further, it would be well to note the height limitation on the tidal calculations that is implied by the preceding assumptions.

The assumption of hydrostatic equilibrium will be true so long as the tidal frequency is much smaller than the Brunt-Vaisala frequency in the atmosphere ($\Omega^2 << N^2$) . This is true so long as the undisturbed temperature is less than about 10^6 °K. This assumption will certainly be justified below the exosphere ($\approx$ 1000 km), where even the assumption of continuum mechanics breaks down.

The assumption of uniform composition is good up to about 120 km where the mean molecular weight falls to 93.3% of its value at sea level[1].

The acceleration due to gravity at 120 km is 96.2% of its value at the ground indicating that this assumption is also good through 120 km.

Kato and Matsushita (1968) have made estimates on the electromagnetic effects on tides in the upper atmosphere. They found that the electromagnetic interaction time-scale becomes equal to the tidal time-scale at about 130 km.

Newell[2] has performed rough calculations of the kinematic viscosity of the atmosphere at various levels. With his values it

---

1. CIRA 1965
2. unpublished calculations

can be shown that viscosity is negligible for vertical wavelengths of about 100 km so long as the motion being considered takes place below about 250 km[1].

Knowing the height limitations on the equations to be used (below about 130 km), it is possible to proceed with the derivation of the tidal equations.

The set of equations (IIA-4) - (IIA-8), with the stated assumptions, becomes

$$\frac{\partial u}{\partial t} - (2\Omega \sin\varphi)v + \frac{1}{a\cos\varphi}\frac{\partial \phi'}{\partial \lambda} = 0 \qquad \text{IIA-9}$$

$$\frac{\partial v}{\partial t} + (2\Omega \sin\varphi)u + \frac{1}{a}\frac{\partial \phi'}{\partial \varphi} = 0 \qquad \text{IIA-10}$$

$$\frac{1}{a\cos\varphi}\frac{\partial u}{\partial \lambda} + \frac{1}{a\cos\varphi}\frac{\partial}{\partial \varphi}(v\cos\varphi) + \frac{\partial w}{\partial z} - w = 0 \qquad \text{IIA-11}$$

$$\frac{\partial T'}{\partial t} + w(\bar{T}_z + \gamma_B \bar{T}) = \frac{Q}{c_p} \qquad \text{IIA-12}$$

$$\frac{\partial \phi'}{\partial z} = RT' . \qquad \text{IIA-13}$$

Q is the total diabatic term in the thermodynamic equation

---

1. The lunar tide has wavelength of this order.

and will be divided into two parts — J, the solar heating, and $-a_0 T'$, the cooling-to-space term (Newtonian Cooling approximation)[1].

It is now assumed that all perturbation variables and the heating J are proportional to $\exp[im\lambda + i\nu t]$ and that the latitudinal variable φ is changed to $\mu (= \sin\varphi)$. The following equations are then obtained:

$$i\nu U - 2\Omega\mu V + \frac{im}{a(1-\mu^2)^{\frac{1}{2}}}\phi' = 0 \qquad \text{IIA-14}$$

$$i\nu V + 2\Omega\mu U + \frac{(1-\mu^2)^{\frac{1}{2}}}{a}\frac{\partial\phi'}{\partial\mu} = 0 \qquad \text{IIA-15}$$

$$\frac{im}{a(1-\mu^2)^{\frac{1}{2}}}U + \frac{1}{a}\frac{\partial}{\partial\mu}\left[V(1-\mu^2)^{\frac{1}{2}}\right] + \frac{\partial W}{\partial z} - W = 0 \qquad \text{IIA-16}$$

$$(i\nu + a_0)T' + W(\bar{T}_z + \varkappa\bar{T}) = \frac{J}{c_p} \qquad \text{IIA-17}$$

$$\frac{\partial\phi'}{\partial z} = RT' \,. \qquad \text{IIA-18}$$

Equations IIA-14 and IIA-15 may be used in solving for U and V. The results are as follows:

---

1. Dickinson and Geller (1968) carry through this derivation with a more general operator on the perturbation temperature.

$$U = \frac{1}{\nu^2-(2\Omega\mu)^2}\left[-\frac{\nu m\phi'}{a(1-\mu^2)^{\frac{1}{2}}} + \frac{(2\Omega\mu)}{a}(1-\mu^2)^{\frac{1}{2}}\frac{\partial\phi'}{\partial\mu}\right] \qquad \text{IIA-19}$$

and

$$V = \frac{1}{\nu^2-(2\Omega\mu)^2}\left[-\frac{(2\Omega\mu)im}{a(1-\mu^2)^{\frac{1}{2}}}\phi' + \frac{i\nu}{a}(1-\mu^2)^{\frac{1}{2}}\frac{\partial\phi'}{\partial\mu}\right] \qquad \text{IIA-20}$$

These relations for U and V can be put into equation (16), the continuity equation, to give the following equation,

$$i\nu F[\phi'] + (2\Omega a)^2\left[\frac{\partial W}{\partial z} - W\right] = 0 \qquad \text{IIA-21}$$

where the operator F is defined by

$$F \equiv \frac{d}{d\mu}\frac{(1-\mu^2)}{(\tilde{\nu}^2-\mu^2)}\frac{d}{d\mu} - \frac{1}{\tilde{\nu}^2-\mu^2}\left[\frac{m}{\tilde{\nu}}\frac{\tilde{\nu}^2+\mu^2}{\tilde{\nu}^2-\mu^2} + \frac{m^2}{1-\mu^2}\right] \qquad \text{IIA-22}$$

$(\tilde{\nu} = \nu/2\Omega)$.

Equation IIA-21 can be treated by a classical method of solution that is applicable to certain types of partial differential equations. The method to be used is that of separation of variables.

The equation for Hough functions is

$$F[H^m_n] + \gamma^m_n H^m_n = 0 \qquad \text{IIA-23}$$

where geophysically reasonable boundary conditions are assumed at $\mu = \pm 1$ that is, $H^m_n(\mu)$ is assumed to remain finite at the poles[1]. The eigenvalue of the problem is taken to be γ^m_n and of course is a constant.

T' may now be eliminated from the equations by combining equations IIA-17 and IIA-18 to yield

$$(i\nu + a_0)\frac{\partial \phi'}{\partial z} + (2\Omega a)^2 S' w = \mathcal{H} J \qquad \text{IIA-24}$$

where $S' = \frac{g}{(2\Omega a)^2}\left[\mathcal{H}\bar{H} + \frac{d\bar{H}}{dz}\right]$ is the nondimensional spherically-averaged static stability.

It is now appropriate to expand ϕ', w, J, and $\phi^{(\tau)}$ as sums of Hough functions. The coefficients of ϕ' and w will be determined from equation IIA-24 (when J is replaced by its Hough function coefficient);

$$(i\nu + a_0)\frac{d\phi'^m_n}{dz} + (2\Omega a)^2 S' w^m_n = \mathcal{H} J^m_n \qquad \text{IIA-24'}$$

and by the separability condition

$$-i\nu\gamma^m_n \phi'^m_n + (2\Omega a)^2\left[\frac{dw^m_n}{dz} - w^m_n\right] = 0 \qquad \text{IIA-21'}$$

---

1. For the gravitational modes, $H^m_n(\mu)$ represents wavenumber m motion with n nodes. These gravitational modes are also symmetric in μ (see Flattery (1967)).

Eliminating ϕ'^m_n from these two equations gives

$$(1+\frac{a_0}{\lambda\nu})\left(\frac{d^2W^m_n}{dz^2}-\frac{dw^m_n}{dz}\right)+\gamma^m_n w^m_n S'=\frac{\gamma^m_n \beta J^m_n}{(2\Omega a)^2} \quad \text{IIA-25}$$

Taking $w^m_n = e^{z/2} Y^m_n(z)$ leads to the vertical structure equation in its simplest form

$$\frac{d^2Y^m_n}{dz^2}+\left[-\frac{1}{4}+\frac{\gamma^m_n S'}{1+\frac{a_0}{\lambda\nu}}\right]Y^m_n=\frac{\gamma^m_n \beta J^m_n}{(2\Omega a)^2(1+\frac{a_0}{\lambda\nu})} \quad \text{IIA-26}$$

Equation IIA-26 is a second-order ordinary differential equation; therefore, two boundary conditions are required to complete a proper formulation of the tidal problem.

The lower boundary condition, at $z=0$, is that there should be no vertical motion at $z=0$; or to express it mathematically

$$w=\frac{dh}{dt}=0 \quad \text{at} \quad z=0 \quad . \quad \text{IIA-27}$$

Linearizing IIA-27 leads to

$$\left(\frac{\partial}{\partial t}+w\frac{\partial}{\partial z}\right)\left(\frac{\phi'-\phi^{(T)}}{g}\right)=0 \quad , \quad \text{IIA-28}$$

which may be rewritten in terms of the coefficients of the Hough functions as

$$i\nu\phi'^{m}_{n} - i\nu\Omega^{m}_{n} + w^{m}_{n}\bar{H} = 0 \quad . \qquad \text{IIA-29}$$

By substituting, as before, $w^{m}_{n} = e^{z/2} Y^{m}_{n}(z)$, the final form of the bottom boundary condition is seen to be

$$\frac{dY^{m}_{n}}{dz} + \left(\frac{\bar{H}}{D^{m}_{n}} - \frac{1}{2}\right) Y^{m}_{n} = \frac{i\nu\Omega^{m}_{n}}{g D^{m}_{n}} \quad \text{at } z=0 \quad . \qquad \text{IIA-30}$$

($D^{m}_{n} = (2\Omega a)^2 \div g\gamma^{m}_{n}$ is the so-called "equivalent depth".)

To complete the tidal formulation the upper boundary condition must be considered. This upper condition is taken to be the requirement that the solutions to equation IIA-26 be either evanescent or propagate outward as waves for large z .

Section B: Formulation of Variables

The previous formulation of the tidal equations had Y^{m}_{n} as the dependent variable where

$$w^{m}_{n}(z) = e^{z/2} Y^{m}_{n}(z) \quad . \qquad \text{IIB-1}$$

When a solution of these tidal equations is calculated, it will still be necessary to calculate the usual meteorological variables from this solution. Once these meteorological variables are computed, the tidal solution is complete and can be compared directly with observations.

In this study the final variables to be computed will be as follows:

(1) h' -- the pressure perturbation in geopotential height units

(2) U -- the eastward tidal wind velocity

(3) V -- the northward tidal wind velocity

(4) W -- the upward tidal wind velocity

(5) T' -- the tidal temperature perturbation.

This section will be devoted to finding equations for these meteorological variables in terms of $Y^m_n(z)$[1].

h'

The starting point for this variable is eqn. (21') in the previous section

$$-i\nu\gamma^m_n\phi'^m_n + (2\Omega a)^2\left[\frac{dw^m_n}{dz} - w^m_n\right] = 0 \quad . \qquad \text{IIB-2}$$

---

1. In this section the z -dependent Hough function coefficients will be subscripted and superscripted. The full variable (with (λ, φ, z, t) dependence will not be scripted even though a single tidal mode is meant.

Substituting for w^m_n with equation II B-1 and solving for ϕ'^m_n gives

$$\phi'^m_n = \frac{(2\Omega a)^2}{\nu \gamma^m_n} e^{z/2} i \left[\frac{1}{2} Y^m_n - \frac{dY^m_n}{dz}\right] \quad \text{II B-3}$$

Since $\phi'^m_n = g h'^m_n + \Omega^m_n$, eqn. II B-3 can be solved for h' giving

$$h' = \mathcal{R}e\left[\left\{H^m_n(\mu) \frac{(2\Omega a)^2}{\nu \gamma^m_n g} e^{z/2} i\left[\frac{1}{2} Y^m_n - \frac{dY^m_n}{dz}\right] - \frac{\Omega^m_n}{g}\right\} \exp[im\lambda + i\nu t]\right] \quad \text{II B-4}$$

[1]

U

Equation II A-19 implies

$$U = \left\{\frac{1}{\nu^2 - (2\Omega\mu)^2}\left[-\frac{\nu m \phi'}{a(1-\mu^2)^{\frac{1}{2}}} + \frac{(2\Omega\mu)}{a}(1-\mu^2)^{\frac{1}{2}} \frac{\partial \phi'}{\partial \mu}\right]\right\} \exp[im\lambda + i\nu t]. \quad \text{II B-5}$$

Equation II B-3 along with equation II B-5 yields the following formula for U :

$$U = \mathcal{R}e\left\{\frac{(2\Omega a)^2}{a\nu\gamma^m_n} e^{z/2} i \left[\frac{-\nu m H^m_n(\mu)}{(1-\mu^2)^{1/2}} + (2\Omega\mu)(1-\mu^2)^{\frac{1}{2}} \frac{\partial H^m_n}{\partial \mu}\right] \left(\frac{1}{2} Y^m_n - \frac{dY^m_n}{dz}\right) \exp[im\lambda + i\nu t]\right\} \quad \text{II B-6}$$

$$\nu^2 - (2\Omega\mu)^2$$

---

1. $\mathcal{R}e(\,)$ = real part of $(\,)$
   $\mathcal{I}m(\,)$ = imaginary part of $(\,)$

V

Equation II A-20 implies

$$V=\frac{1}{\nu^2-(2\Omega\mu)^2}\left[-\frac{(2\Omega\mu)im}{a(1-\mu^2)^{1/2}}\phi'+\frac{i\nu}{a}(1-\mu^2)^{\frac{1}{2}}\frac{\partial\phi'}{\partial\mu}\right]\exp[im\lambda+i\nu t] \qquad \text{II B-7}$$

Equation II B-3 along with equation II B-7 yields the following formula for V :

$$V=\sum_n\left\{\frac{(2\Omega a)^2}{a\nu\gamma_n^m}e^{a/2}\left[\frac{(2\Omega\mu)m}{(1-\mu^2)^{1/2}}H_n^m+\nu(1-\mu^2)^{\frac{1}{2}}\frac{\partial H_n^m}{\partial\mu}\right]\Big/\left[\nu^2-(2\Omega\mu)^2\right]\left(-\frac{1}{2}Y_n^m+\frac{dY_n^m}{d\bar{z}}\right)\exp[im\lambda+i\nu t]\right\} \qquad \text{II B-8}$$

W

The vertical velocity W is defined by

$$W=\frac{dh'}{dt} \qquad \text{II B-9}$$

Linearizing equation II B-9, and remembering that $\phi'=gh'+\phi^{(T)}$, implies

$$W=\frac{1}{g}\frac{\partial\phi'}{\partial t}-\frac{1}{g}\frac{\partial\phi^{(T)}}{\partial t}+\bar{H}w \qquad \text{II B-10}$$

or alternatively

$$W_n^m=i\nu\frac{\phi_n'^m}{g}-i\nu\frac{\Omega_n^m}{g}+\bar{H}w_n^m \qquad \text{II B-11}$$

Hence

$$w=\mathcal{R}\left\{H_n^m(\mu)\left[\frac{(2\Omega a)^2}{\delta_n^m g}e^{s/2}\left(-\tfrac{1}{2}Y_n^m+\frac{dY_n^m}{d\xi}\right)-\frac{i\nu\Omega_n^m}{g}+\bar{H}e^{s/2}Y_n^m\right]\exp[im\lambda+i\nu\tau]\right\} \quad \text{II B-12}$$

T'

Equations II A-18 and II A-24 may be combined to give

$$(i\nu+a_0)RT'^m_n+(2\Omega a)^2\mathcal{S}'w^m_n=\mathcal{H}J^m_n \quad \text{II B-13}$$

From equation II B-13 T' may be seen to be given by

$$T'=\mathcal{R}\left\{H_n^m(\mu)\left[\frac{(2\Omega a)^2\mathcal{S}'}{R(i\nu+a_0)}e^{s/2}Y_n^m+\frac{\mathcal{H}}{R(i\nu+a_0)}J_n^m\right]\exp[im\lambda+i\nu\tau]\right\} \quad \text{II B-14}$$

The final formulae are found from equations II B-4, II B-6, II B-8, II B-12, and II B-14 to be

$$h'=H_n^m(\ell)\frac{D_n^m}{\nu}e^{s/2}\left\{\left(-\tfrac{1}{2}Y_i^{(m,n)}+\frac{dY_i^{(m,n)}}{d\xi}-\frac{\nu e^{-s/2}}{gD_n^m}\Omega_n^m\right)\cos[\nu t+m\lambda]\right.$$
$$\left.+\left(-\tfrac{1}{2}Y_r^{(m,n)}+\frac{dY_r^{(m,n)}}{d\xi}\right)\sin[\nu\tau+m\lambda]\right\} \quad \text{II B-15}$$

$$u=\frac{gD_n^m}{a\nu}e^{s/2}\left[\frac{-\nu m H_n^m(\ell)}{\cos\ell}+f\frac{dH_n^m}{d\ell}\right]\left\{\begin{array}{l}\left(-\tfrac{1}{2}Y_i^{(m,n)}+\frac{dY_i^{(m,n)}}{d\xi}\right)\cos[\nu t+m\lambda]+\\ \left(-\tfrac{1}{2}Y_r^{(m,n)}+\frac{dY_r^{(m,n)}}{d\xi}\right)\sin[\nu\tau+m\lambda]\end{array}\right\} \quad \text{II B-16}$$

$$V=\frac{gD_n^m}{a\nu}e^{z/2}\left[\frac{-\frac{mf}{\cos\varphi}H_n^m(\varphi)+\nu\frac{dH_n^m}{d\varphi}}{\nu^2-f^2}\right]\begin{Bmatrix}(-\frac{1}{2}Y_r^{(m,n)}+\frac{dY_r^{(m,n)}}{dz})\cos[\nu t+m\lambda]-\\(-\frac{1}{2}Y_i^{(m,n)}+\frac{dY_i^{(m,n)}}{dz})\sin[\nu t+m\lambda]\end{Bmatrix}$$ [1] II B-17

$$W=D_n^m e^{z/2}H_n^m(\varphi)\begin{Bmatrix}[(-\frac{1}{2}+\frac{\bar{H}}{D_n^m})Y_r^{(m,n)}+\frac{dY_r^{(m,n)}}{dz}]\cos[\nu t+m\lambda]+\\[(\frac{1}{2}-\frac{\bar{H}}{D_n^m})Y_i^{(m,n)}-\frac{dY_i^{(m,n)}}{dz}+e^{z/2}\frac{\nu\Omega_n^m}{gD_n^m}]\sin[\nu t+m\lambda]\end{Bmatrix}$$ II B-18

$$T'=\frac{(2\Omega a)^2\delta'}{R(\nu^2+a_0^2)}e^{z/2}H_n^m(\varphi)\begin{Bmatrix}(a_0Y_r^{(m,n)}-\nu Y_i^{(m,n)}-\frac{a_0\beta J_n^m}{R(\nu^2+a_0^2)})\cos[\nu t+m\lambda]+\\(-a_0Y_i^{(m,n)}-\nu Y_r^{(m,n)}+\frac{\nu\beta J_n^m}{R(\nu^2+a_0^2)})\sin[\nu t+m\lambda]\end{Bmatrix}$$ II B-19

where $Y_n^m(z)=Y_r^{(m,n)}(z)+iY_i^{(m,n)}(z)$ ($Y_r^{(m,n)}$ and $Y_i^{(m,n)}$ are real functions of z).

Equations (II B-15) - (II B-19)are the formulae to be used in calculating the meteorological variables.

---

1. $f\ (=2\Omega\mu)$ is the Coriolis parameter.

CHAPTER III

PROCEDURE

Section A: Gravitational Forcing

The lunar atmospheric tide is quite unlike the solar diurnal and semidiurnal atmospheric tides. The main source of forcing for the solar tides is thought to be solar heating (see Siebert (1961), Eutler and Small (1963), Lindzen (1968), etc). This insolational heating displays an annual variation both due to the variation of the incoming solar radiation and due to variation in absorber amounts. The first impulse would be, for this reason, to explain the annual variation of a solar tide by utilizing the variation of the solar heating. In fact Lindzen (1967) did just this for the solar diurnal tide.

The lunar tide is quite different from the solar tide since there is negligible heating of the atmosphere with the lunar period. The lunar tide is forced purely by the moon's tidal forces acting on the earth-ocean-atmosphere system.

These lunar tidal forces may be obtained from the lunar tidal potential which was derived by Lamb (1932). His expression for this tidal potential is

$$\Omega = -\frac{3}{4} g \frac{M}{E} \left(\frac{a}{D}\right)^3 \frac{(a+z)^2}{a} \left[3\left(\cos^2\Delta - \tfrac{1}{3}\right)\left(\cos^2\theta - \tfrac{1}{3}\right)\right.$$

$$+ \sin 2\Delta \cdot \sin 2\theta \cdot \cos(\alpha+\lambda) \qquad \text{IIIA-1}$$

$$\left. + \sin^2\Delta \cdot \sin^2\theta \cdot \cos 2(\alpha+\lambda)\right]$$

where the symbols have the following meaning:

g = acceleration of gravity (= 980.6 cm sec^{-2})

M = mass of the moon (= 7.349×10^{25} gm)

E = mass of the earth (= 5.977×10^{27} gm)

a = mean radius of the earth (= 6.371×10^{8} cm)

D = mean distance between the center of the earth and of the moon (= 3.844×10^{10} cm)

z = height above the surface of the earth

Δ, α = north-polar distance, and the hour-angle of the moon

θ, λ = colatitude and longitude.

Since the lunar semidiurnal tide is known to far exceed the lunar diurnal tide the term of interest is the potential for the semidiurnal lunar forces,

$$\Omega_{\text{semidiurnal}} = -\frac{3}{4} g \frac{M}{E} \left(\frac{a}{D}\right)^3 \frac{(a+z)^2}{a} \sin^2\Delta \cdot \sin^2\theta \cdot \cos 2(\alpha+\lambda) \qquad \text{IIIA-2}$$

As is usual in tidal theory the vertical tidal forces are neglected[1] and Δ is taken to be $\frac{\pi}{2}$. (The moon is located over the earth's equator.) The hour-angle of the moon can also be expressed in time units so that the expression for the tidal potential becomes

$$\phi^{(T)} = -\frac{3}{4} g \frac{M}{E} \frac{a^4}{D^3} \cdot \sin^2\theta \cdot \cos(\nu t + 2\lambda) \qquad \text{IIIA-3}$$

where $$\nu = \frac{2\pi}{\frac{T}{2}} = 1.407 \times 10^{-4}\ \text{sec}^{-1}$$

(T is the lunar day which equals 24.8412 mean solar hours.)

It is seen that the lunar tidal potential is proportional to $\sin^2\theta$; but $\sin^2\theta = \frac{\sqrt{15}}{4} P_2^2(\mu)$[2], where $P_2^2(\mu)$ is the normalized (2, 2) spherical harmonic.

It only remains to expand $P_2^2(\mu)$ in Hough functions. This expansion has been done by Flattery (1967). His expansion of $P_2^2(\mu)$ in normalized Hough functions is

---

1. This is true since the tidal potential varies little over the depth of the atmosphere — $\frac{z}{a} << 1$.

2. $\mu = \sin\varphi = \cos\theta$

$$P^2_2(\mu) = 0.962708\, H^2_2(\mu) + 0.228431\, H^2_4(\mu) +$$

$$0.105893\, H^2_6(\mu) - 0.062925\, H^2_8(\mu) -$$

$$0.042627\, H^2_{10}(\mu) - 0.031293\, H^2_{12}(\mu) - \qquad \text{IIIA-4}$$

$$0.024243\, H^2_{14}(\mu) + 0.019515\, H^2_{16}(\mu) + \cdots \quad [1]$$

Putting numbers into expression IIIA-3 and using the first three terms in expansion IIIA-4 yields the required expansion of $\phi^{(\tau)}$ in Hough functions:

$$\phi^{(\tau)} \approx -2.60787\times10^4 H^2_2(\mu) - 6.18794\times10^3 H^2_4(\mu) \qquad \text{IIIA-5}$$

$$- 2.86852\times10^3 H^2_6(\mu) .$$

It is thus seen that the forcing for the (2, 2) mode is, roughly speaking, four times larger than the (2, 4) mode. It is also true that D^2_2 = 7.07009 km. while D^2_4 = 3.24857 km and h^m_n, U^m_n, V^m_n, and W^m_n depend linearly on D^m_n. With this in mind, only the (2, 2) mode will be considered as representing the lunar tide in the remainder of this study.

---

1. These differ slightly from the calculations of Sawada (1954).

Section B: Stability Function

The vertical structure equation was derived in a previous section (equation II B-26) to be

$$\frac{d^2Y_n^m}{dz^2} + \left[-\frac{1}{4} + \frac{\gamma_n^m S'}{1 + \frac{a_0}{i\nu}}\right] Y_n^m = \frac{\gamma_n^m \mathcal{B} J_n^m}{(2\Omega a)^2 (1 + \frac{a_0}{i\nu})} \qquad \text{III B-1}$$

This equation for the lunar tide is

$$\frac{dY_n^m}{dz^2} + \left[-\frac{1}{4} + \frac{\gamma_n^m S'}{1 + \frac{a_0}{i\nu}}\right] Y_n^m = 0 \qquad \text{III B-2}$$

since, as stated before, the atmosphere experiences negligible heating with the lunar period.

For the time being, the effects of Newtonian Cooling will be ignored leaving the equation

$$\frac{d^2Y_n^m}{dz^2} + \left[-\frac{1}{4} + \gamma_n^m S'\right] Y_n^m = 0 \qquad \text{III B-3}$$

Equation III B-3 is of similar structure to the time-independent one-dimensional Schrodinger equation

$$\frac{d^2\psi}{dz^2} + \frac{2m}{\hbar^2}\left[-V(z) + E(z)\right]\psi = 0 \qquad \text{III B-4}$$

where

ψ = wave-function of particle with mass m

$\hbar$ = (Plank's constant) $\div 2\pi$

$V(z)$ = potential energy function

$E(z)$ = total energy function[1].

The comparison between equations III B-3 and III B-4 is complete if $V(z) = \frac{\hbar^2}{2m} \cdot \frac{1}{4}$ and $E(z) = \frac{\hbar^2}{2m} \cdot \gamma_n^m S'$. With this comparison, it should be possible to carry over at least part of the physical reasoning so common in Schrodinger equation usage, that of the potential barrier, to the tidal problem.

A mean profile of $S'(z)$ is shown in figure III B-1. This profile above 30 km was constructed by using the 1965 CIRA mean atmosphere. The lower part of this profile was calculated by averaging temperatures collected in a five year study by the Planetary Circulations Project under Prof. V. P. Starr at the Massachusetts Institute of Technology. These temperatures were first time-averaged for the five years and then averaged with respect to area over the Northern Hemisphere[2, 3]. The lower and upper parts of $S'(z)$

---

1. Equations III B-3 and III B-4 are both examples of a more general class of equations -- the Helmholtz equation.
2. The hemispheric average is computed by the following formula:

$$\overline{(\,)} = \frac{\int_0^{\pi/2} \left\{ \int_0^{2\pi} (\,) \frac{d\lambda}{2\pi} \right\} \cos\varphi \, d\varphi}{\int_0^{\pi/2} \cos\varphi \, d\varphi}$$

3. Rigorously the calculation of $S'(z)$ should be carried out as follows:

(1) Calculate $\frac{g}{(2\Omega a)^2} \left[\gamma H(\lambda, \varphi, z, t) + \frac{\partial}{\partial z} H(\lambda, \varphi, z, t) \right]$

(2) Average with respect to time and area. At what is considered a small loss in accuracy, H was first averaged and $S'(z)$ was computed with this.

were then connected smoothly.

The vertical line in the middle of the figure is $S = S_{crit}^{(2,2)}$, where $\gamma_2^2 S_{crit}^{(2,2)} = \frac{1}{4}$ $(\gamma_2^2 = 12.4618)$. In the parts of $S(z)$ where $S(z) < S_{crit}^{(2,2)}$, the (2, 2) tidal mode is evanescent; however, where $S(z) > S_{crit}^{(2,2)}$ the (2, 2) mode has the characteristics of a travelling wave.

Preserving the terminology of the Schrodinger equation, the regions where $S(z) < S_{crit}^{(2,2)}$ will be called "barriers". The author has named the various regions of the stability curve in figure III B-1 according to whether the solutions to equation III B-3 are evanescent or wavelike.

Figures (III B-2) - (III B-13) display the author's calculations of the monthly-averaged values of $S(z)$ and $\bar{H}(z)$. The data used in these monthly calculations were as follows:

(1) 1000 mb to 50 mb (approximately the ground to 20 km)

The temperature data of Starr, et al. is used to calculate $[H]$ [1]. For example, the January $[H]$ is the average of January 1957, January 1958, January 1959, January 1960, and January 1961. This data is then hemispherically averaged.

(2) 30 km to 80 km

Zonal averages of temperature are obtained from the CIRA

---

1. $[(\,)] = \frac{1}{2\pi}\int_0^{2\pi} (\,)\, d\lambda$

atmospheres. $\tilde{H}(z)$ is then calculated by hemispherically averaging these CIRA values.

(3) 100 km $\rightarrow \infty$

The CIRA mean atmosphere is used for this region.

These three regions were then connected as simply as possible with a smooth curve. This smooth curve is shown as the dashed line in figures (III B-2) - (III B-13).

This curve for $\tilde{H}(z)$ is then used to calculate $S'(s)$ up to $z = 14.8$. Above $z = 14.8$ a straight line was fitted to the calculations of $S'(z)$. All months are thus fitted to a standard thermosphere.

The values for $S'(z)$, computed as explained above, are shown as the solid curves in figures (III B-2) - (III B-13).

The annual variation in $S'(z)$, which is depicted in these figures, will cause a corresponding variation in the lunar tide. For this reason, the character of the seasonal changes in $S'(z)$ will be discussed.

The temperatures at the ground, tropopause, stratopause, and mesopause levels are marked to emphasize the regions where there is most seasonal variation.

The temperature at the ground in January is 281°K. It rises to a maximum of 294°K in July and August. The range of

seasonal variation in $\bar{T}$ at the ground is then $13^{o}K$.

The temperature at the tropopause in mid-winter is $208^{o}K$ and reaches its maximum value of $211^{o}K$ in mid-summer. The range of seasonal variation in $\bar{T}$ at the tropopause is $3^{o}K$.

The minimum stratopause temperature is $263^{o}K$ and occurs in February; while the maximum stratopause temperature is $278^{o}K$ and occurs in June. The range of seasonal variation in $\bar{T}$ at the stratopause is $15^{o}K$.

At the mesopause the minimum temperature, $183^{o}K$, is seen in July while the maximum temperature, $225^{o}K$, is seen in December. The range of seasonal variation in $\bar{T}$ at the mesopause is $42^{o}K$.

From the preceding, it is clear that the seasonal variation in $\bar{H}(z)$ is most pronounced at the mesopause level. This seasonal variation in the region of the mesopause is also evident in the changing size of the "mesospheric barrier" (the shaded regions) in figures (III B-2) - (III B-13). It will be noted that the "mesospheric barrier" is much larger in the summer months than during the winter.

This means that the lunar tide should experience more trapping in summer than in winter. It would follow that the

tidal wave should more closely resemble a standing wave in summer; while in winter the tide should show more characteristics of a propagating wave. This change in wave structure could be a very important effect in explaining the observed annual changes in the lunar tide.

Before proceeding further it should be noted that $S'(z)$ is a Northern Hemisphere average but is assumed to be true over the entire sphere. It is not possible to get a globally averaged stability function due to the paucity of Southern Hemisphere data at high levels. This limitation of the calculations which follow should be kept in mind.

Section C: Newtonian Cooling

In section II A, it was assumed that the diabatic term in the thermodynamic equation is expressable as the sum of a solar heating term and a Newtonian Cooling term, $Q = J - a_0 \delta T$ (δT being a temperature perturbation). In this section the Newtonian Cooling term will be examined.

There are two distinct contributions to the Newtonian Cooling term with one part of this effect being due to the temperature dependent effect of CO_2 infra-red cooling and the other part of the Newtonian Cooling term being due to the temperature depen-

dence of O_3 photochemistry.

The contribution due to CO_2 will be treated first[1]. A formula for the net monochromatic radiant flux at a given level z is given by

$$F_\nu(z) = \int_0^z B_\nu(\theta(z')) \frac{\partial T_\nu(z,z')}{\partial z'} dz' + \int_z^\infty B_\nu(\theta(z')) \frac{\partial T_\nu(z,z')}{\partial z'} dz' \qquad \text{III C-1}$$

$$+ B_\nu(\theta(0)) T_\nu(0,z) + B_\nu(\theta(\infty)) T_\nu(\infty,z)$$

where

$F_\nu(z)$ = net radiative flux at frequency ν and level z

$\theta(z)$ = temperature at level z

$B_\nu(\theta)$ = Plank function at frequency ν and temperature θ

$T_\nu(z,z')$ = transmissivity function from level z to z' evaluated at frequency ν .

The terms in equation III C-1 represent, proceeding from left to right; the flux arriving at z from atmospheric layers below, the flux arriving at z from atmospheric layers above, the flux arriving at z from the ground, and finally the flux at z originating at infinity.

The flux convergence, or "heating", at z is given by differentiating equation III C-1 with respect to z giving

1. This discussion is the author's understanding of an unpublished derivation due to C. D. Rodgers.

$$H_\nu(z) = -\frac{dF_\nu}{dz} = -\int_0^z B_\nu(\theta(z'))\frac{\partial^2 T_\nu(z,z')}{\partial z' \partial z}dz' - \int_z^\infty B_\nu(\theta(z'))\frac{\partial^2 T_\nu(z,z')}{\partial z' \partial z}dz'$$

$$+ B_\nu(\theta(0))\frac{dT_\nu(z,0)}{dz} - B_\nu(\theta(\infty))\frac{dT_\nu(z,\infty)}{dz} \qquad \text{III C-2}$$

As noted in Rogers and Walshaw (1966) the complete radiative heating equation III C-2 includes the following effects:

(a) a cooling-to-space effect

(b) a flux exchange with other atmospheric layers

(c) a boundary flux from the ground

(d) a boundary flux from infinity.

Ignoring all these effects except (a) is the cooling-to-space approximation. This cooling-to-space term, integrated over all frequencies, is seen to be

$$C_s = \text{cooling-to-space (in } ^\circ\text{C/day)} = \frac{1}{c_p \rho}\int_0^\infty E_\nu(z)\frac{dT_\nu(z,\infty)}{dz}d\nu \qquad \text{III C-3}$$

Since the main contribution to CO_2 infrared transfer is in the strong band centered at $\lambda \sim 15\mu$, the integral in equations III C-3 may be approximated by

$$\bar{C}_s \approx \frac{1}{c_p \rho}\bar{B}_{15\mu}(z)\frac{\overline{dT_{15\mu}(z,\infty)}}{dz} \qquad \text{III C-4}$$

where $\bar{(\,)} = \frac{1}{\Delta\nu}\int_{\Delta\nu}(\,)d\nu$ (the average over the absorption

band). The emissivity is defined to be equal to $1-\bar{T}_\nu$ so that, after putting in numerical values for c_p and adjusting to proper time units. the CO_2 cooling is approximated by

$$\text{Cooling} \approx 8.31\times10^{-6}\cdot \bar{B}_{15\mu}(\theta)\cdot\frac{d\bar{\varepsilon}_{15\mu}(z,\infty)}{dp}\quad \frac{^oC}{day}\ .^{1} \qquad \text{III C-5}$$

Rodgers (1967) has fitted analytical expressions to approximate the CO_2 emissivity. His expressions are as follows:

$$\bar{\varepsilon}(U) \approx 160\sqrt{U} \quad \text{above 10 mb} \qquad \text{III C-6}$$

$$\bar{\varepsilon}(U) \approx 20 \ln U \quad \text{below 10 mb} \ . \qquad \text{III C-7}$$

These emissivity formulae are valid for U (the optical path) given by $U(p,p') = \frac{p_s}{g}\int_p^{p'} c(p)\,p\,dp$

where p is in atmospheres with p_s being 10^6 dynes cm^{-2} while $c(p)$ is the CO_2 mixing ratio. As is customary, when treating CO_2, $c(p)$ is taken to be constant giving

$$U = U_0 p^2 \ . \qquad \text{III C-8}$$

Using these approximations, the cooling due to CO_2 may be calculated by noting $\frac{d\bar{\varepsilon}}{dp} = \frac{d\bar{\varepsilon}}{dU}\cdot\frac{dU}{dp}$. For the log region

---

1. Note the change to pressure coordinates.

$$\frac{d\bar{\varepsilon}}{dv} = \frac{20}{v} = \frac{20}{v_0 p^2} \qquad \text{while} \quad \frac{dv}{dp} = 2v_0 p \ ;$$

thus, $\frac{d\bar{\varepsilon}}{dp} = \frac{40}{p}$ below 10 mb. III C-9

The band-averaged Plank function is approximated by the value of the Plank function at the center of the band,

$$\text{i.e.} \quad \bar{B}_\nu = \frac{2h\nu^3}{c^2(e^{h\nu/kT} - 1)} \approx \frac{2h\nu^3}{c^2} e^{-\frac{h\nu}{kT}} \qquad \text{III C-10}$$

(This approximation is good to about 5% for the 15 μ band at reasonable temperatures.)

Using formulae III C-5, III C-9, and III C-10 the cooling for the log region (below 10 mb) is given by

$$\text{Cooling} \approx \frac{3.66}{p} e^{-\frac{960}{T}} \qquad \text{III C-11}$$

with p in atmospheres and T in ^{o}K.

For the square-root region $v = 125\, p^2$ gm. cm.$^{-2}$ (p in atm.) if the constant CO_2 mixing ratio is taken to be 250 atm. cm. Hence in this region, $\bar{\varepsilon} = 1.8 \times 10^3\, p$ which implies

$$\frac{d\bar{\varepsilon}}{dp} = 1.8 \times 10^3 \qquad \text{III C-12}$$

Therefore, using formulae III C-5, III C-9, and III C-12,

$$\text{Cooling} \approx 160\, e^{-\frac{960}{T}} \qquad \text{above 10 mb .} \qquad \text{III C-13}$$

In summary, the approximate formulae for CO_2 cooling are as follows:

$$CO_2 \text{ cooling} = \begin{cases} \frac{3.66}{p} e^{-\frac{960}{T}} & \text{below 10 mb} \\ 160\, e^{-\frac{960}{T}} & \text{above 10 mb} \end{cases} \quad \text{III C-14}$$

The corresponding Newtonian Cooling formulae are obtained by linearizing expressions III C-14 with $T = \bar{T} + \delta T$. These formulae are as follows:

$$\alpha_{CO_2} = \begin{cases} 3.52 \times 10^3 \frac{1}{p\bar{T}^2} e^{-\frac{960}{\bar{T}}} & \text{below 10 mb} \\ 1.54 \times 10^5 \frac{1}{\bar{T}^2} e^{-\frac{960}{\bar{T}}} & \text{above 10 mb} \end{cases} \quad \text{III C-15}$$

An average profile of α_{CO_2} is calculated from the hemispherically-averaged temperature profile. This temperature profile is shown in figure III C-1. The Newtonian Cooling function, α_{CO_2} (figure III C-2) is arbitrarily set to zero at $z = 14.8$. This should not affect any calculations since all energy reaching $z = 14.8$ leaves the system because of the upper radiation condition. It is important to have a constant value of α_{CO_2} above $z = 14.8$ for consistency of this radiation condition.

The Newtonian Cooling effects due to ozone will now be discussed. Classical ozone photochemistry predicts that ozone concentrations should be strongly temperature dependent between about 40 and 70 km. (see Leovy (1964) and Lindzen and Goody (1965)). This is due to the strong temperature dependence of the reaction

$$O + O_3 \longrightarrow 2O_2 \quad . \qquad \text{III C-16}$$

Because of the ozone photochemistry, the ozone heating rate should be strongly temperature dependent. This heating rate is given by the following equation which has been taken from Leovy (1964):

$$q_s \simeq \frac{\text{const.}}{\rho} J_3^{\frac{1}{2}} \exp\left(\frac{\Delta Q}{2 R_* T}\right) \qquad \text{III C-17}$$

where J_3 is the rate of absorption of solar photons by an ozone molecule, ΔQ is the activation energy for reaction III C-16 (ΔQ = 6 Kcal. mole^{-1}), and R_* is the universal gas constant.

J_3 is dependent on the ozone concentration at all levels above that being considered and therefore is dependent on the atmospheric temperature structure. This temperature dependence of J_3 is,however, taken to be secondary to the temperature

dependence of the ozone concentration and is disregarded for this reason.. Differentiating equation III C-17 with respect to T gives the following:

$$a_{O_3} = \left(\frac{\partial q_s}{\partial T}\right)_{eq} = -\frac{\Delta Q}{2R_* \bar{T}^2} q_s(\bar{T}) \qquad \text{III C-18}$$

Upper and lower limits for a_{O_3} are shown in figure III C-3. These profiles were computed from curves of "observed" ozone heating rates prepared by Leovy (1967), and the temperature structure in figure III C-1[1].

Section D: Numerical Procedure

In section (II A) the lunar tidal equations were formulated and in sections (III A), (III B), and (III C) the coefficients in the tidal equations and boundary conditions were found. It only remains for the means of solution to be discussed.

The vertical equation along with boundary conditions can be written as

$$\frac{d^2 Y_n^m}{dz^2} - \frac{1}{4} Y_n^m + \left[\left(1 + \frac{a_0}{L\nu}\right)^{-1} \gamma_n^m S'\right] Y_n^m = 0 \qquad \text{III D-1}$$

with

---

1. The author is very grateful to Capt. Thomas Dopplick and Mr. Herbert Jacobowitz for their help in understanding the radiative transfer considerations contained in this section.

$$\frac{dY_n^m}{dz} - \left(\frac{1}{2} - \frac{\bar{H}}{D_n^m}\right) Y_n^m = i \frac{\nu \Omega_n^m}{g D_n^m} \quad \text{at } z=0$$

III D-2

and Radiation Condition as $z \to \infty$

III D-3

Although some solutions to this lunar tidal problem can be obtained analytically, any realistic problem must be treated numerically. The plan of attack is illustrated in figure III D-1.

Equation III D-1 along with conditions III D-2 and III D-3 constitute a boundary-value problem. Such problems are amenable to two types of solution

(1) an iterative procedure and

(2) a matrix approach.

The iterative procedures are quite tedious and the rate of convergence of such procedures is sometimes a problem. For this reason, the method used in this study is a matrix approach.

Equation III D-1 should more precisely be written as the two equations

$$\frac{d^2 Y_r^{(m,n)}}{dz^2} - \left[\frac{1}{4} - \frac{\gamma_n^m \beta'}{1 + \frac{a_0^2}{\nu^2}}\right] Y_r^{(m,n)} - \frac{\gamma_n^m \beta' \frac{a_0}{\nu}}{1 + \frac{a_0^2}{\nu^2}} Y_i^{(m,n)} = 0 \quad \text{III D-4}$$

and

$$\frac{d^2 Y_i^{(m,n)}}{dz^2} - \left[\frac{1}{4} - \frac{\gamma_n^m \delta'}{1+\frac{a_0^2}{\nu^2}}\right] Y_i^{(m,n)} + \frac{\gamma_n^m \delta' \frac{a_0}{\nu}}{1+\frac{a_0^2}{\nu^2}} Y_r^{(m,n)} = 0 \qquad \text{III D-5}$$

In order to simplify the notation, the following variables are defined:

$$\eta(z) = Y_r^{(m,n)}(z)$$

$$w(z) = Y_i^{(m,n)}(z)$$

$$f(z) = -\left[\frac{1}{4} - \frac{\gamma_n^m \delta'}{1+\frac{a_0^2}{\nu^2}}\right]$$

$$g(z) = \frac{\gamma_n^m \delta' \frac{a_0}{\nu}}{1+\frac{a_0^2}{\nu^2}} .$$

Equations III D-4 and III D-5 become

$$\frac{d^2\eta}{dz^2} + f(z)\eta - g(z)w = 0 \qquad \text{III D-6}$$

$$\frac{d^2 w}{dz^2} + f(z)w + g(z)\eta = 0 . \qquad \text{III D-7}$$

Equations III D-6 and III D-7 will now be put into finite-difference form. The following finite-difference notation will be needed:

$$h = \Delta z = \frac{z_{TOP}}{N}$$

$$z_n = n\Delta z$$

$$()_n = ( ) \text{ evaluated at } z_n$$

$$\delta^2()_K = ()_{K+1} - 2()_K + ()_{K-1} .$$

The starting point for the finite-difference equations will be the following formula which is taken out of Hildebrand (p. 241).

$$U_{n+1} - 2U_n + U_{n-1} = h^2\left(1 + \tfrac{1}{12}\delta^2\right)U''_n + T_n \qquad \text{III D-8}$$

where the truncation error is given by

$$T_n = -\frac{h^6}{240}\,U^{vi}(\xi) \qquad (z_{n-1} < \xi < z_{n+1}) \,. \qquad \text{III D-9}$$

Equation III D-6 can be put into finite-difference form, by using equation III D-8 and ignoring T_n, as

$$\eta_{n+1} - 2\eta_n + \eta_{n-1} = h^2\left(1 + \frac{\delta^2}{12}\right)(-f_n\eta_n + g_n w_n) \qquad \text{III D-10}$$

while equation III D-7 is written

$$w_{n+1} - 2w_n + w_{n-1} = h^2\left(1 + \frac{\delta^2}{12}\right)(-f_n w_n - g_n\eta_n) \,. \qquad \text{III D-11}$$

By expanding δ^2, in equations III D-10 and III D-11, the following equations are derived:

$$\left(1 + \tfrac{h^2}{12}f_{n+1}\right)\eta_{n+1} - 2\left(1 - \tfrac{5h^2}{12}f_n\right)\eta_n + \left(1 + \tfrac{h^2}{12}f_{n-1}\right)\eta_{n-1}$$
$$- \tfrac{h^2}{12}g_{n+1}w_{n+1} - \tfrac{5h^2}{6}g_n w_n - \tfrac{h^2}{12}g_{n-1}w_{n-1} = 0 \qquad \text{III D-12}$$

$$\left(1 + \tfrac{h^2}{12}f_{n+1}\right)w_{n+1} - 2\left(1 - \tfrac{5h^2}{12}f_n\right)w_n + \left(1 + \tfrac{h^2}{12}f_{n-1}\right)w_{n-1} \qquad \text{III D-13}$$
$$+ \tfrac{h^2}{12}g_{n+1}\eta_{n+1} + \tfrac{5h^2}{6}g_n\eta_n + \tfrac{h^2}{12}g_{n-1}\eta_{n-1} = 0 \,.$$

Equations III D-12 and III D-13 give a fifth-order system of finite-difference equations as an approximation to equations III D-6 and III D-7.

The boundary conditions must now be put into finite-difference form in order to complete the formulation of the numerical problem. It will, for this purpose, be necessary to expand $\frac{d}{dz}$ numerically at both the upper and lower boundaries.

Using finite-difference operators (see Hildebrand, p. 138) the following relations are found to exist

$$\Delta = \frac{h\partial}{1!} + \frac{h^2\partial^2}{2!} + \frac{h^3\partial^3}{3!} + \cdots \qquad \text{III D-14}$$

$$\nabla = -\frac{h\partial}{1!} + \frac{h^2\partial^2}{2!} - \frac{h^3\partial^3}{3!} + \cdots \qquad \text{III D-15}$$

where

$$\Delta(\ )_n = (\ )_{n+1} - (\ )_n$$
$$\Delta(\ )_n = (\ )_n - (\ )_{n-1}$$
$$\partial(\ )_n = \frac{d(\ )_n}{dz}$$

Using equation III D-14 at $z=0$ $(n=0)$ and equation III D-15 at $z = z_{TOP}$ $(n = N)$, the following expressions are obtained:

$$U_1 - U_0 = hU_0' + \frac{h^2}{2}U_0'' + \mathcal{O}(h^3) \qquad \text{III D-16}$$

$$U_N - U_{N-1} = hU_N' + \frac{h^2}{2}U_N'' + O(h^3) \qquad \text{III D-17}$$

Hence to second-order[1]

$$\left\{ \begin{aligned} \eta_0' &= \frac{1}{h}[\eta_1 - \eta_0] - \frac{h}{2}[-f_0\eta_0 + g_0 w_0] \\ w_0' &= \frac{1}{h}[w_1 - w_0] - \frac{h}{2}[-f_0 w_0 - g_0\eta_0] \end{aligned} \right\} \qquad \text{III D-18}$$

and

$$\left\{ \begin{aligned} \eta_N' &= \frac{1}{h}[\eta_N - \eta_{N-1}] - \frac{h}{2}[-f_N\eta_N + g_N w_N] \\ w_N' &= \frac{1}{h}[w_N - w_{N-1}] - \frac{h}{2}[-f_N w_N - g_N\eta_N] \end{aligned} \right\} \qquad \text{III D-19}$$

The lower boundary condition III D-2 can then be written in finite-difference form as

$$\frac{1}{h}[\eta_1 - \eta_0] - \frac{h}{2}[-f_0\eta_0 + g_0 w_0] - \left(\frac{1}{2} - \frac{\bar{H}}{D_n^m}\right)\eta_0 = 0 \qquad \text{III D-20}$$

$$\frac{1}{h}[w_1 - w_0] - \frac{h}{2}[-f_0 w_0 - g_0\eta_0] - \left(\frac{1}{2} - \frac{\bar{H}}{D_n^m}\right)w_0 = i\frac{\nu\Omega_n^m}{g D_n^m} . \qquad \text{III D-21}$$

The upper boundary condition is handled in a different way. The upper boundary condition is taken to be the requirement that

---

1. In approximating to second-order, the writer has compromised the accuracy in order to keep the boundary conditions near the boundary.

there be no downward energy flux at infinity. In order to treat this condition numerically the stability function above z_{TOP} is assumed to be $\delta = az + b$ (assumption of a thermosphere).

In the last section it was stated that the Newtonian Cooling coefficient was assumed to vanish above z_{TOP} ; thus, the vertical structure equation, above z_{TOP} , becomes

$$\frac{d^2 Y^m_n}{dz^2} + \left[-\tfrac{1}{4} + \gamma^m_n (az + b)\right] Y^m_n = 0 \qquad \text{III D-22}$$

The solution to equation III D-22 is

$$Y^m_n(z) = A\,Ai\left\{-(a\gamma^m_n)^{\frac{1}{3}} z - \frac{(b\gamma^m_n - \frac{1}{4})}{(a\gamma^m_n)^{2/3}}\right\} + B\,Bi\left\{-(a\gamma^m_n)^{\frac{1}{3}} z - \frac{(b\gamma^m_n - \frac{1}{4})}{(a\gamma^m_n)^{2/3}}\right\} \qquad \text{III D-23}$$

where Ai and Bi are the two Airy functions (A and B are complex constants)[1].

Since the radiation condition applies at infinity, it is of interest to look at the asymptotic behavior of $Ai(-x)$ and $Bi(-x)$ as $x \to \infty$. These asymptotic formulae are

$$Ai(-x) \sim \pi^{-\frac{1}{2}} x^{-\frac{1}{4}} \sin\left(\tfrac{2}{3} x^{3/2} + \tfrac{\pi}{4}\right) \qquad \text{III D-24}$$

and

$$Bi(-x) \sim \pi^{-\frac{1}{2}} x^{-\frac{1}{4}} \cos\left(\tfrac{2}{3} x^{3/2} + \tfrac{\pi}{4}\right) \qquad \text{III D-25}$$

1. Airy functions satisfy the equation $U'' = zU$.

From expressions III D-24 and III D-25 it follows that

$$Bi(-x) + i\,Ai(-x) \sim \pi^{-\frac{1}{2}} x^{-\frac{1}{4}} \exp\left[i\left(\frac{2}{3}x^{\frac{3}{2}} + \frac{\pi}{4}\right)\right] \qquad \text{III D-26}$$

The combination $Bi(-x) + i\,Ai(-x)$ is thus seen to lead to downward phase propagation or, since the lunar tidal wave is a gravity wave, upward energy propagation. Therefore,

$$Y_n^m(z) = A\left[i\,Ai\left(-(a\gamma_n^m)^{\frac{1}{3}} z - \frac{(b\gamma_n^m - \frac{1}{4})}{(a\gamma_n^m)^{2/3}}\right) + Bi\left(-(a\gamma_n^m)^{\frac{1}{3}} z - \frac{(b\gamma_n^m - \frac{1}{4})}{(a\gamma_n^m)^{2/3}}\right)\right] \qquad \text{III D-27}$$

above $z = z_{TOP}$.

For the numerical solution it will be assumed that $Y_n^m(z)$ and $\frac{dY_n^m}{dz}$ are continuous across z_{TOP}. Mathematically speaking, these conditions are as follows

$$Y_n^m(z_{TOP}) = A\left[i\,Ai\left(-(a\gamma_n^m)^{\frac{1}{3}} z_{TOP} - \frac{(b\gamma_n^m - \frac{1}{4})}{(a\gamma_n^m)^{2/3}}\right) + Bi\left(-(a\gamma_n^m)^{\frac{1}{3}} z_{TOP} - \frac{(b\gamma_n^m - \frac{1}{4})}{(a\gamma_n^m)^{2/3}}\right)\right] \qquad \text{III D-28}$$

$$\left.\frac{dY^m}{dz}\right|_{z_{TOP}} = -A(a\gamma_n^m)^{\frac{1}{3}}\left[i\,Ai'\left((-a\gamma_n^m)^{\frac{1}{3}} z_{TOP} - \frac{(b\gamma_n^m - \frac{1}{4})}{(a\gamma_n^m)^{2/3}}\right) + Bi'\left((-a\gamma_n^m)^{\frac{1}{3}} z_{TOP} - \frac{(b\gamma_n^m - \frac{1}{4})}{(a\gamma_n^m)^{2/3}}\right)\right] \qquad \text{III D-29}$$

Equation III D-28 can be separated into real and imaginary parts giving <u>two</u> equations. When these two equations are solved for $Re(A)$ and $Im(A)$, equation III D-29 becomes the following two equations:

$$\left.\begin{aligned} \frac{dY_r^{(m,n)}}{dz} &= a_{TOP} Y_r^{(m,n)} + b_{TOP} Y_i^{(m,n)} \\ \frac{dY_i^{(m,n)}}{dz} &= -b_{TOP} Y_r^{(m,n)} + a_{TOP} Y_i^{(m,n)} \end{aligned}\right\} \quad \text{at } z = z_{TOP} \qquad \text{III D-30, III D-31}$$

where

$$a_{TOP} = -(a\gamma_n^m)^{\frac{1}{3}}\left[\frac{Bi(\xi_{TOP})Bi'(\xi_{TOP}) + Ai(\xi_{TOP})Ai'(\xi_{TOP})}{Ai^2(\xi_{TOP}) + Bi^2(\xi_{TOP})}\right] \qquad \text{III D-32}$$

and

$$b_{TOP} = -(a\gamma_n^m)^{\frac{1}{3}}\left[\frac{Ai(\xi_{TOP})Bi'(\xi_{TOP}) - Bi(\xi_{TOP})Ai'(\xi_{TOP})}{Ai^2(\xi_{TOP}) + Bi^2(\xi_{TOP})}\right] \qquad \text{III D-33}$$

(with $\xi_{TOP} = -(a\gamma_n^m)^{\frac{1}{3}} z_{TOP} - \frac{(b\gamma_n^m - \frac{1}{4})}{(a\gamma_n^m)^{2/3}}$).

Equations III D-30 and III D-31 can be put into finite difference form by the use of relations III D-19 giving

$$\frac{1}{h}[w_N - w_{N-1}] - \frac{h}{2}[-f_N w_N + g_N W_N] = a_{TOP} w_N + b_{TOP} W_N \qquad \text{III D-34}$$

and

$$\frac{1}{h}[W_N - W_{N-1}] - \frac{h}{2}[-f_N W_N - g_N f_N] = -b_{TOP} w_N + a_{TOP} W_N \qquad \text{III D-35}$$

The total finite-difference system can be written in matrix form as

$$\bar{\bar{A}}\,\bar{Y} = \bar{B} \qquad \text{III D-36}$$

where

$$\bar{Y} = \begin{pmatrix} \gamma_0 \\ W_0 \\ \gamma_1 \\ W_1 \\ \gamma_2 \\ W_2 \\ \vdots \\ \gamma_{N-2} \\ W_{N-2} \\ \gamma_{N-1} \\ W_{N-1} \\ \gamma_N \\ W_N \end{pmatrix} \qquad \bar{B} = \begin{pmatrix} 0 \\ \frac{\nu \Omega_n^m}{g D_n^m} \\ 0 \\ 0 \\ \vdots \\ 0 \\ 0 \\ 0 \\ 0 \end{pmatrix}$$

and $\bar{\bar{A}}$ is a $(2N+2)\times(2N+2)$ matrix given on the following page.

The set of simultaneous linear equations given by the matrix equation III D-36 is then solved numerically by GELB, an IBM subroutine suitable for solving such matrix equations as III D-36 with a band-structured matrix such as $\bar{\bar{A}}$.

The numerical method derived in this section is shown to be accurate with about 1-2% error. In testing the accuracy, the analytical results of a later section were used to compare the nu-

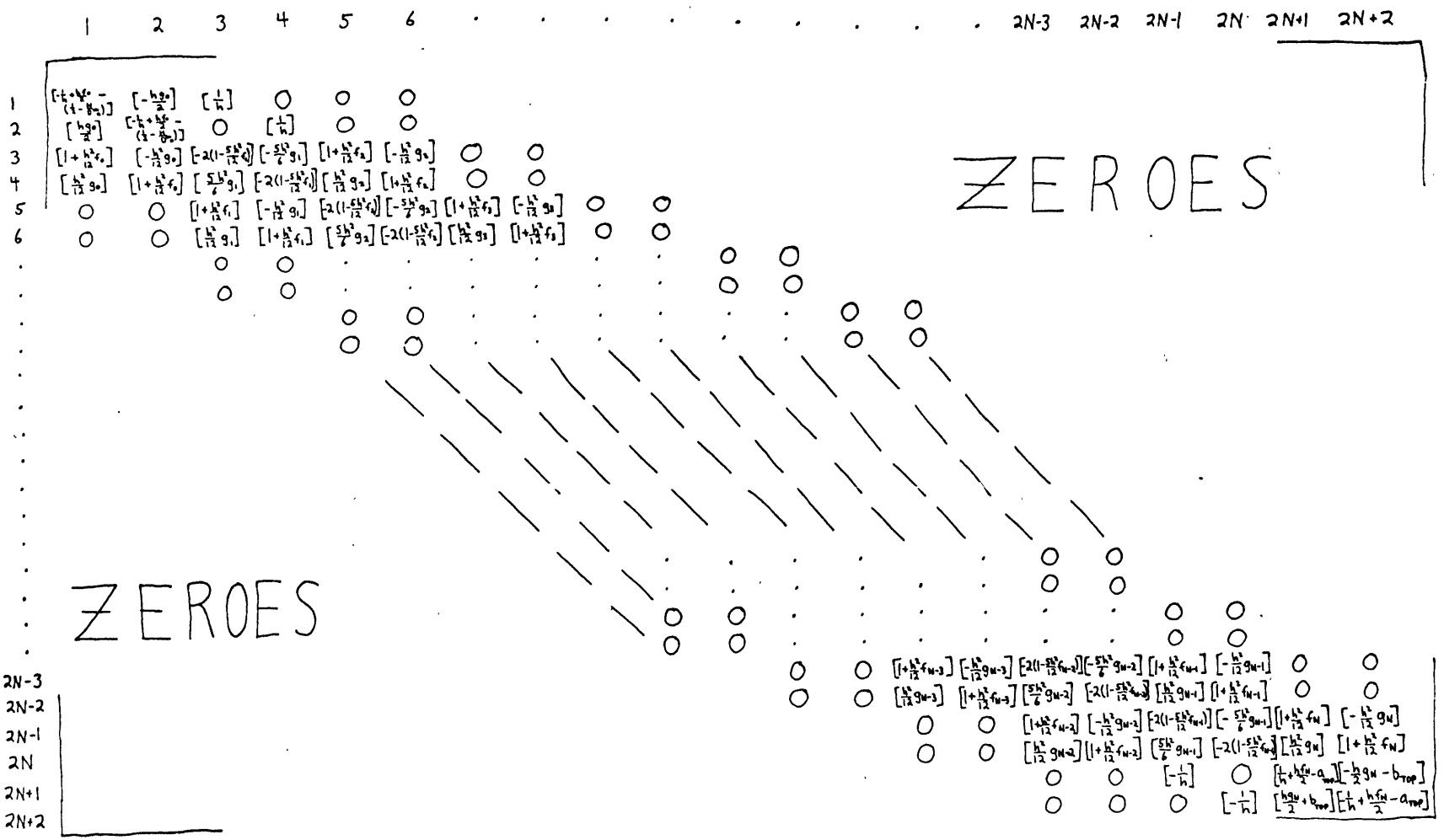
1 2 3 4 5 6 . . . . . 2N-3 2N-2 2N-1 2N 2N+1 2N+2
1
2
3
4
5
6
.
.
.
.
.
.
.
.
.
.
.
.
2N-3
2N-2
2N-1
2N
2N+1
2N+2
ZEROES
ZEROES

merical solution to the analytic solution in the special case of an isothermal atmosphere[1].

---

1. In both this test and actual calculations the following parameters are used: $h = 0.1$, $Z_{TOP} = 14.8$, and $N = 148$.

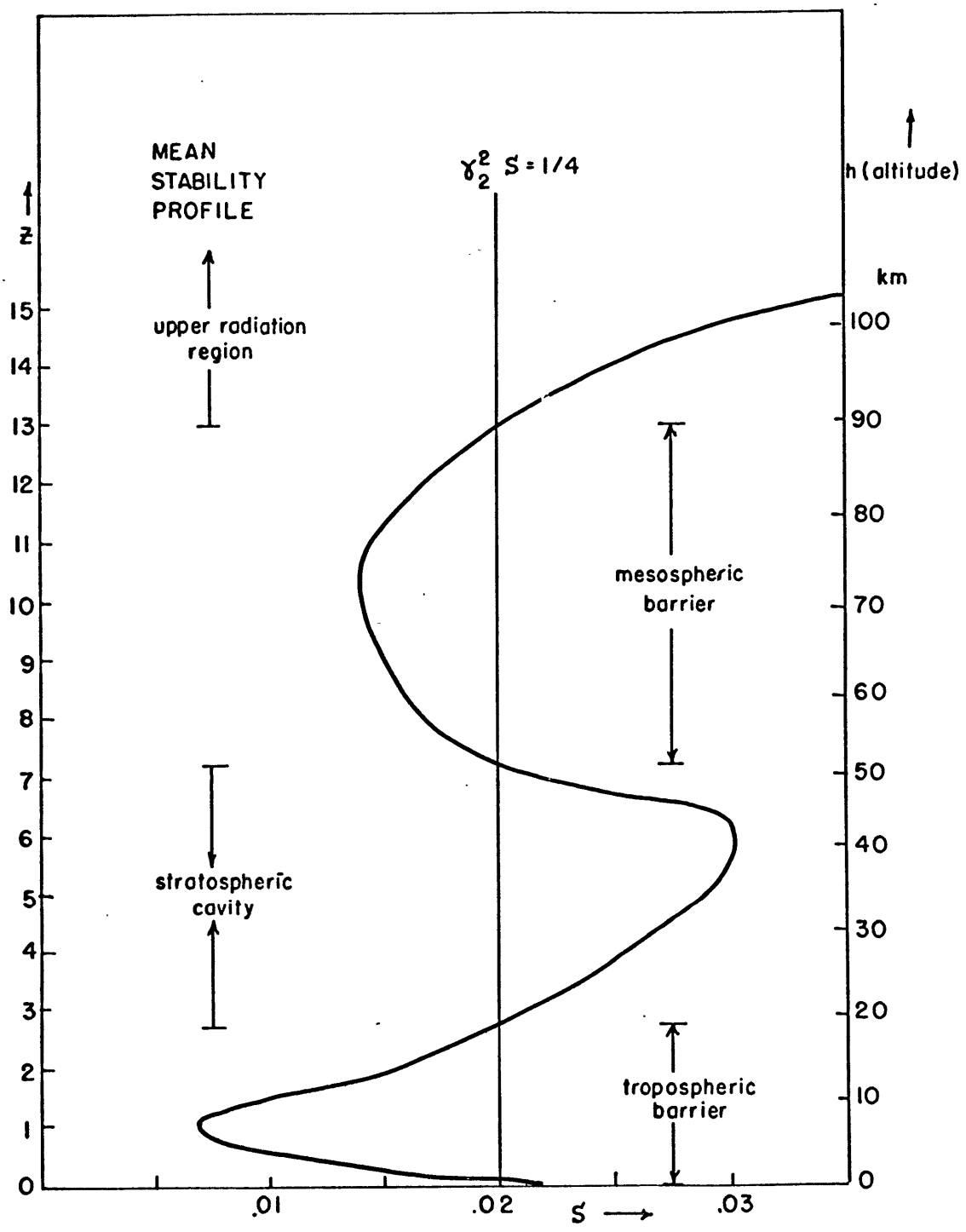

Figure III B-1

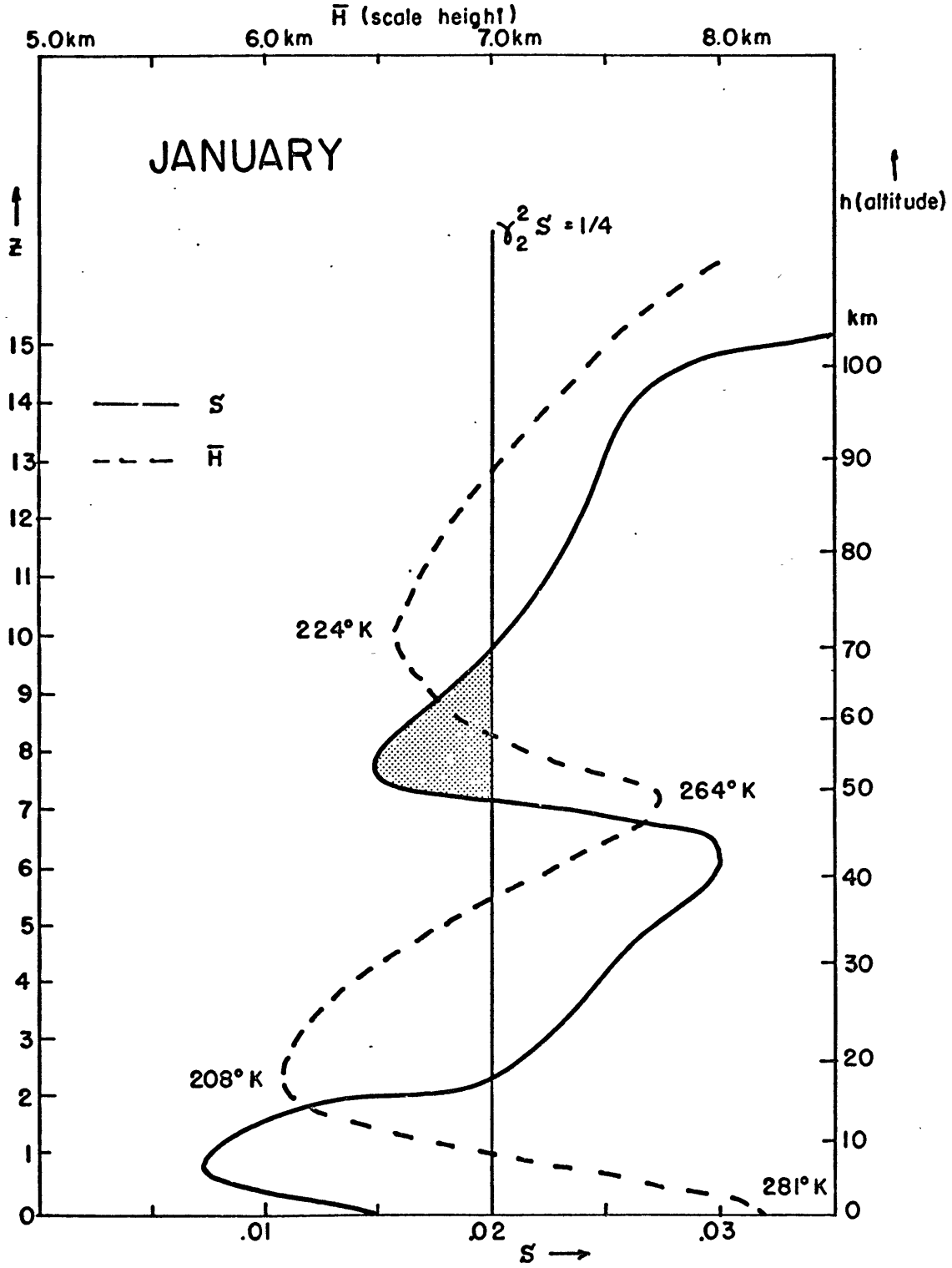

Figure III B-2

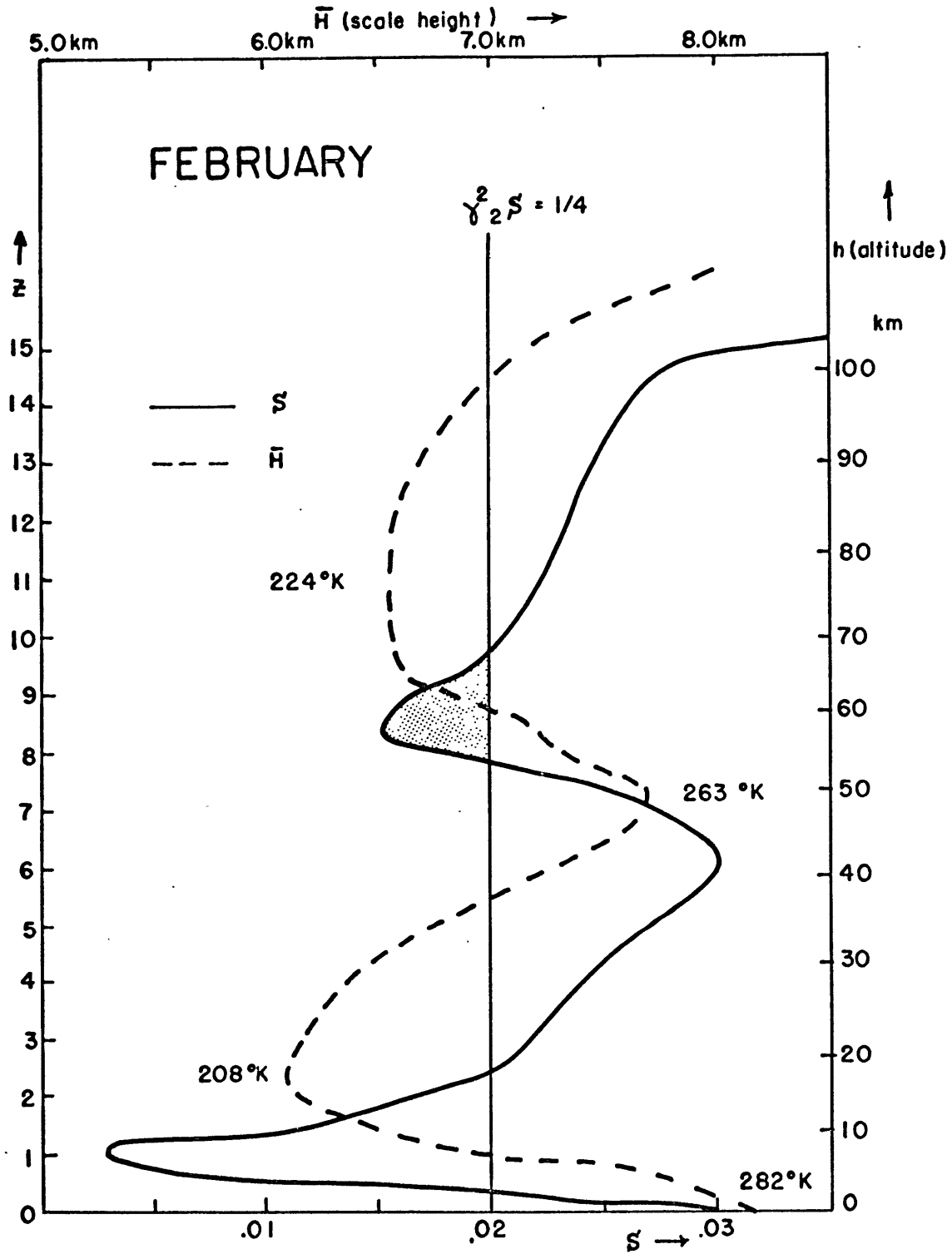

Figure III B-3

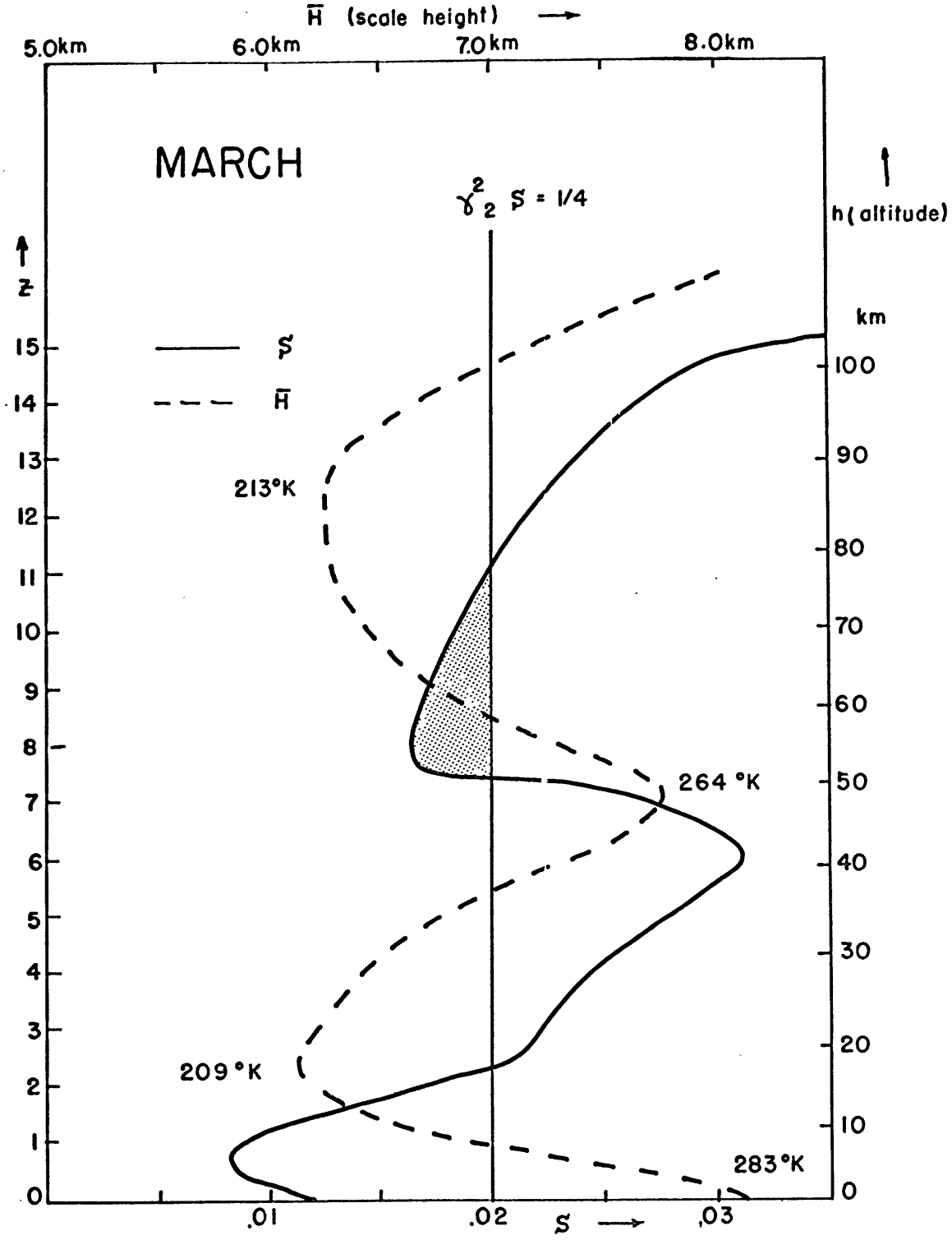

Figure III B-4

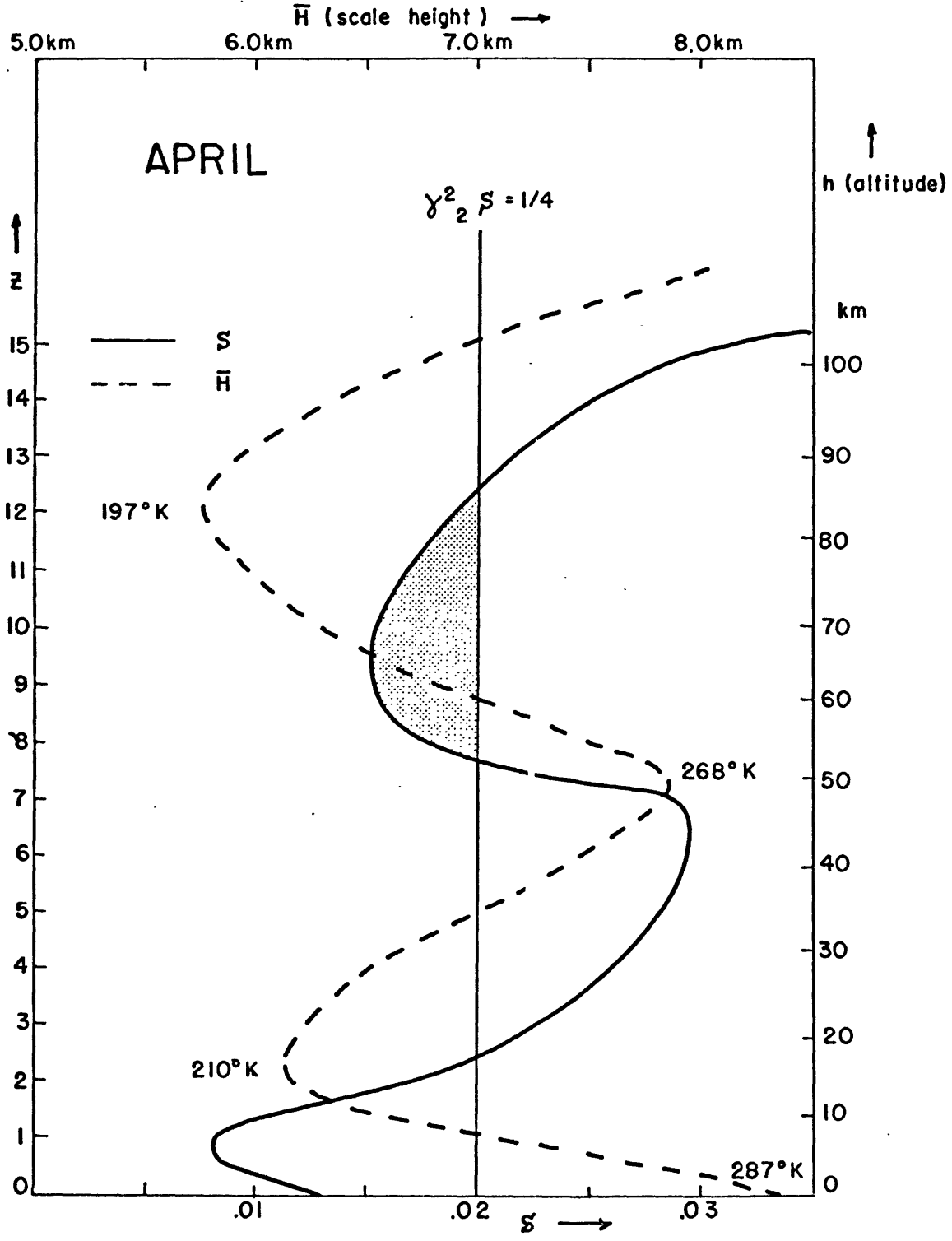

Figure III B-5

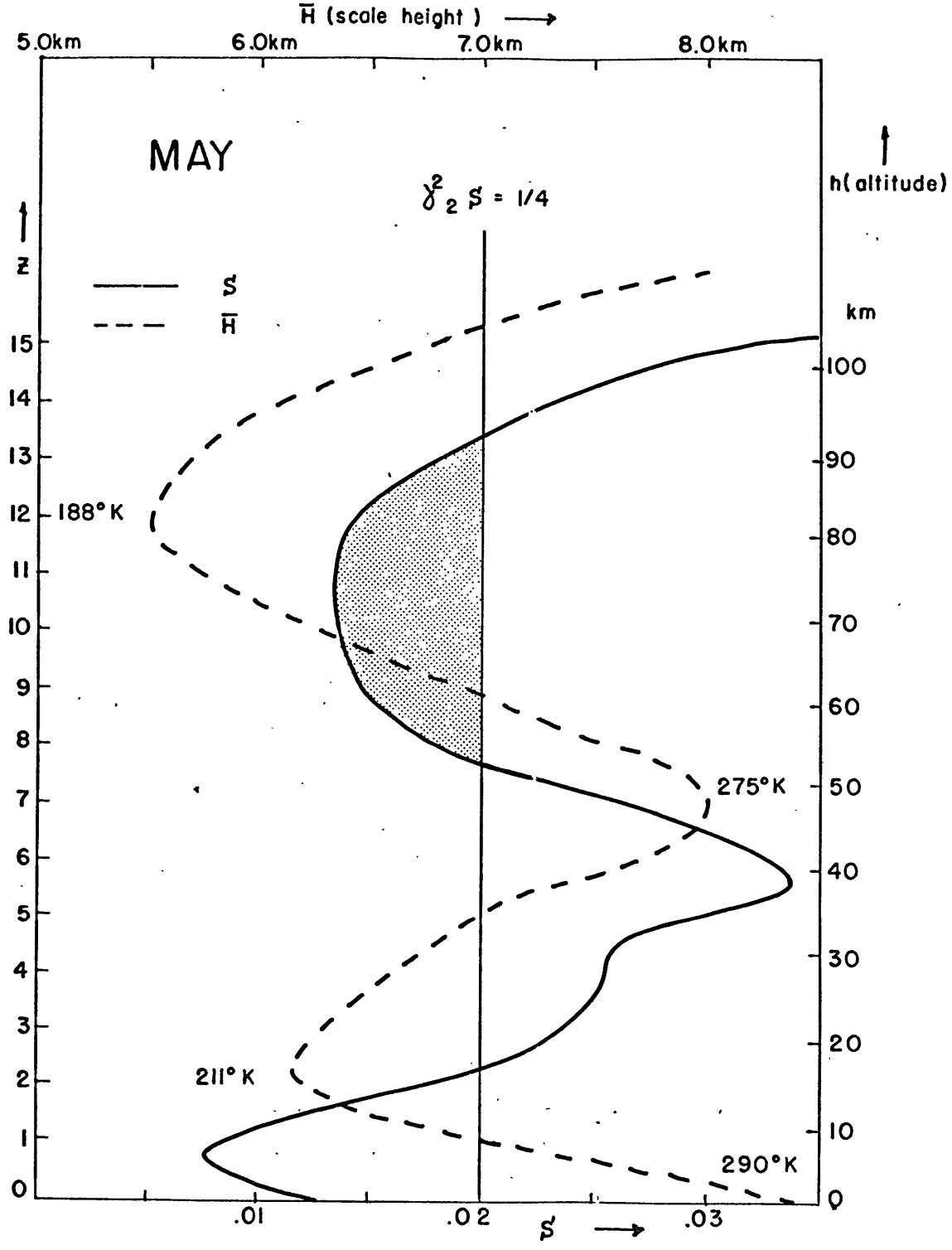

Figure III B-6

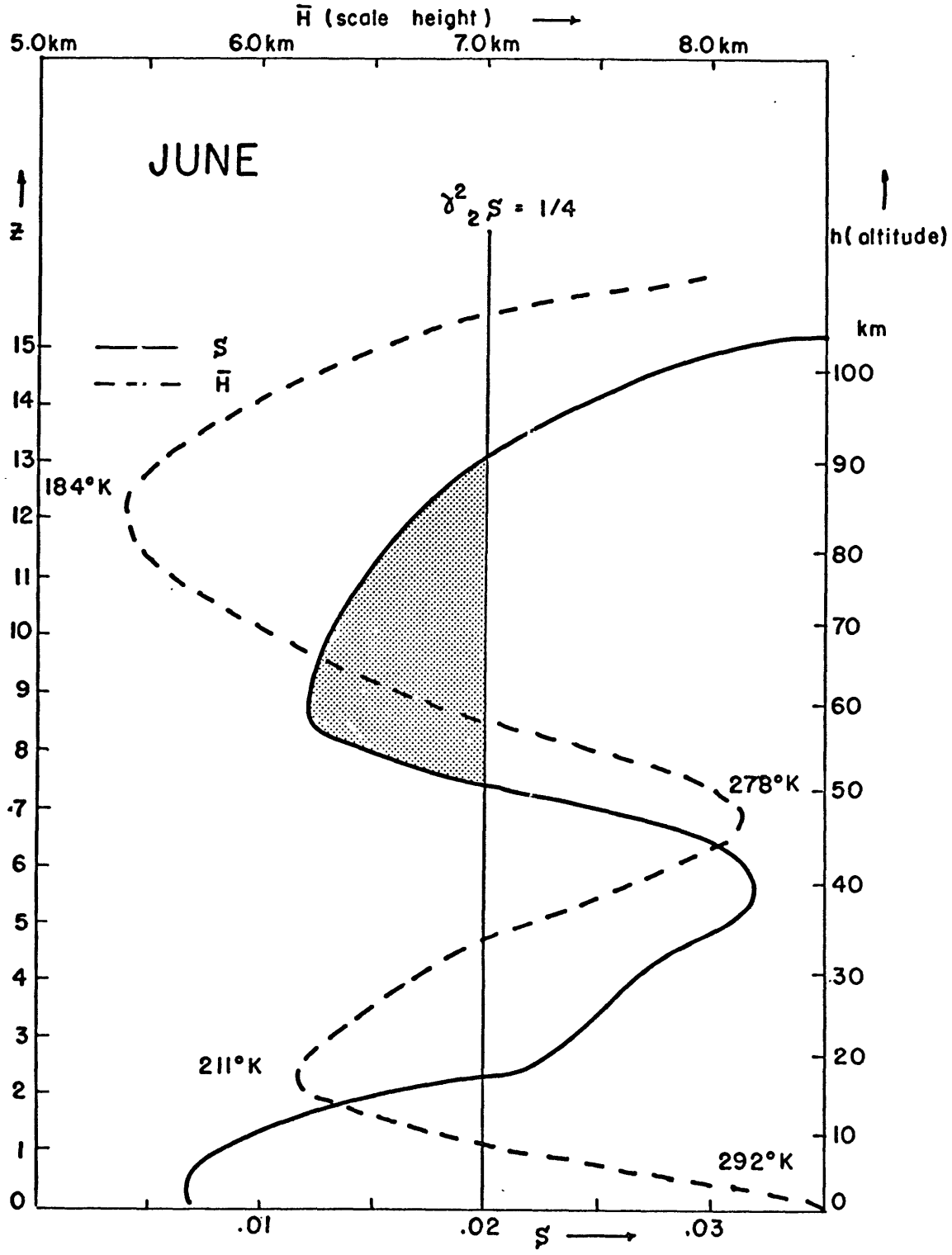

Figure III B-7

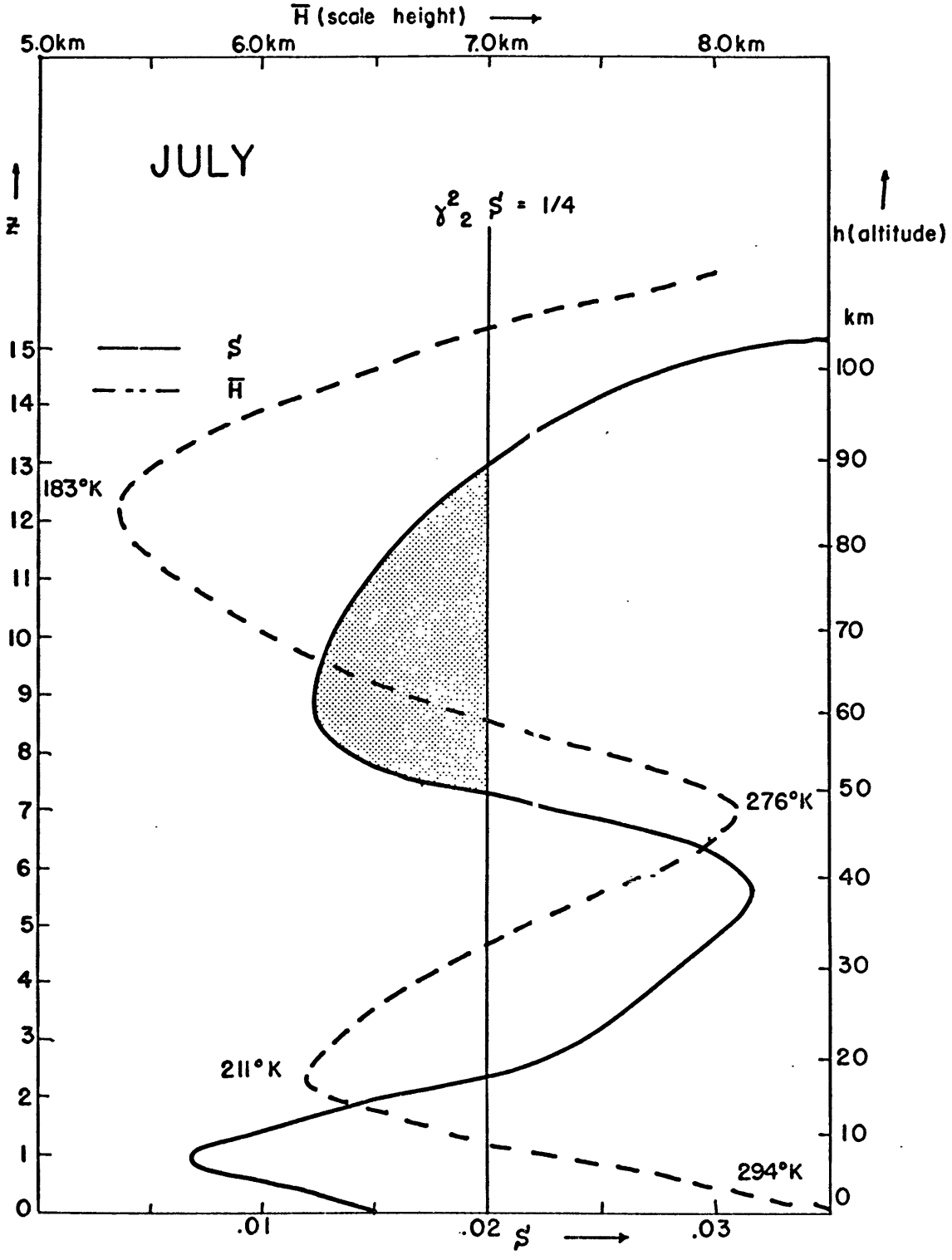

Figure III B-8

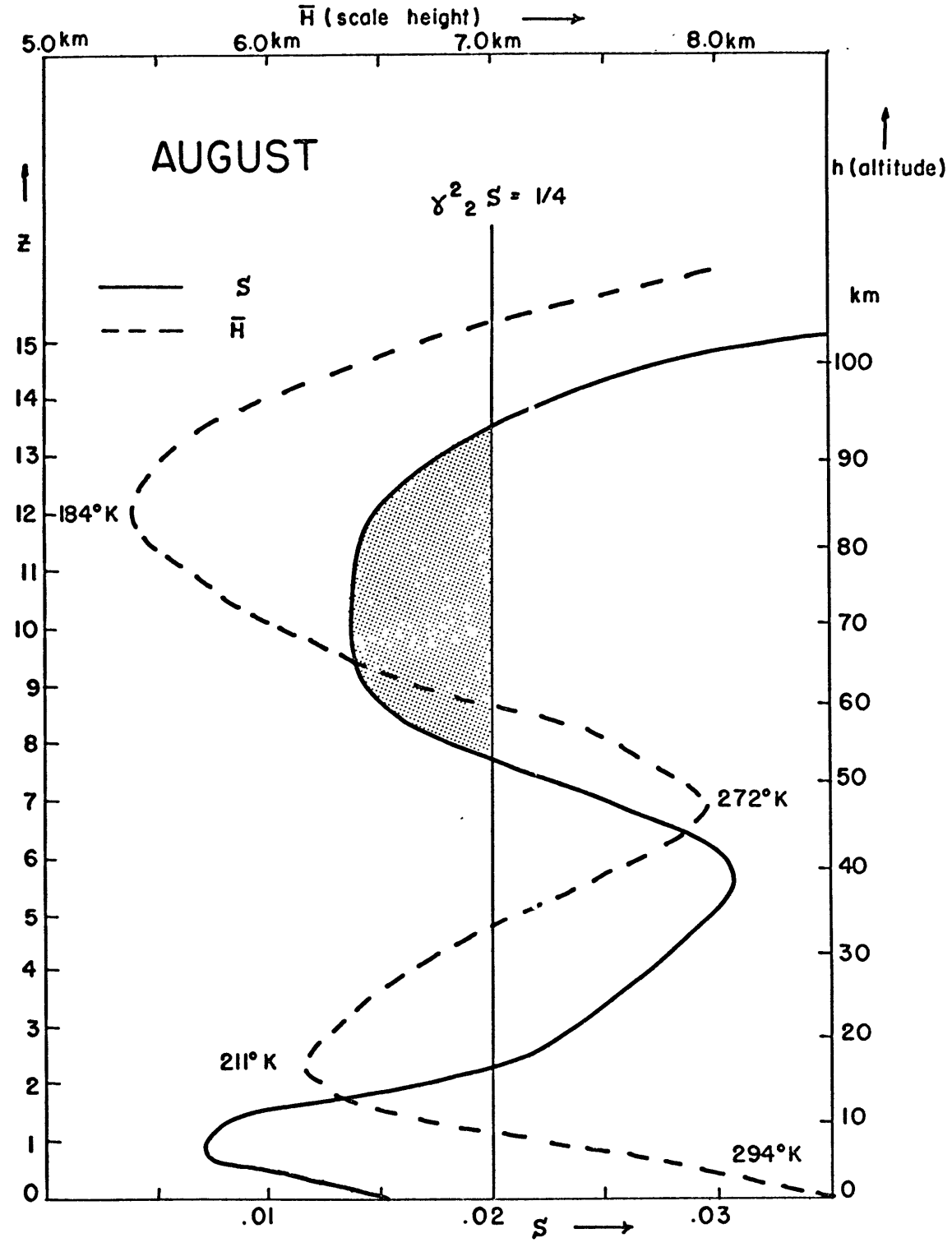

Figure III B-9

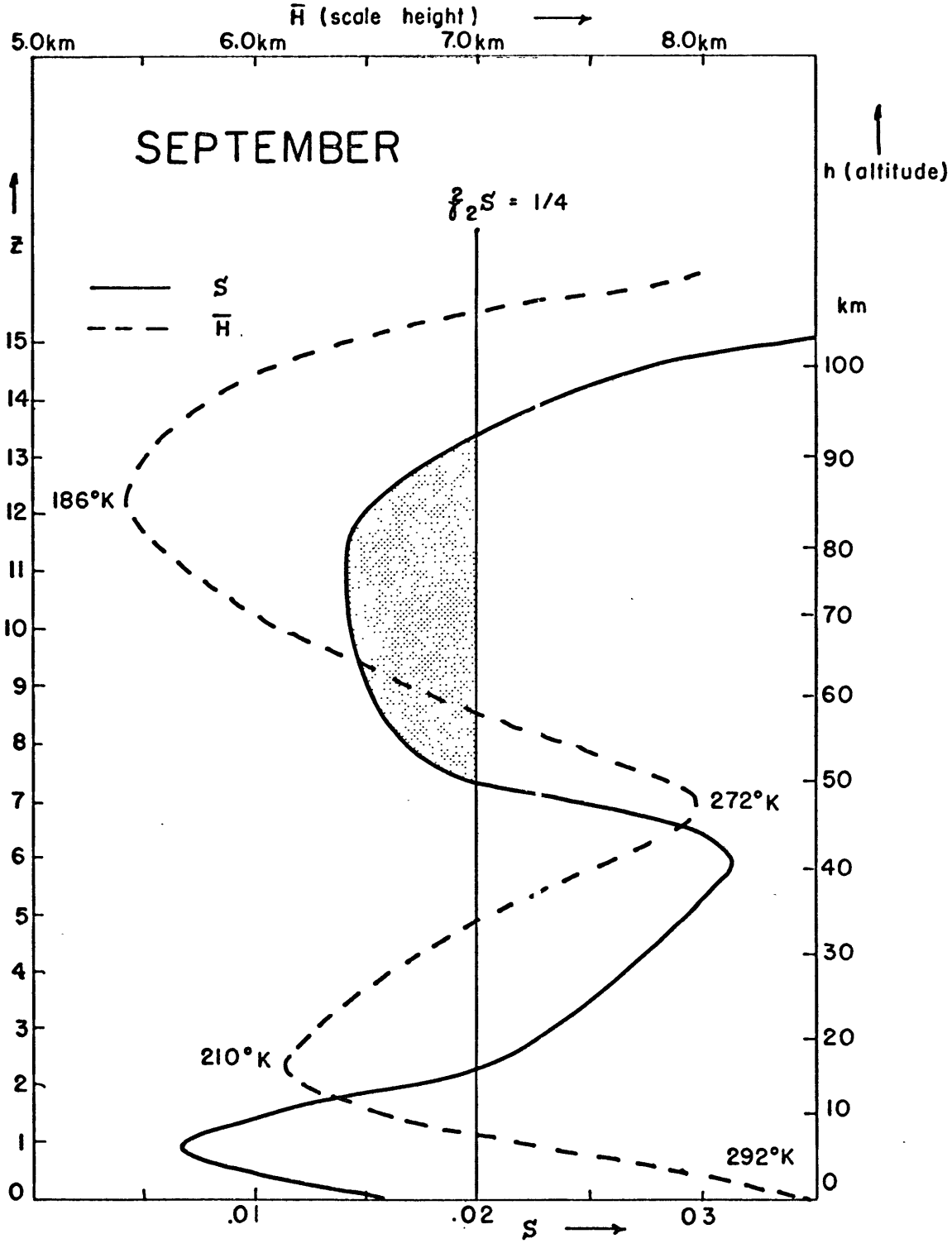

Figure III B-10

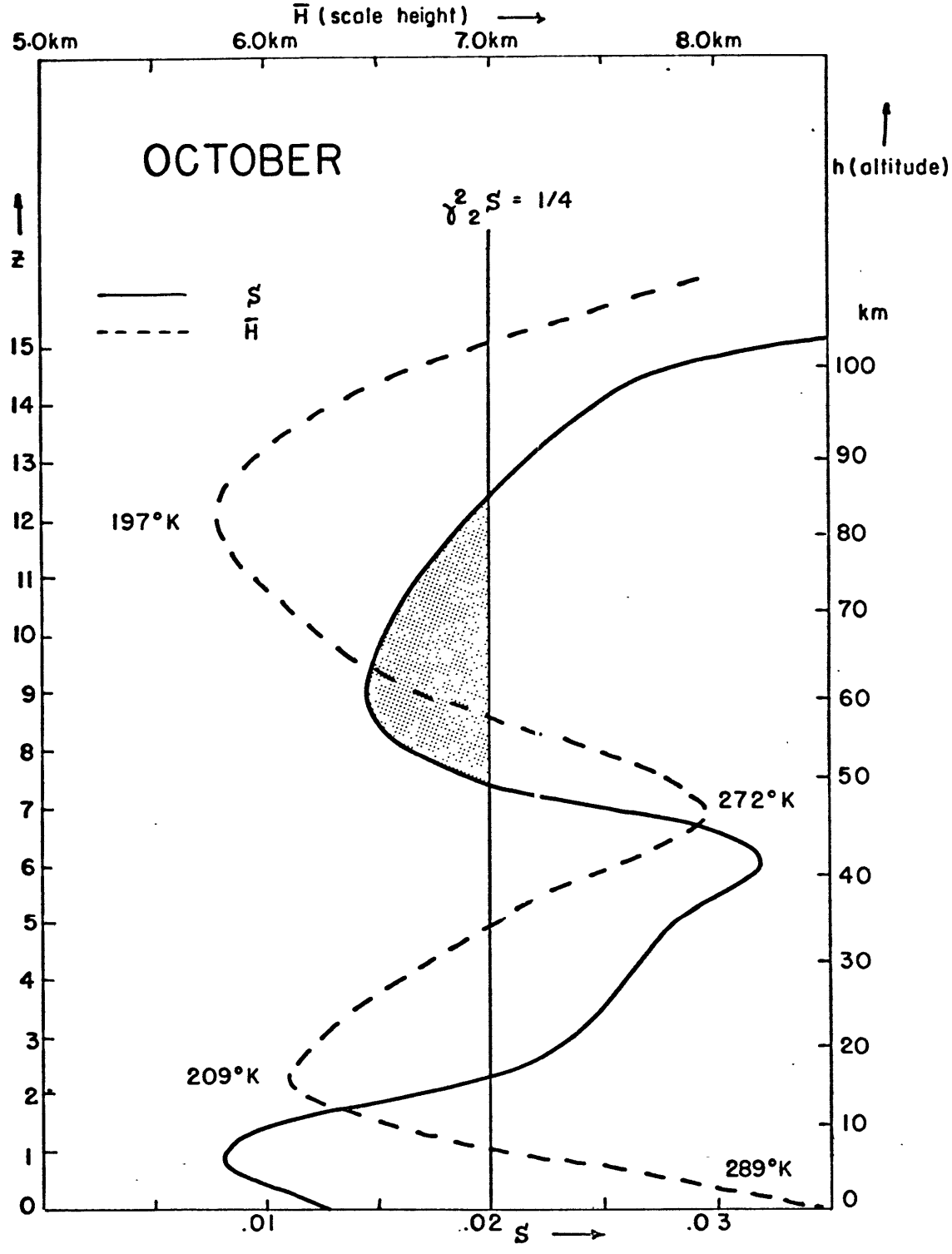

Figure III B-11

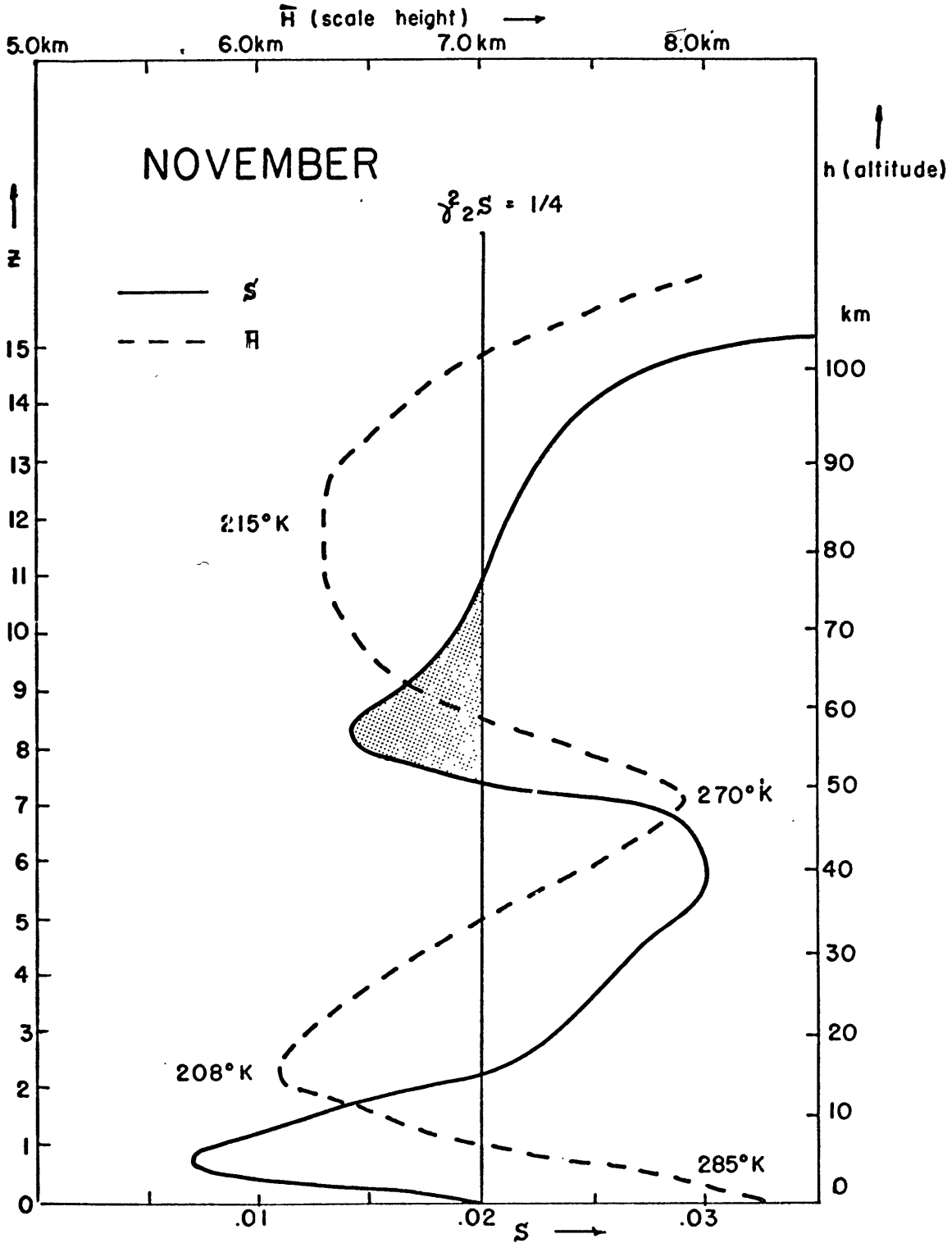

Figure III B-12

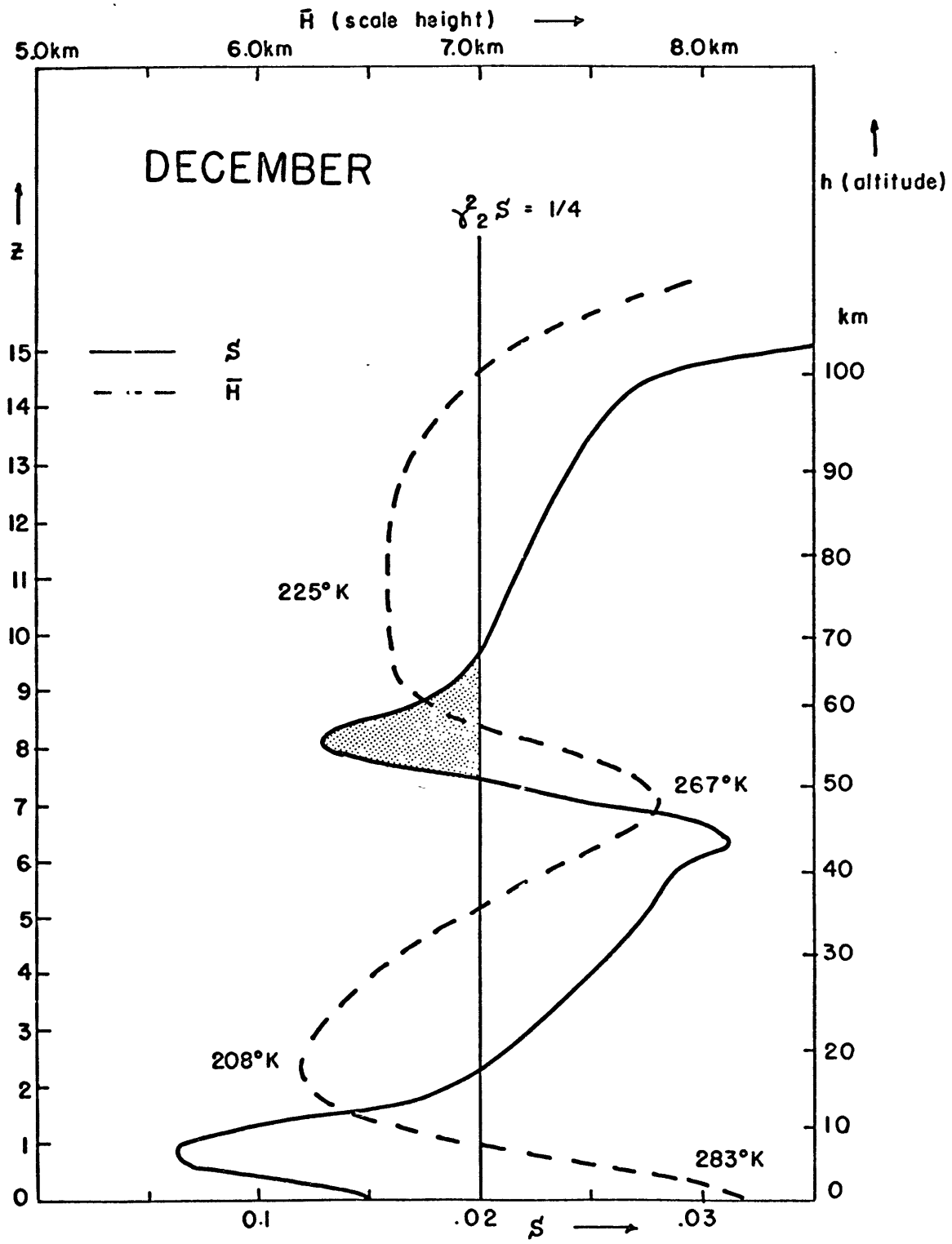

Figure III B-13

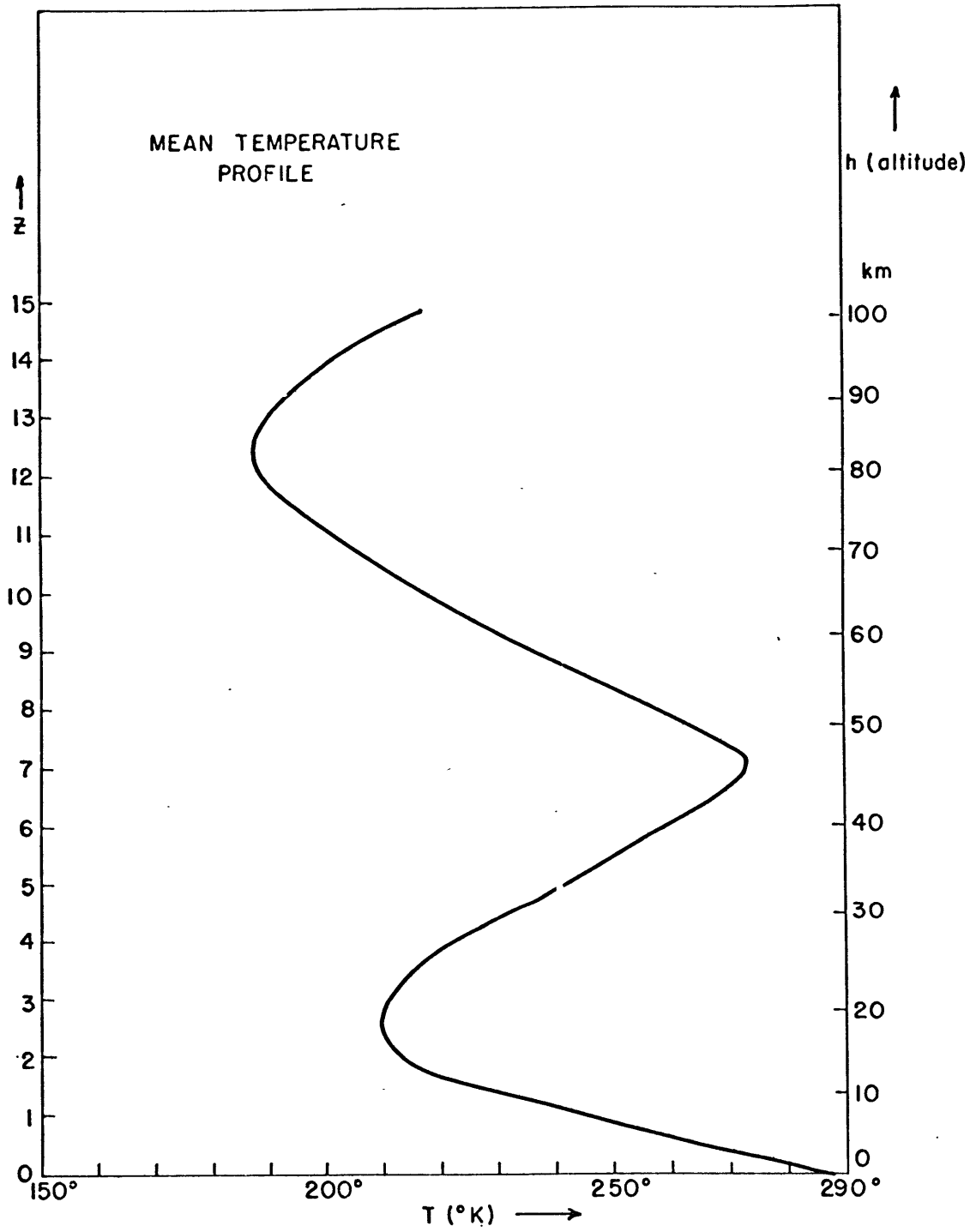

Figure IIIC- 1

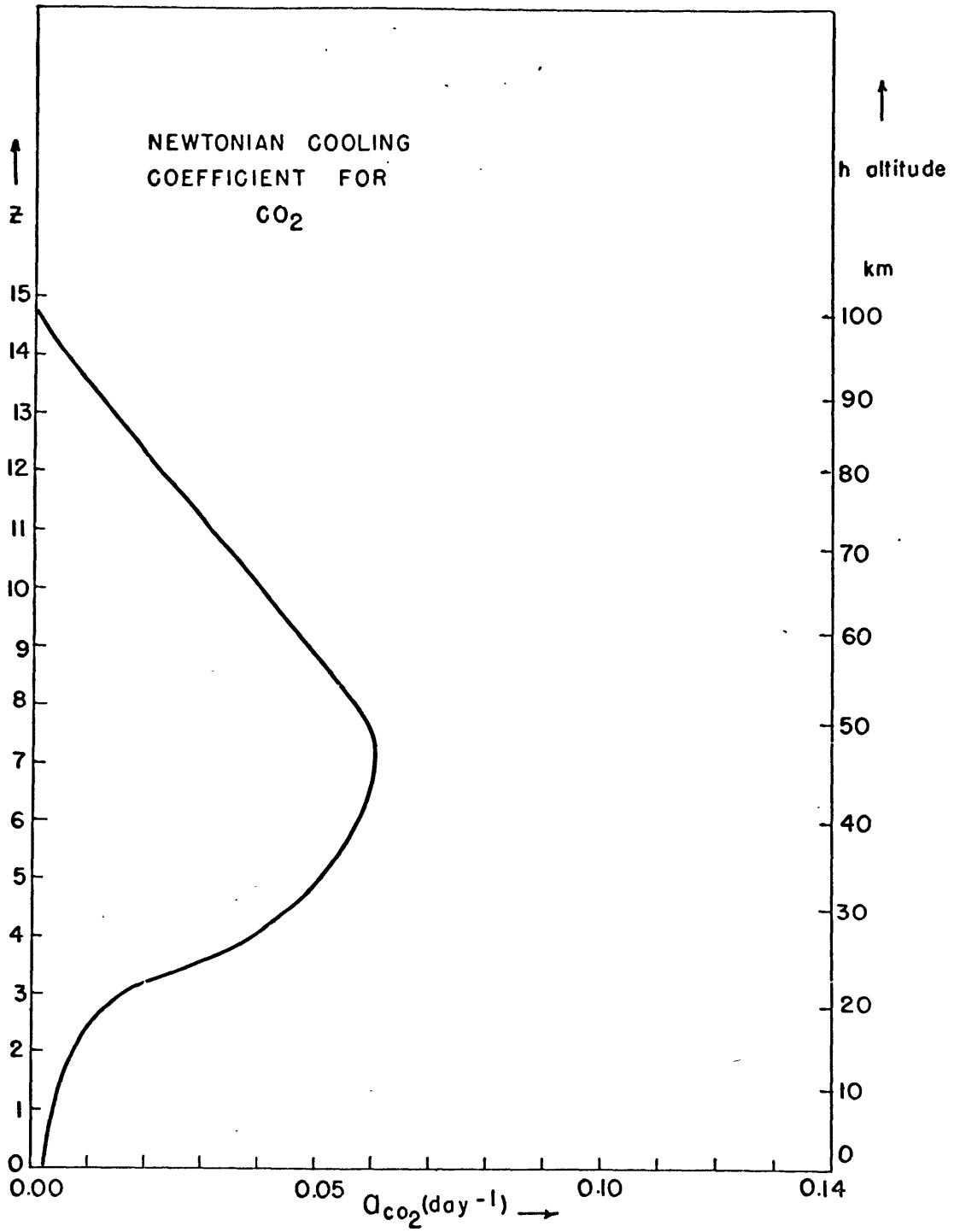

Figure III C- 2

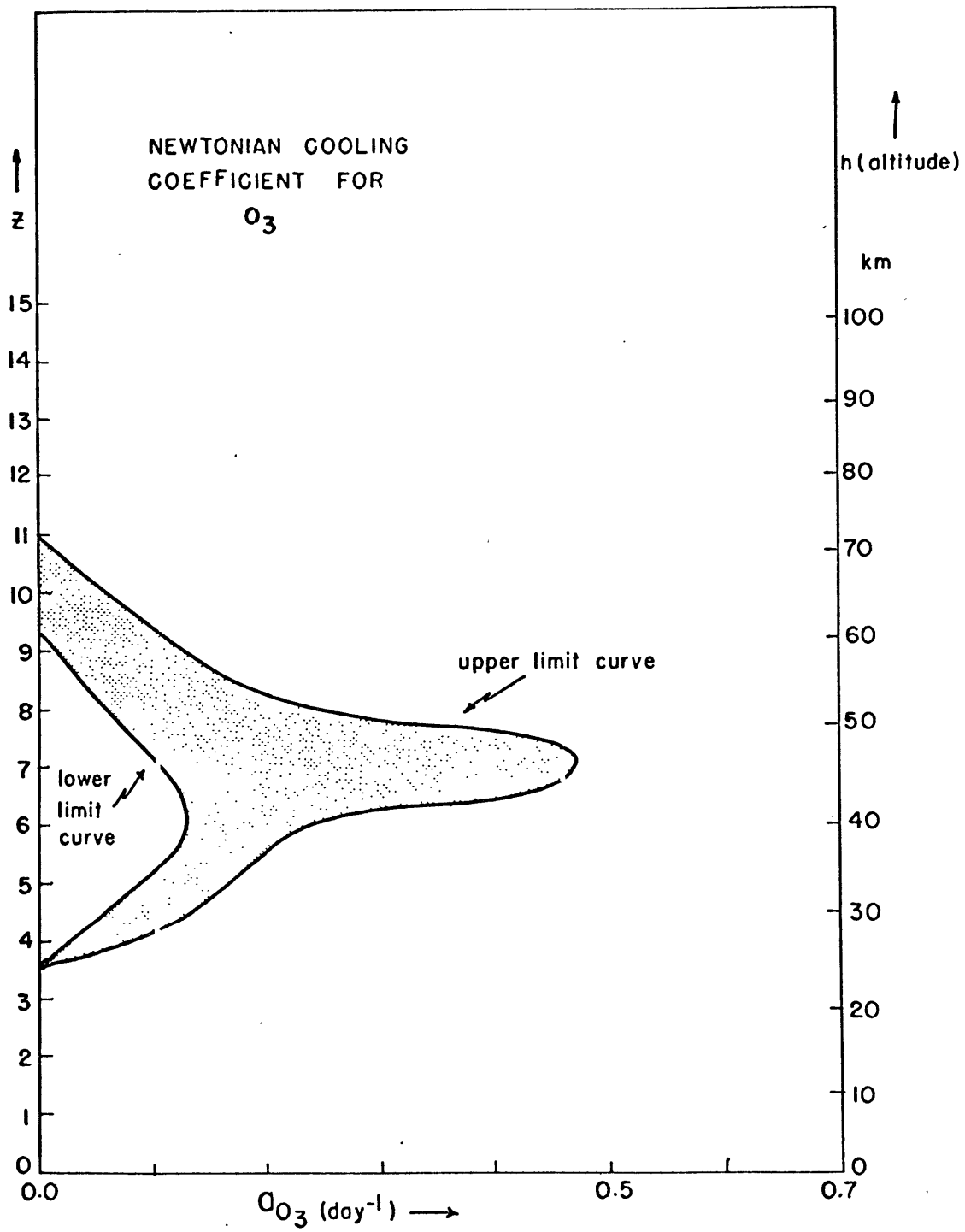

Figure III C- 3

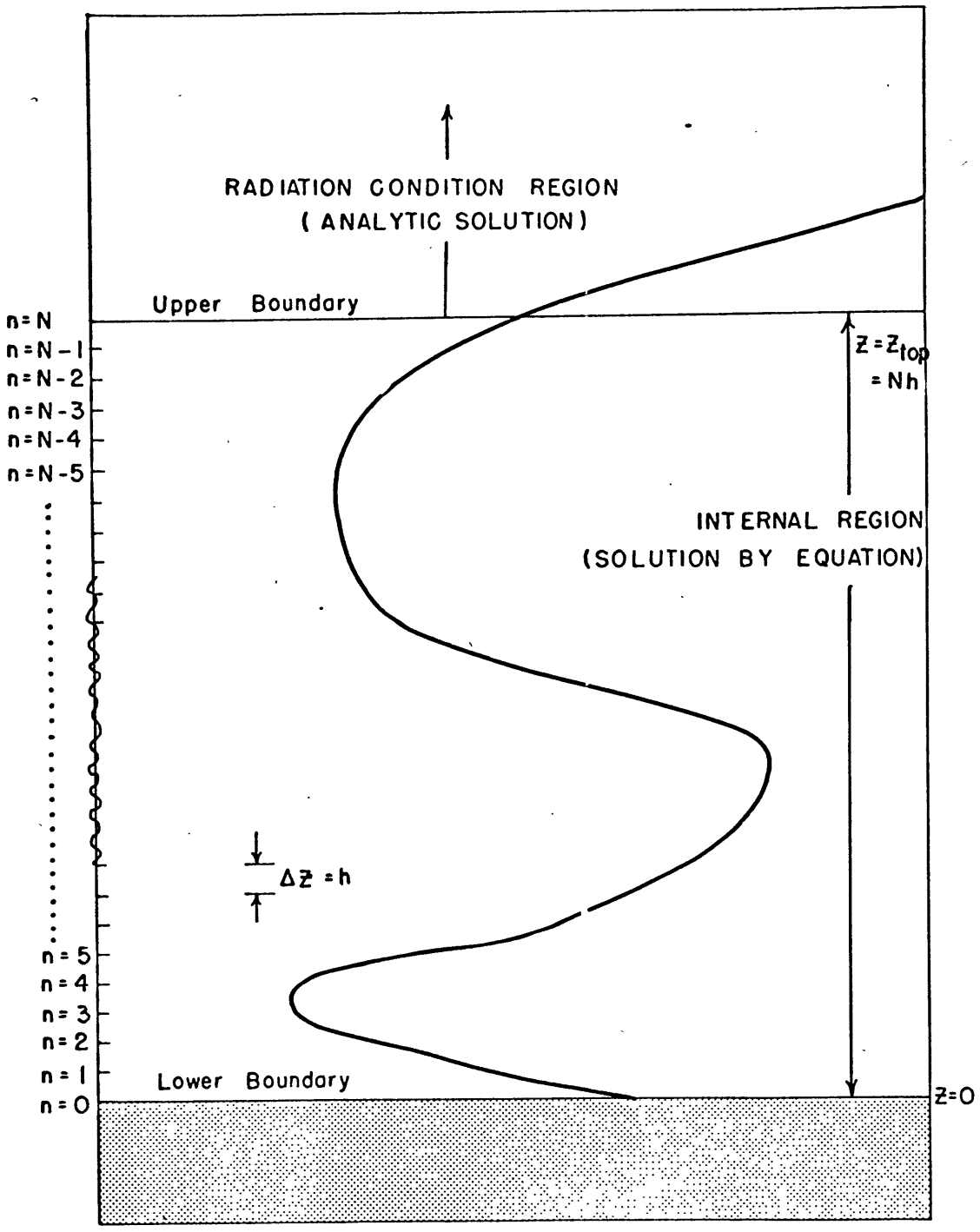

Figure III D-1

CHAPTER IV

RESULTS AND OBSERVATIONAL AGREEMENT

Section A: Results With No Newtonian Cooling

In the previous sections the methods of calculating the lunar tidal response were presented. The inputs for such calculations were shown along with discussions of them. Having done all of this, the results of these computations are given in this chapter.

The first results will be calculations of the lunar tide with no Newtonian Cooling for each of the twelve months. These calculations were carried out for the twelve monthly stability profiles which were presented previously in figures (III B-2) - (III B-13). These stability curves were all analyzed before any calculations had been performed, with a view towards eliminating any bias in the analysis.

Figures (IV A-1) - (IV A-12) show these results. The final variables are presented as being proportional to $\cos[\nu t + 2\lambda + \phi(z)]$. Here $\phi(z)$ is the phase of the variation; that is, the variation reaches maximum at $\frac{\phi(z)}{30^\circ}$ and $\frac{\phi(z)}{30^\circ} + 12$ lunar hours before lunar transit. A negative ϕ will imply a phase lag. Each of the variables is represented by a curve in which the phase ϕ is plotted as a function of z. The amplitudes of the variables at

the equator are also put on the curve at integral values of z . Each of these variables h' , u , v , w , and T' will be discussed separately.

h (geopotential height)

The pressure variation is expressed in geopotential height units for two reasons. First, where equations have been formulated in pressure coordinates it is customary in meteorology to use the geopotential height variable. Second, geopotential height is a more convenient variable for upper atmosphere work. Geopotential height variations may be related to pressure variations as follows:

$$\delta h = \frac{1}{\bar{\rho} g} \delta p$$ for hydrostatic motions.

For instance at the ground $\rho \approx 1.2 \times 10^{-3}$ gm cm^{-3} , so a 1 cm change in geopotential height implies a change of approximately 1.2×10^{-3} mb in pressure. The observed lunar variation in surface pressure at the equator averages about 0.06 mm (.079 mb) which implies a variation in geopotential height of about 66 cm.

The vertical structure of the geopotential variation is given by the solid lines in figures (IV A-1) - (IV A-12). The h -curve, as all of the other curves, shows a positive slope as is required in order that there should be an upward energy flux. This lunar variation in geopotential height varies from tens of centimeters at

the surface to fractions of a kilometer at about 95 km.

The lunar semidiurnal variation in pressure changes appreciably with latitude. This latitudinal dependence is given by the principal lunar semidiurnal Hough function (figure IV A-13), $H^2_2(\varphi)$; thus, by latitude 30° the lunar variation in geopotential height has fallen to less than half of its amplitude at the equator[1].

It is important to note that there is a phase lag in the h -curve at the surface in every month.

U and V (eastward and northward wind)

The eastward wind, U , and the northward wind, V , due to the lunar semidiurnal tide are shown in figures (IV A-1)-(IV B-12) by the dotted line and the dot-dash-dot line respectively. There are no amplitudes next to the V -line, since the northward wind velocity is identically zero at the equator. Note that the phase of the V -curve is always 90° ahead of the U -curve. This can also be seen from the formulae for U and V in section II B.

The eastward wind varies in amplitude from a fraction of a cm sec^{-1} at the surface to some m sec^{-1} at 95 km.

The latitudinal variations of the lunar tidal wind velocities are

1. $H^2_2(\varphi)$ is shown normalized so that $H^2_2(0)=1$.

shown in figures IV A-14 and IV A-15. To obtain the amplitude of U or V, the amplitude of U at the equator is multiplied by the value that is read from these curves.

W (vertical velocity)

The vertical tidal velocity is shown in figures (IV A-1) - (IV A-12) by the dash-dot-dash line. The W -curve does not extend to the surface, since the bottom boundary condition forces W to be identically zero at the surface thus making the phase indeterminate. The W -curve has been arbitrarily cut off at $Z = 1.0$.

The vertical wind velocity varies in amplitude from thousanths of a cm sec^{-1} at the surface to some cm sec^{-1} at 95 km.

The latitudinal variation of this tidal vertical velocity is given by $H_2^2(\varphi)$ which is pictured in figure IV A-13.

T (temperature)

The lunar tidal temperature variation is shown in figures (IV A-1)- IV A-12) by the dashed line. This temperature variation varies from thousanths of a degree Centigrade at the surface to 1-7 degrees Centigrade at around 95 km.

The latitudinal dependence of the lunar tidal temperature variation is given by $H_2^2(\varphi)$ which is pictured in figure IV A-13.

After looking at the results of these calculations of the lunar semidiurnal tide, neglecting the effects of Newtonian Cooling,

these results will now be compared with observations that were cited in Chapter I.

Recalling figure I-4, it was seen that there was a marked annual variation in the phase lag of the surface barometric lunar tide but not in its amplitude. The amplitude of the pressure variation was seen to vary between about .055 mm - .065 mm (or in geopotential height units 61 cm - 72 cm). The phase lag at the equator was seen to vary from about -10^{o} (20 min) in northern hemisphere summer to about -40^{o} (-1 1/3 hrs) in northern hemisphere winter. The annual variations in the amplitudes and phase lags in the calculated lunar tidal variations of geopotential height at $Z = 0$ as read off from figures (IV A-1) - (IV A-12) are shown in figures IV A-16 and IV A-17. In figure IV A-16, there is no apparent organized annual variation of the amplitude even though there is a great scatter of the points from a minimum amplitude of 9.2 cm in May to a maximum amplitude of 49 cm in January. The average amplitude seems to be about 28 cm[1]. The phases in figure IV A-17 do, on the other hand, show an organized seasonal behavior with greater phase lags in winter than in summer, as is observed. The maximum phase lag of -59^{o} ($\approx$ 2 hrs) occurs in February with a minimum phase lag of -4^{o} ($\approx$ 8 min) occurring in

1. The smallness in the calculated amplitudes relative to the observed amplitudes will be explained later.

July. The observed annual variation in the phase lags seems to be explained by the present theory while the calculated amplitude is too small by a factor of about two.

An observation of the lunar tidal variation in temperature at Batavia (7^{o}S, 107^{o}E) was shown in figure I-5. It showed a temperature variation of $.008^{o}$C with a phase lag of about -23^{o} (.75 hrs). The amplitude of the calculated temperature variation varies from a minimum of $.00036^{o}$C in June to a maximum of $.0053^{o}$C in February with the average amplitude being around $.0025^{o}$C. The calculated phase lags lie between -59^{o} ($\approx$ 2 hrs) in February and -4^{o}($\approx$ 8 min) in July. The average phase lag is around -30^{o} ($\approx$ 1 hr). The calculated phase lag is in good agreement with observations while the calculated amplitude is too small by approximately a factor of three.

An observation of the lunar tidal wind variations was shown in figure I-6 at Mauritius (20^{o}S, 55^{o}E). The variation of the eastward wind component showed an amplitude of 1 cm sec^{-1} and phase lag of 230^{o} (7 2/3 hrs) while the variation of the northward wind component had an amplitude 1.2 cm sec^{-1} and phase lag of 90^{o} (3 hrs). The average calculated wind variations, when adjusted to the latitude of Mauritius show amplitudes and phases as follows:

$\overline{u}$ —— amplitude . 5 cm/sec

phase lag -240^{o} (8 hrs)

$\overline{v}$ —— amplitude . 5 cm/sec

phase lag -150^{o} (5 hrs)

There is also a considerable variation in the calculated amplitudes and phase lags from month to month. The average calculated value for the phase lags of the wind observations compare reasonably well with the observations, but once again the amplitudes are too small by a factor of two.

In this section calculations have been presented for the atmospheric response to the lunar gravitational forcing. This is not the only lunar tidal forcing of the atmosphere, though. The oceans move up and down with the lunar semidiurnal period thereby causing an additional forcing. Sawada (1965) investigated the interaction between the lunar tides in the ocean and in the atmosphere. His results indicate that for an ocean covering the entire earth's surface to a depth of 4-5 km, the ocean forcing would cause an atmospheric tide of about the same amplitude as the tide caused directly by the moon's gravitation, while the phase lag would remain unchanged. Since the earth's surface is 71% ocean which, if covering the entire globe, would have a mean depth of about 4 km,

the lunar tide should have about twice the amplitude that was calculated but still have the same phase lag.

The comparison between the theoretical results presented in this section and observations is seen to be quite good when considering the simple model used.

Section B: Results With Newtonian Cooling

In the previous section, it was seen that the calculations which were performed with classical tidal theory gave results that, in many cases, compared quite favorably with observations. The tidal equations were derived, in this study, to include Newtonian Cooling. In this section calculations will be presented for various types of Newtonian Cooling.

Such calculations were performed for all of the monthly temperature profiles, but it would seem redundant to present all of them. Instead the January and July vertical tidal structure is presented along with the monthly values of the geopotential height variation at the surface.

In the previous section it was seen that the calculations with no Newtonian Cooling gave a surface geopotential height variation with amplitudes ranging from 9.2 cm in May to 49 cm in January and phase lags ranging between -59^{o} in February to -4^{o} in July.

The surface geopotential height tidal variations with CO_2 cooling, with CO_2 and small O_3 cooling, and with CO_2 and large O_3 cooling are pictured in figures (IV B-1) - (IV B-3) respectively.

The calculations of the tidal variation of geopotential height at the surface, including CO_2 cooling (figure IV B-1), show amplitudes ranging from 14 cm in May to 53 cm in February and phase lags ranging between -59^o in May to -4^o in July. The same calculation performed with CO_2 and small O_3 cooling (figure IV B-2) gives amplitudes between 24 cm in May and June and 56 cm in February with phase lags between -61^o in May and -15^o in July. The calculations with CO_2 and large O_3 cooling (figure IV B-3) gives amplitudes from 31 cm in June to 65 cm in February with phase lags from -58^o in May to -21^o in July.

The effects of increasing the Newtonian Cooling is to decrease the seasonal differences in the amplitude and phase of the surface pressure tidal variation (both in absolute difference and ratio) while both the amplitudes and phase lags are generally increased.

The seasonal variation in phase lag in figure IV A-17 (no Newtonian Cooling) becomes more obscure with increased Newtonian Cooling while a seasonal variation in amplitude becomes evident with increased Newtonian Cooling (counter to observations).

The vertical structure of the January lunar tide with CO_2

cooling, CO_2 and small O_3 cooling, and CO_2 and large O_3 cooling are shown in figures (IV B-4) - (IV B-6) respectively while the corresponding calculations for July are presented in figures (IV B-7) - (IV B-9).

Figures (IV B-4) - (IV B-9) generally show increased amplitudes with increased Newtonian Cooling at lower altitudes while the amplitudes decrease at higher altitudes. The slopes of the curves also tend to increase with added Newtonian Cooling. The vertical structures, however, do seem qualitatively similar to the results with no Newtonian Cooling.

These Newtonian Cooling calculations are subject to question on at least two grounds. The first is that monthly calculations are being performed with annual Newtonian Cooling profiles. This is certainly not a desirable situation, especially when interested in the seasonal variations of such calculations. This situation is very difficult to remedy at present since ozone observations are poorly known at higher levels (above 30 km), much less the seasonal variation in ozone concentrations at these levels. The seasonal variation in the CO_2 cooling coefficient could have been included but, since there was no hope of treating the variations of ozone, it was not.

The second aspect to be questioned is whether the classical

ozone photochemistry is correct. Hunt (1966a, 1966b) has brought up this question and suggested that the photochemistry of ozone in the upper atmosphere is controlled by a different set of reactions than heretofore had been supposed. Hunt's reactions are not strongly dependent on temperature considerations so that the Newtonian Cooling due to ozone might be significantly smaller than that used in the present investigation.

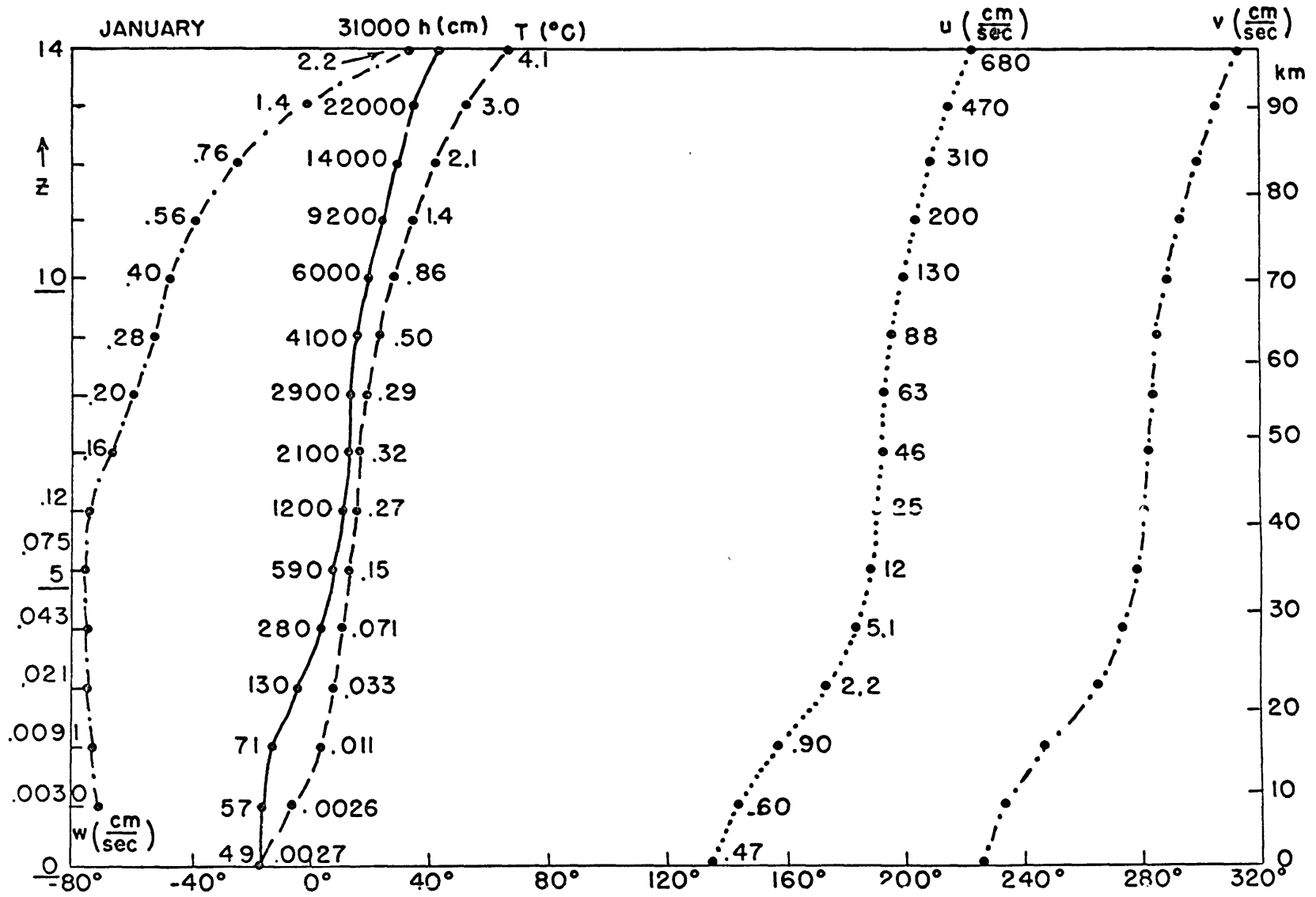
JANUARY
31000 h (cm)
T (°C)
u (cm/sec)
v (cm/sec)
z
km
w (cm/sec)
14
10
5
1
0
.12
.075
.043
.021
.009
.003
2.2
1.4
22000
14000
9200
6000
4100
2900
2100
1200
590
280
130
71
57
49
4.1
3.0
2.1
1.4
.86
.50
.29
.32
.27
.15
.071
.033
.011
.0026
.0027
.76
.56
.40
.28
.20
.16
680
470
310
200
130
88
63
46
25
12
5.1
2.2
.90
.60
.47
90
80
70
60
50
40
30
20
10
0
-80°
-40°
0°
40°
80°
120°
160°
200°
240°
280°
320°

Figure IV A-1

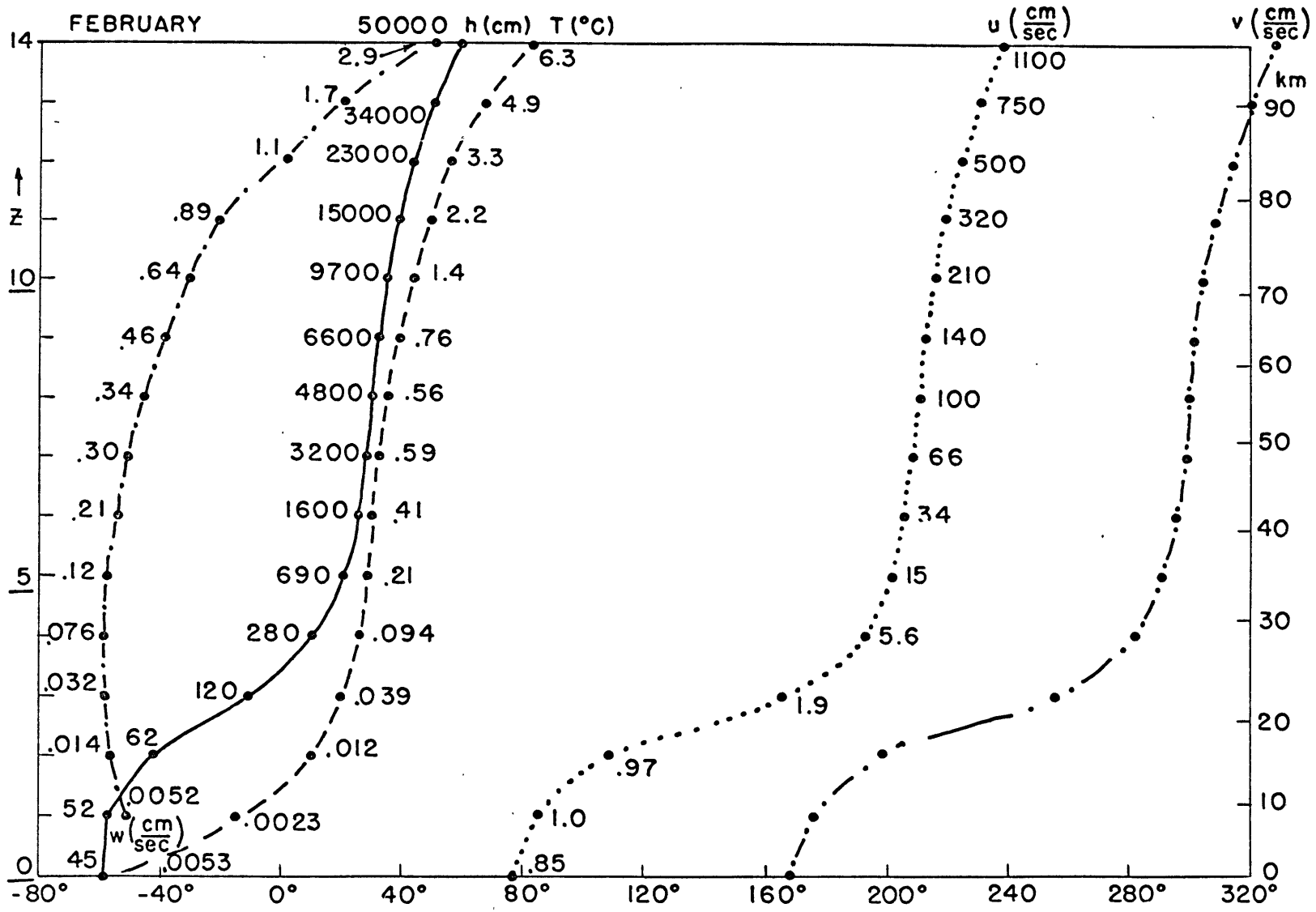
FEBRUARY
50000 h(cm) T(°C)
u (cm/sec)
v (cm/sec)
km
z
w (cm/sec)
14
10
5
0
90
80
70
60
50
40
30
20
10
0
-80°
-40°
0°
40°
80°
120°
160°
200°
240
280°
320°
2.9
1.7
1.1
.89
.64
.46
.34
.30
.21
.12
.076
.032
.014
52
45
34000
23000
15000
9700
6600
4800
3200
1600
690
280
120
62
.0052
.0053
6.3
4.9
3.3
2.2
1.4
.76
.56
.59
.41
.21
.094
.039
.012
.0023
1100
750
500
320
210
140
100
66
34
15
5.6
1.9
.97
1.0
.85

Figure IV A-2

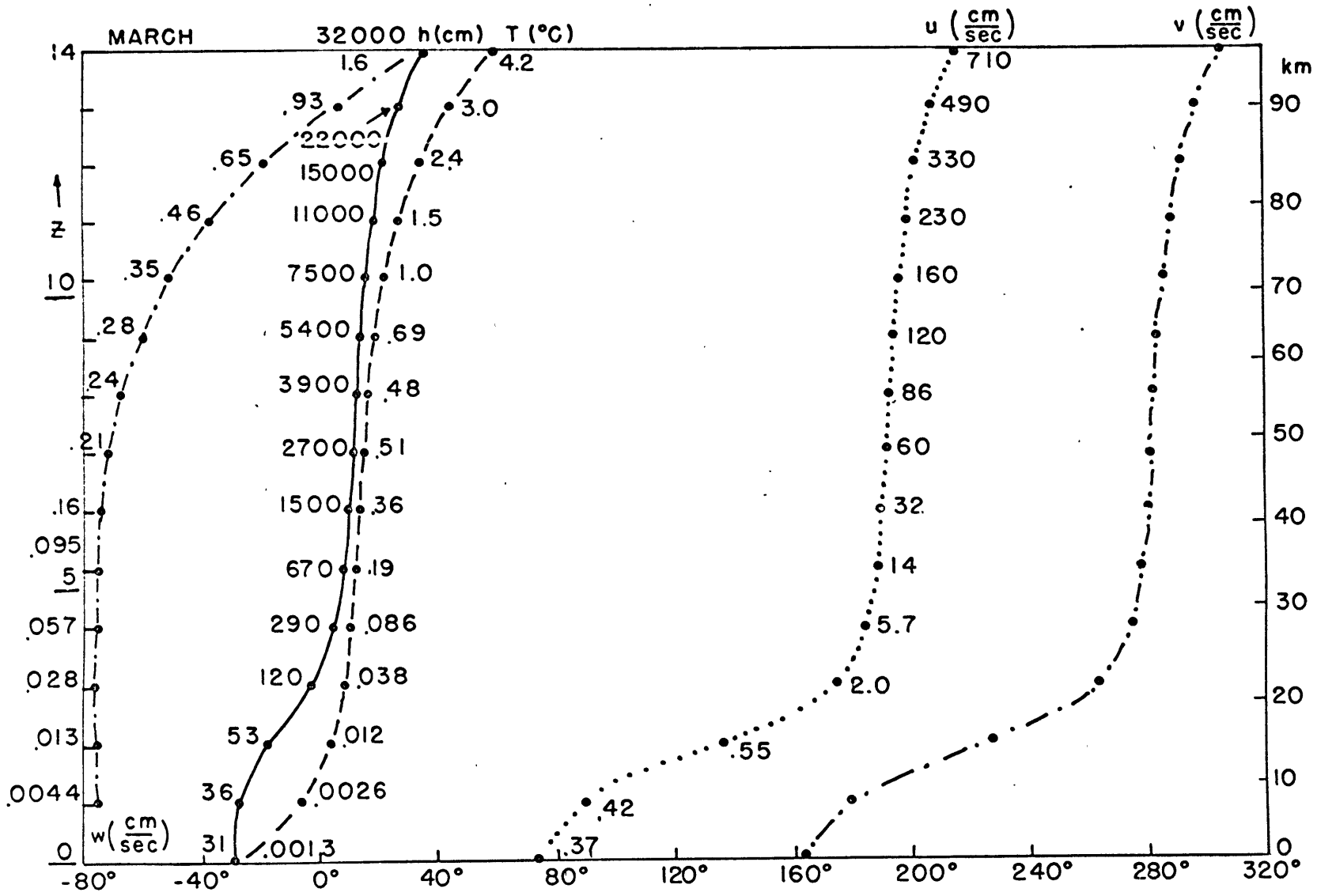
MARCH
32000 h(cm)
T (°C)
u (cm/sec)
v (cm/sec)
km
z
w (cm/sec)
14
10
5
0
1.6
.93
22000
.65
15000
.46
11000
.35
7500
.28
5400
.24
3900
.21
2700
.16
1500
.095
670
.057
290
.028
120
.013
53
.0044
36
31
4.2
3.0
2.4
1.5
1.0
.69
.48
.51
.36
.19
.086
.038
.012
.0026
.0013
710
490
330
230
160
120
86
60
32
14
5.7
2.0
.55
.42
.37
90
80
70
60
50
40
30
20
10
0
-80°
-40°
0°
40°
80°
120°
160°
200°
240°
280°
320°

Figure IV A-3

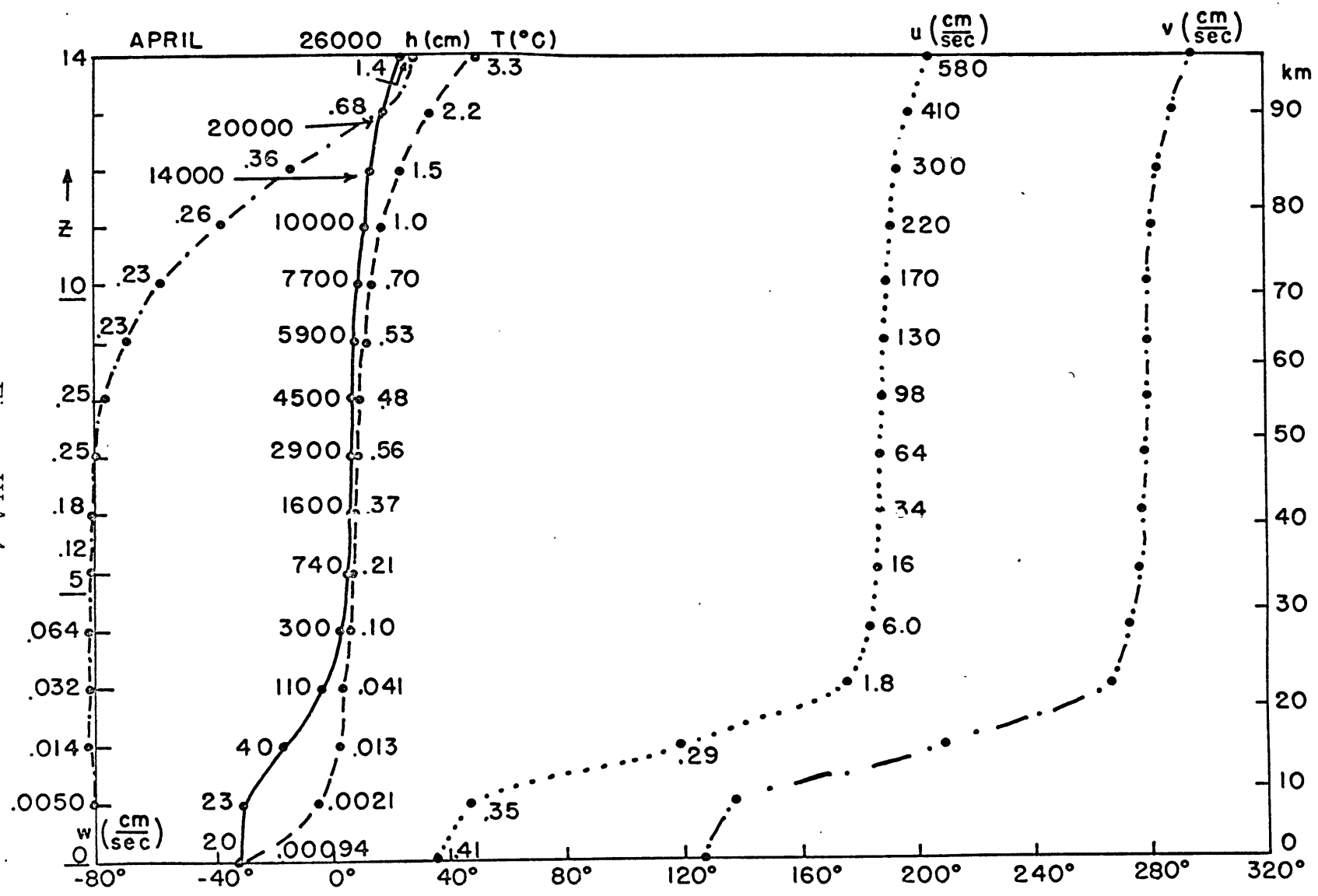
APRIL
26000
h (cm)
T (°C)
u (cm/sec)
v (cm/sec)
km
z
w (cm/sec)
1.4
3.3
.68
2.2
20000
.36
14000
1.5
.26
10000
1.0
.23
7700
.70
.23
5900
.53
4500
.48
2900
.56
1600
.37
740
.21
300
.10
110
.041
40
.013
23
.0021
20
.00094
.41
.35
.29
580
410
300
220
170
130
98
64
34
16
6.0
1.8
14
10
.25
.25
.18
.12
5
.064
.032
.014
.0050
0
90
80
70
60
50
40
30
20
10
0
-80°
-40°
0°
40°
80°
120°
160°
200°
240°
280°
320°

Figure IV A-4

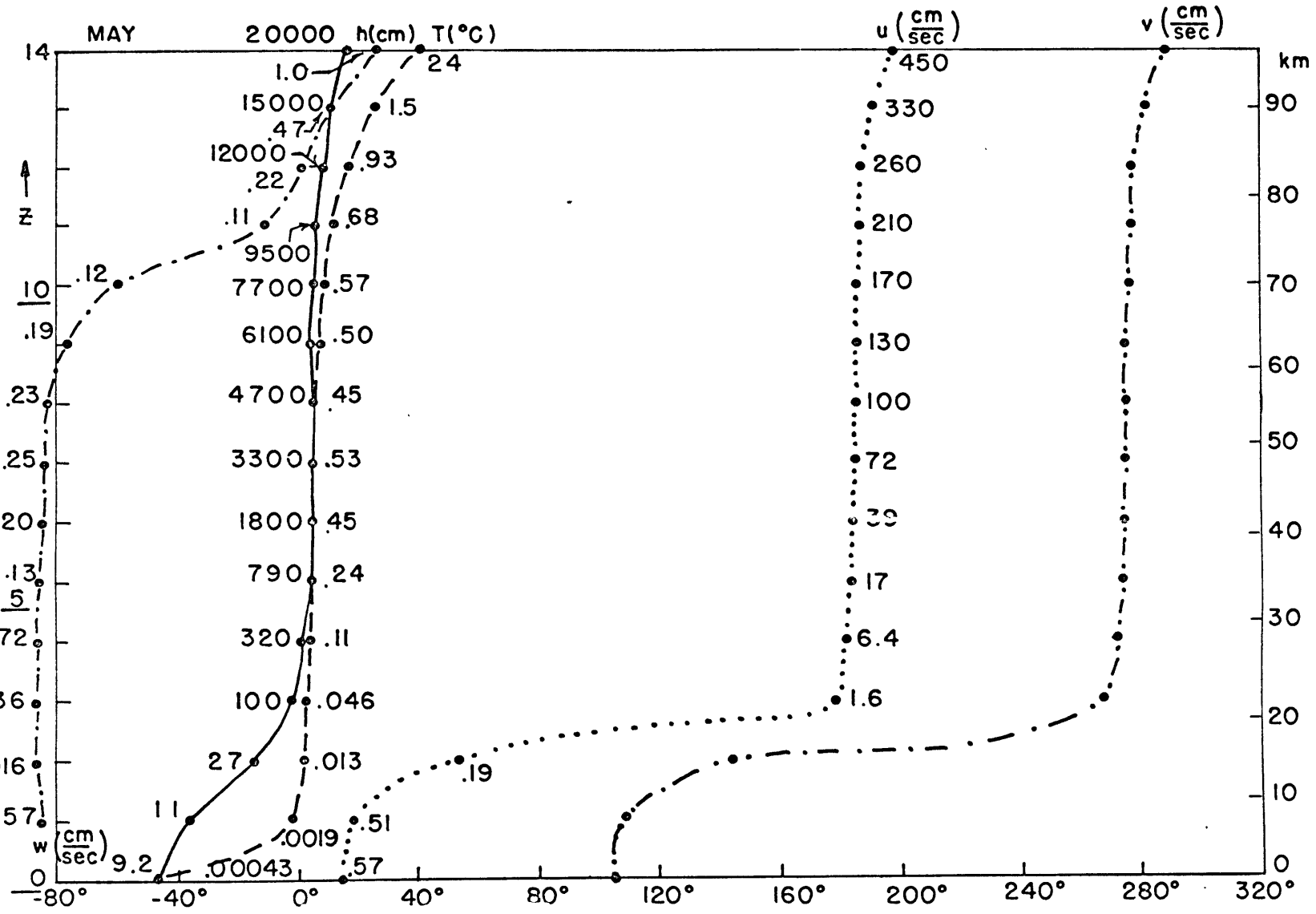
MAY
20000 h(cm) T(°C)
u (cm/sec)
v (cm/sec)
km
z
w (cm/sec)
14
10
5
0
90
80
70
60
50
40
30
20
10
0
-80°
-40°
0°
40°
80°
120°
160°
200°
240°
280°
320°
1.0
15000
.47
12000
.22
.11
9500
7700
6100
4700
3300
1800
790
320
100
27
11
9.2
.00043
.0019
.013
.046
.11
.24
.45
.53
.45
.50
.57
.68
.93
1.5
24
.12
.19
.23
.25
.20
.13
.072
.036
.016
.0057
.51
.57
450
330
260
210
170
130
100
72
17
6.4
1.6
.19

Figure IV A-5

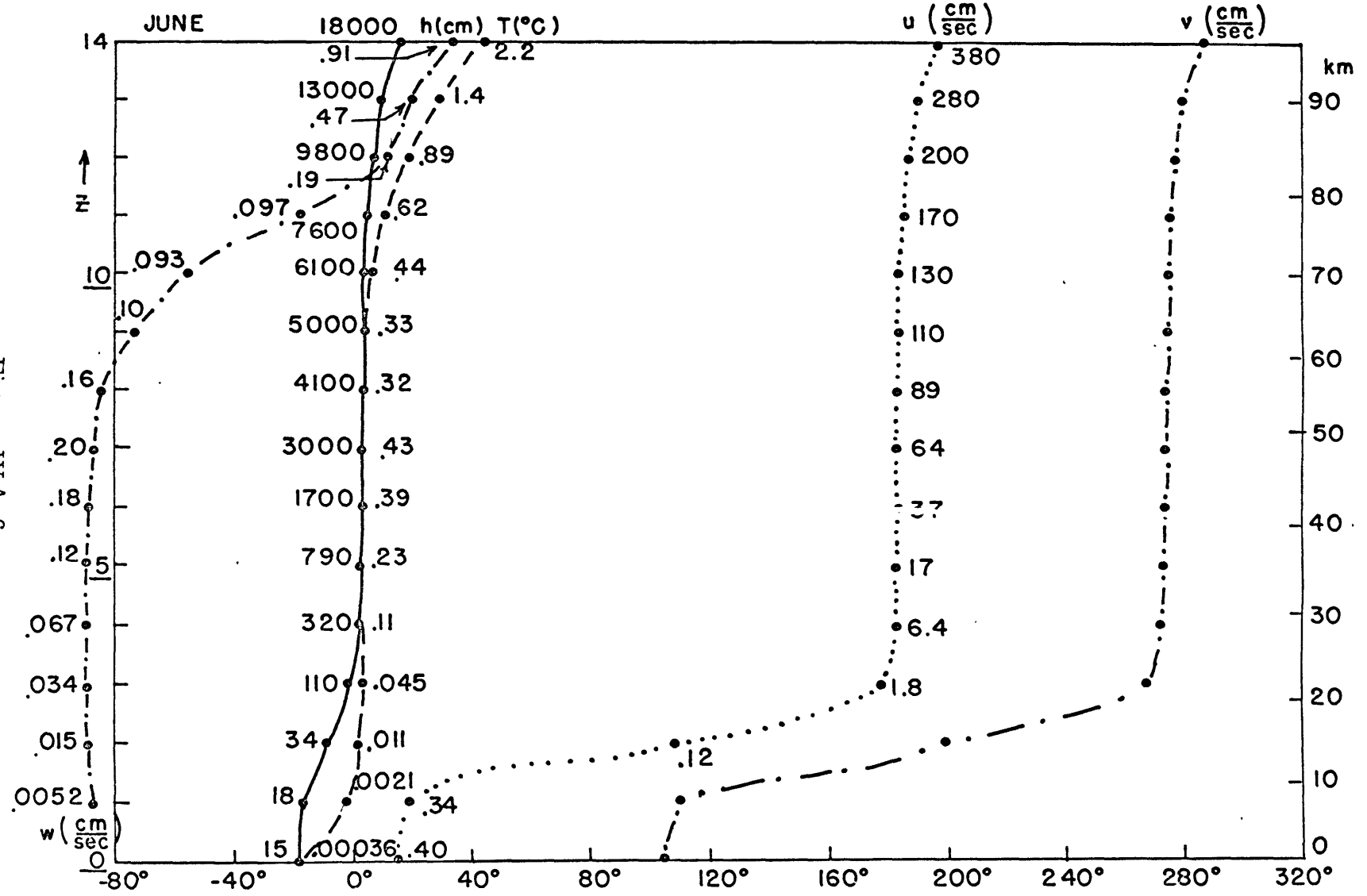
JUNE
18000 h(cm) T(°C)
u (cm/sec)
v (cm/sec)
km
14
10
5
0
N
w (cm/sec)
.91
2.2
13000
1.4
.47
9800
.89
.19
.097
.62
7600
.093
6100
.44
.10
5000
.33
.16
4100
.32
.20
3000
.43
.18
1700
.39
.12
790
.23
.067
320
.11
.034
110
.045
.015
34
.011
.0052
18
.0021
.34
15
.00036
.40
380
280
200
170
130
110
89
64
37
17
6.4
1.8
.12
90
80
70
60
50
40
30
20
10
0
-80°
-40°
0°
40°
80°
120°
160°
200°
240°
280°
320°

Figure IV A-6

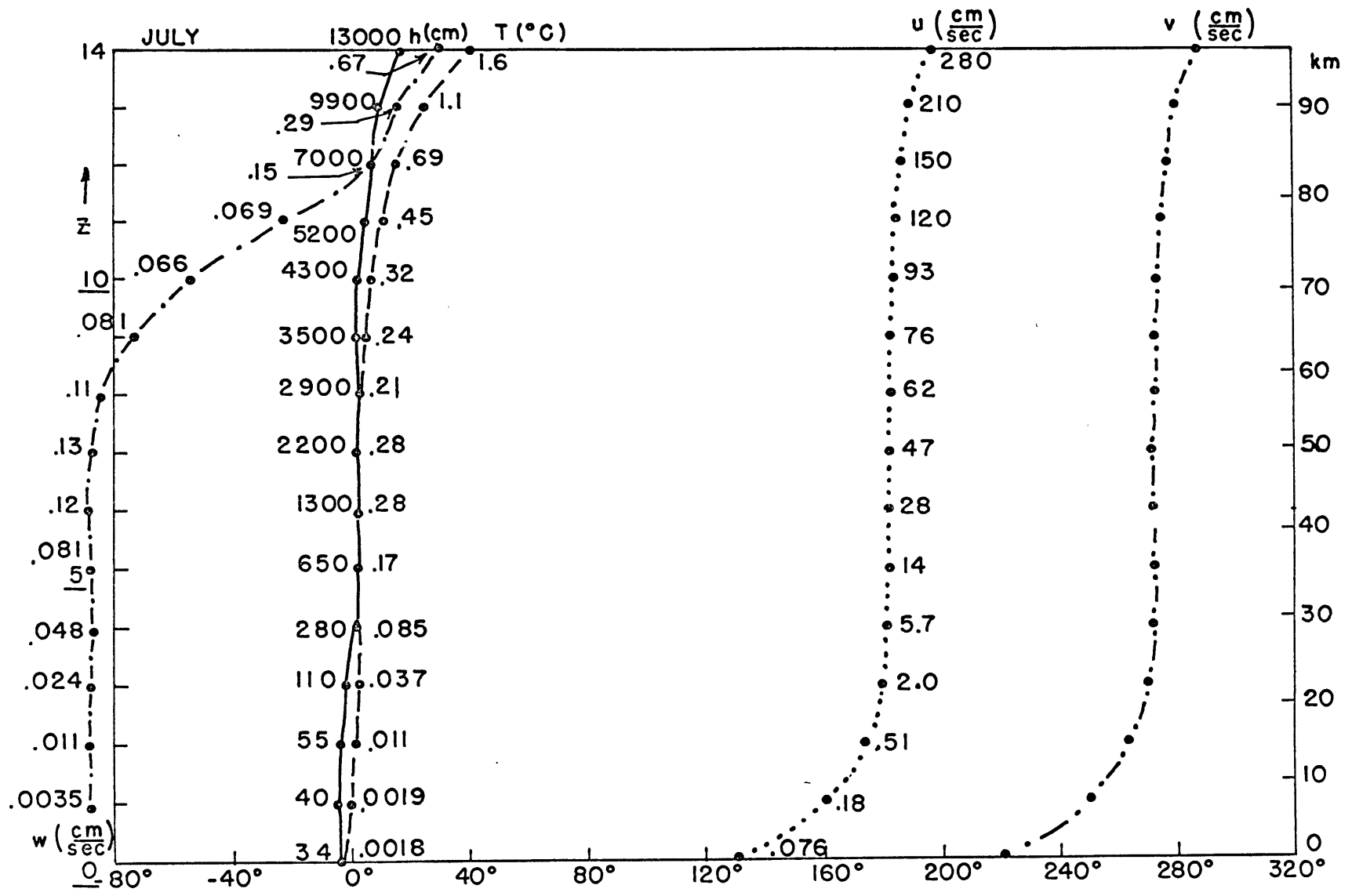
JULY
13000 h(cm)
T (°C)
u (cm/sec)
v (cm/sec)
km
z
w (cm/sec)
14
10
5
0
.067
1.6
9900
1.1
.29
7000
.69
.15
.069
5200
.45
.066
4300
.32
.081
3500
.24
.11
2900
.21
.13
2200
.28
.12
1300
.28
.081
650
.17
.048
280
.085
.024
110
.037
.011
55
.011
.0035
40
.0019
34
.0018
280
210
150
120
93
76
62
47
28
14
5.7
2.0
.51
.18
.076
90
80
70
60
50
40
30
20
10
0
-80°
-40°
0°
40°
80°
120°
160°
200°
240°
280°
320°

Figure IV A-7

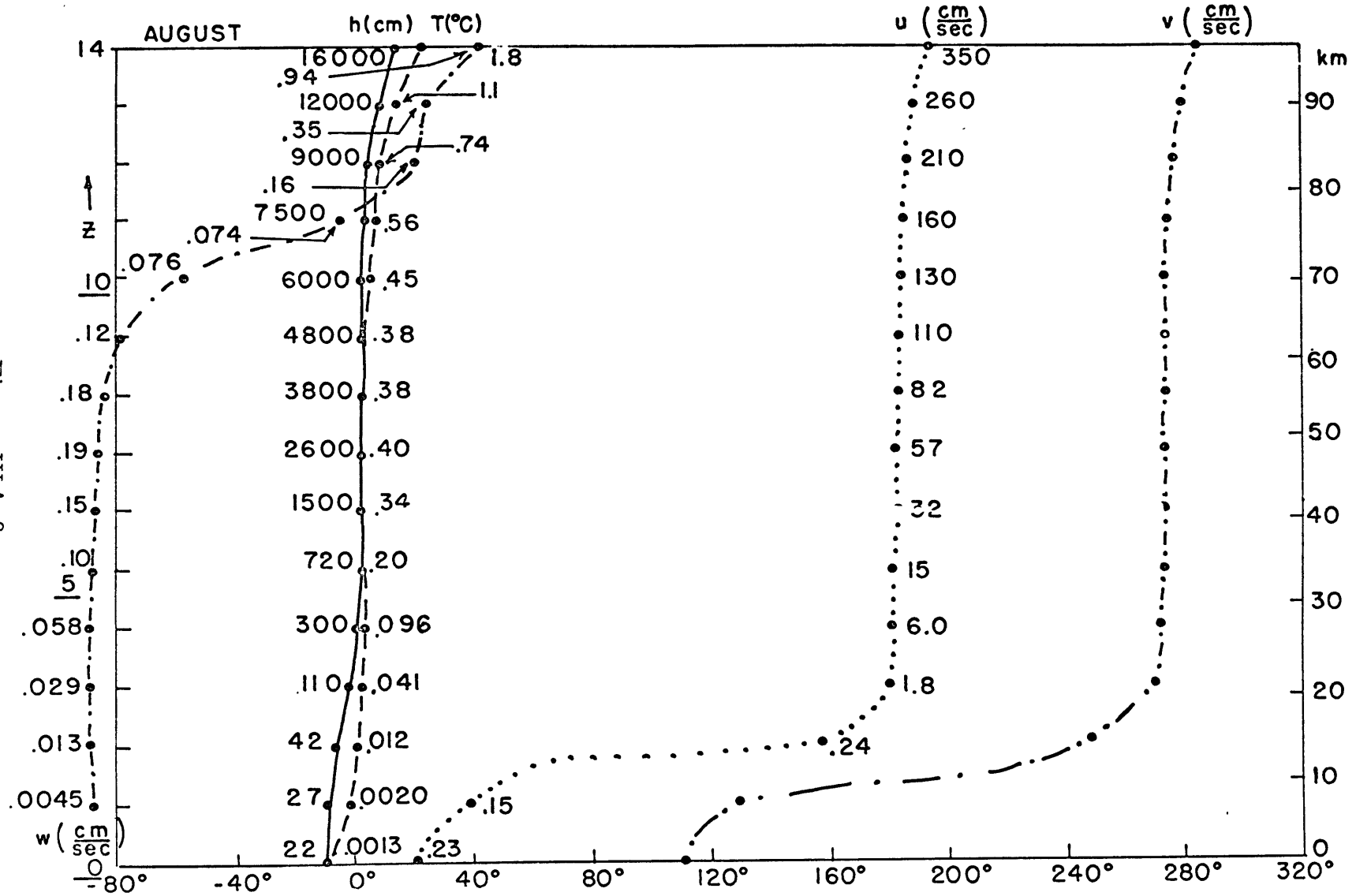
AUGUST
h(cm)
T(°C)
u (cm/sec)
v (cm/sec)
z
km
w (cm/sec)
16000
12000
9000
7500
6000
4800
3800
2600
1500
720
300
110
42
27
22
1.8
1.1
.74
.56
.45
.38
.38
.40
.34
.20
.096
.041
.012
.0020
.0013
.94
.35
.16
.074
.076
.12
.18
.19
.15
.10
.058
.029
.013
.0045
.24
.15
.23
350
260
210
160
130
110
82
57
32
15
6.0
1.8
14
10
5
0
90
80
70
60
50
40
30
20
10
0
-80°
-40°
0°
40°
80°
120°
160°
200°
240°
280°
320°

Figure IV A-8

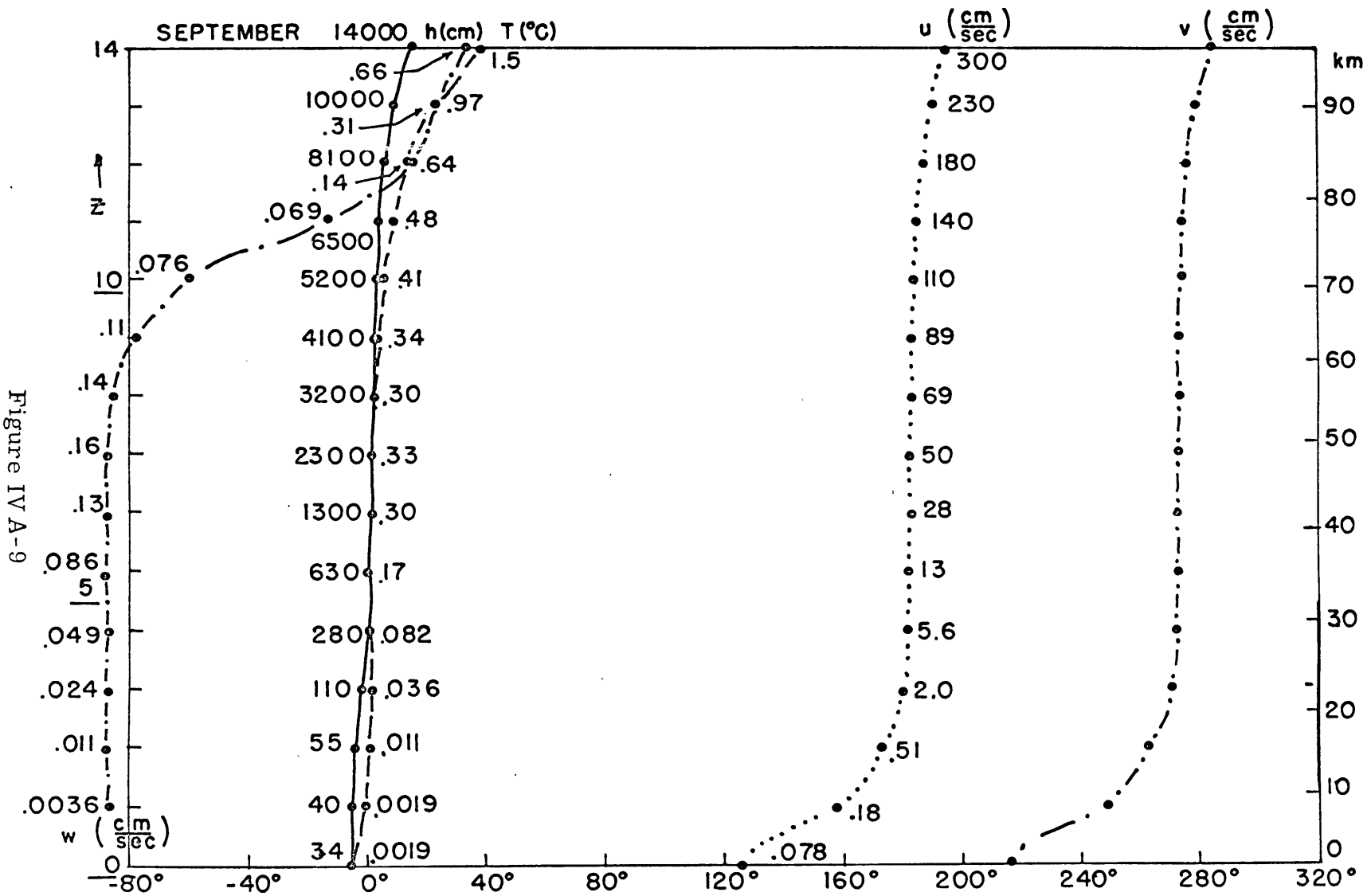
SEPTEMBER 14000 h(cm) T(°C)
u (cm/sec)
v (cm/sec)
km
z
w (cm/sec)
14
10
5
0
-80°
-40°
0°
40°
80°
120°
160°
200°
240°
280°
320°
1.5
.66
10000
.97
.31
8100
.64
.14
.069
.48
6500
.076
5200
.41
.11
4100
.34
.14
3200
.30
.16
2300
.33
.13
1300
.30
.086
630
.17
.049
280
.082
.024
110
.036
.011
55
.011
.0036
40
.0019
34
.0019
0
300
230
180
140
110
89
69
50
28
13
5.6
2.0
.51
.18
.078
90
80
70
60
50
40
30
20
10
0

Figure IV A-9

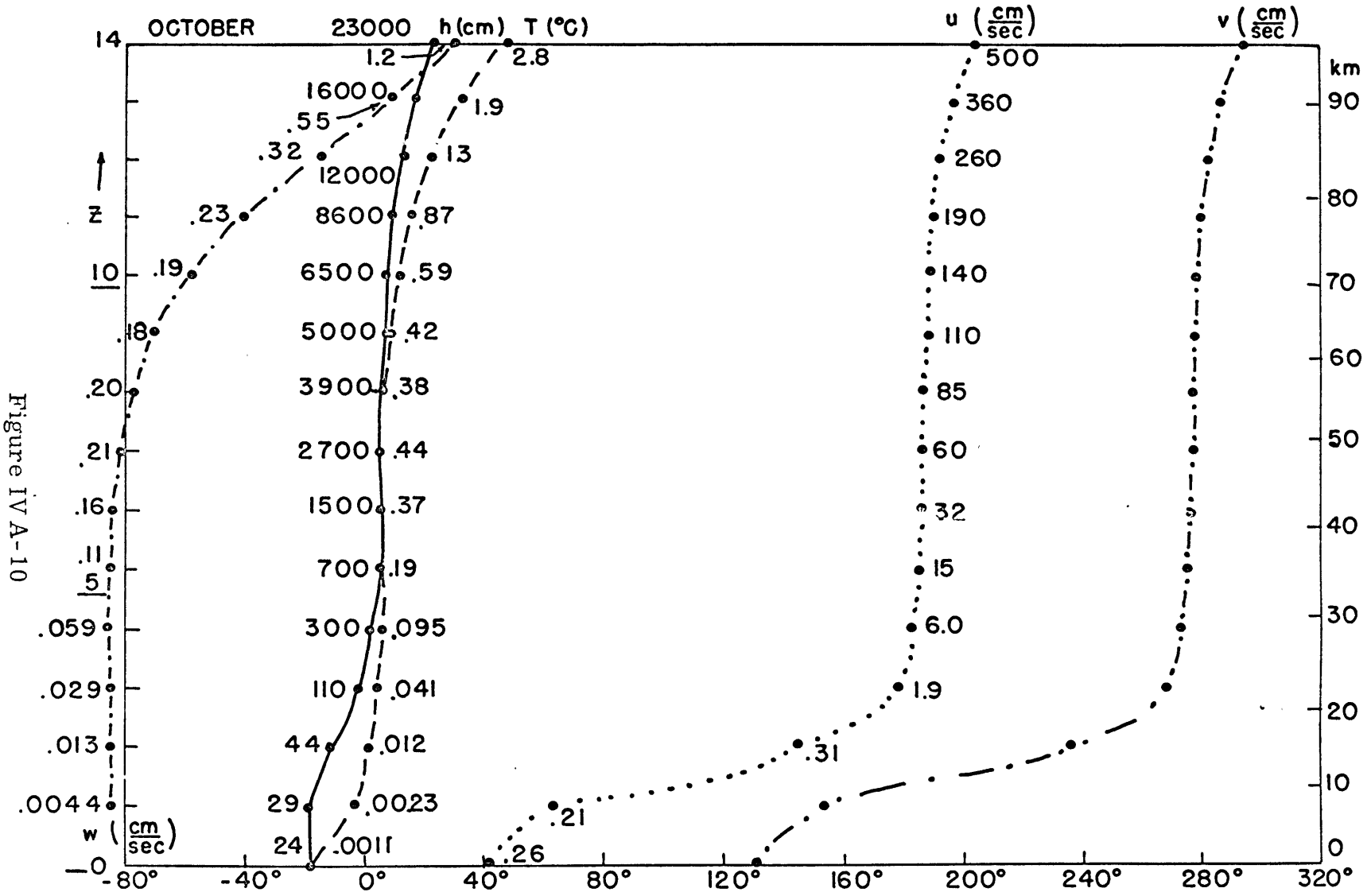

Figure IV A-10

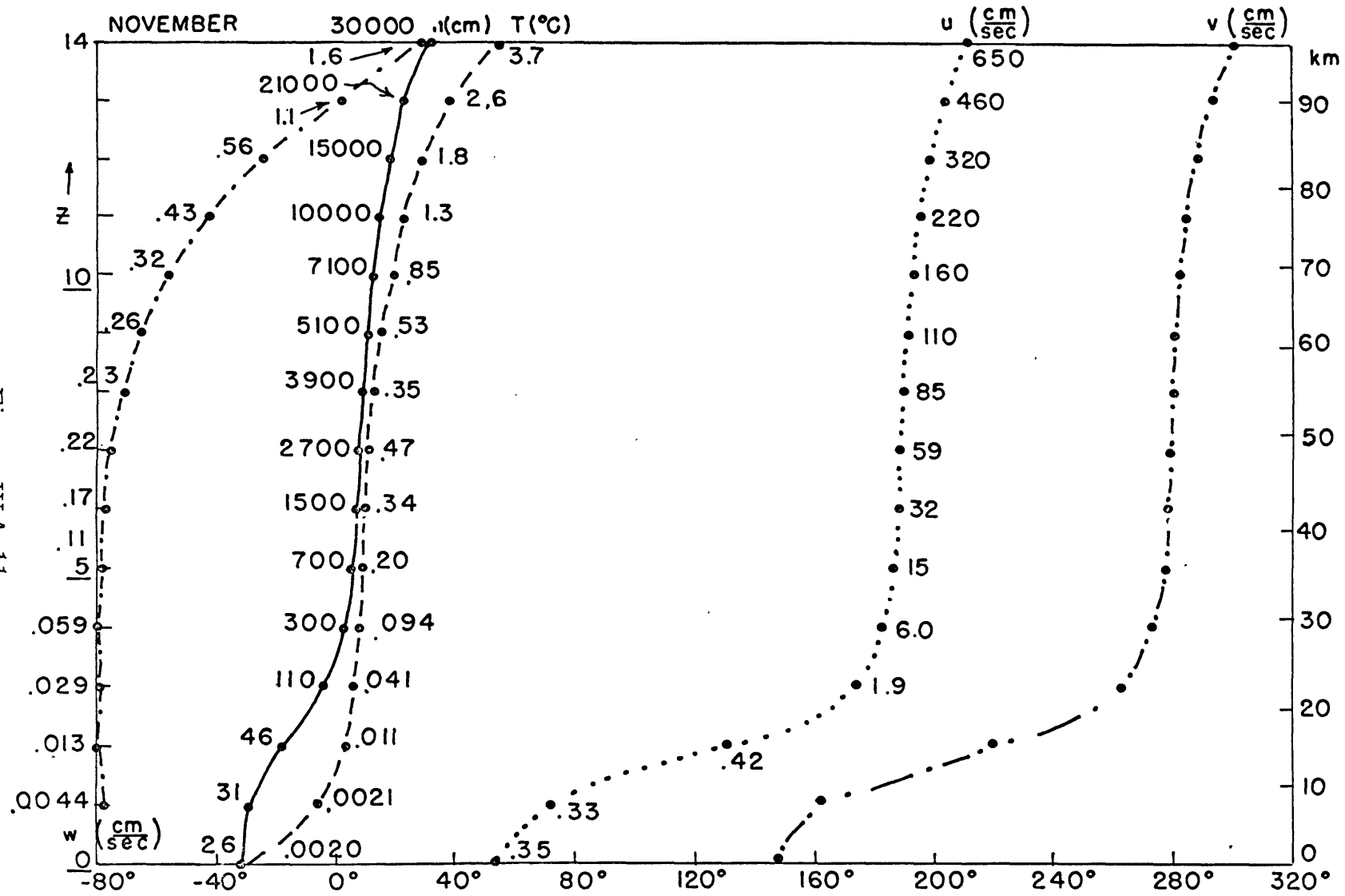

Figure IV A-11

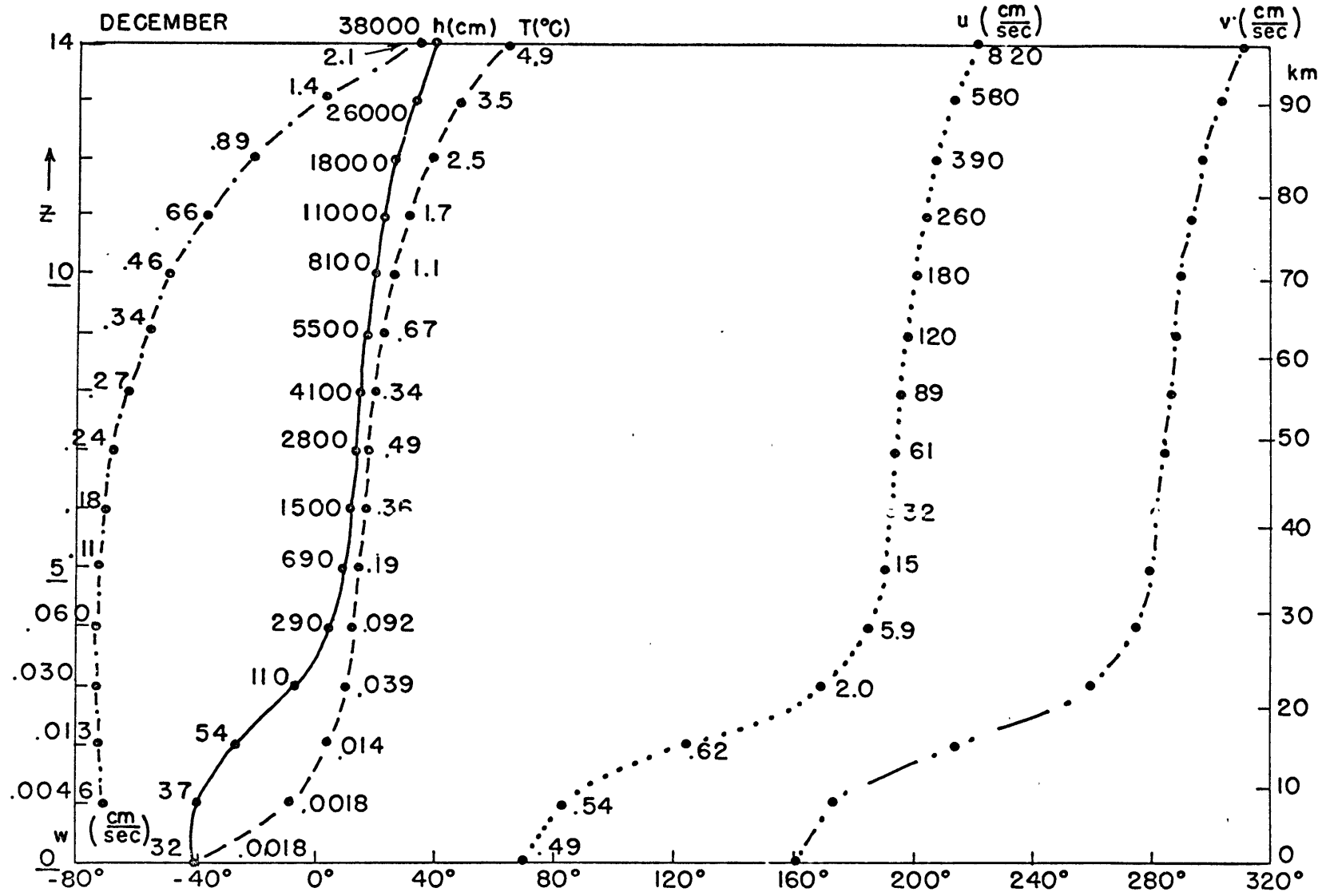

Figure IV A-12

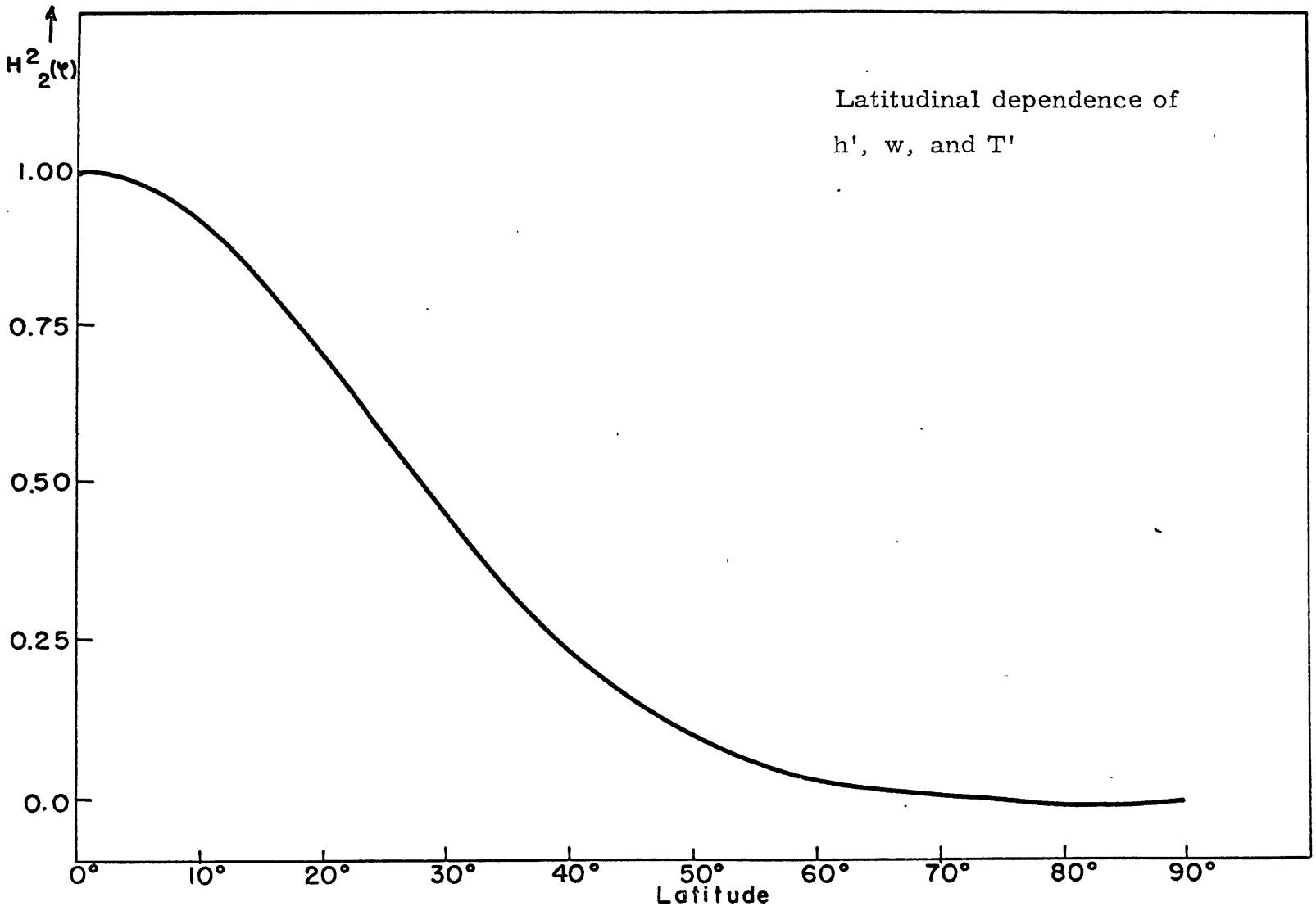

Figure IV A-13

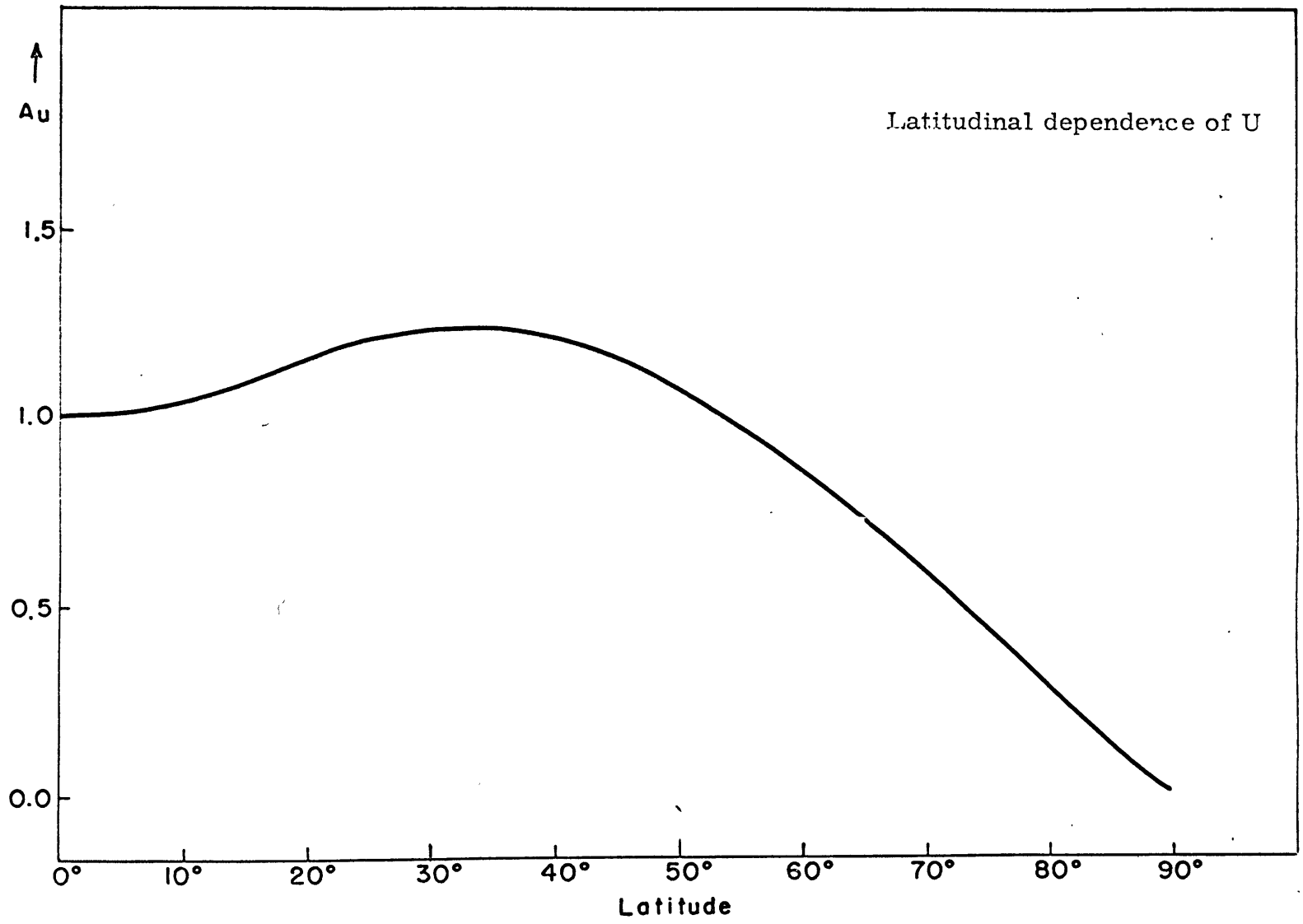

Figure IV A-14

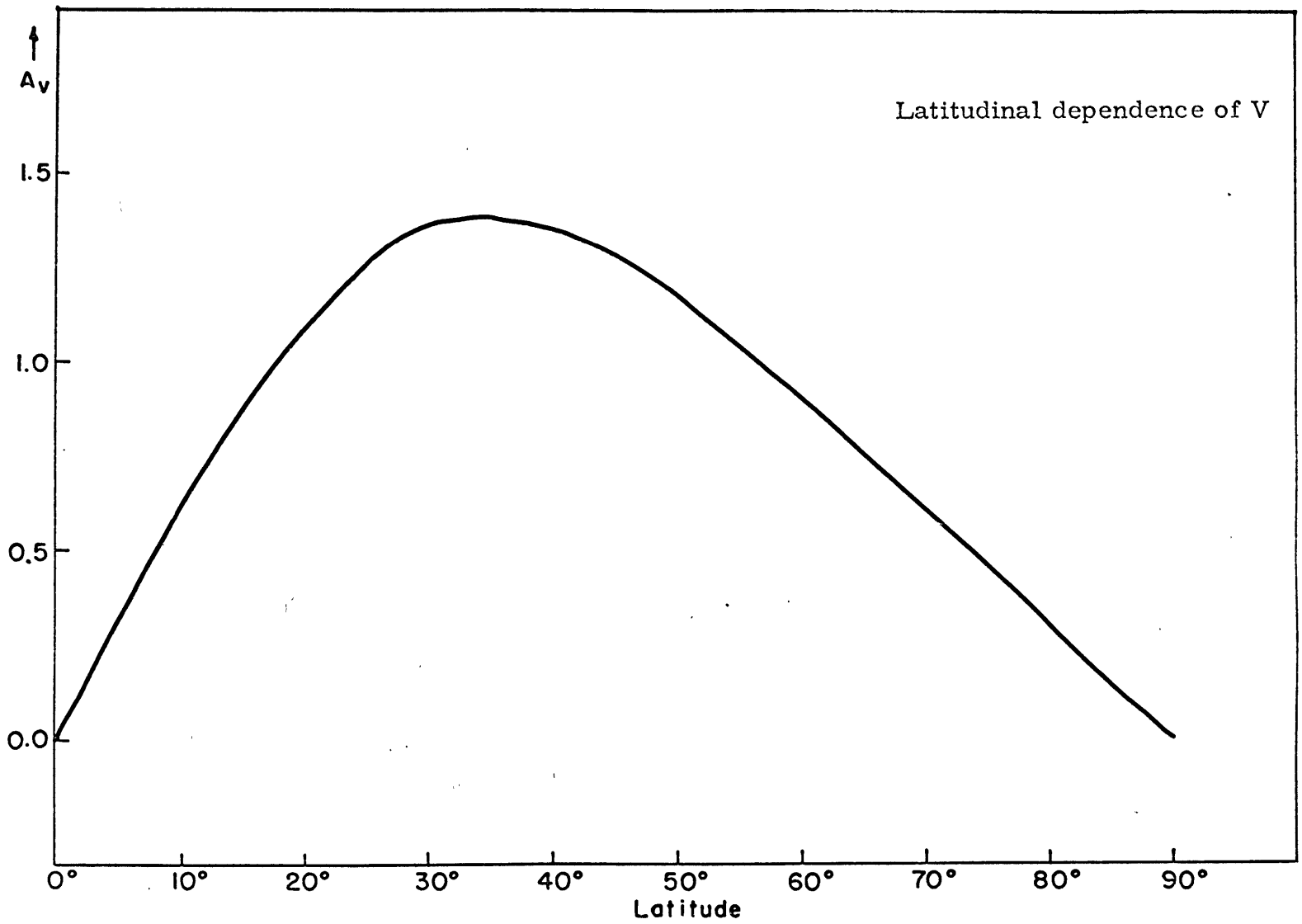

Figure IV A-15

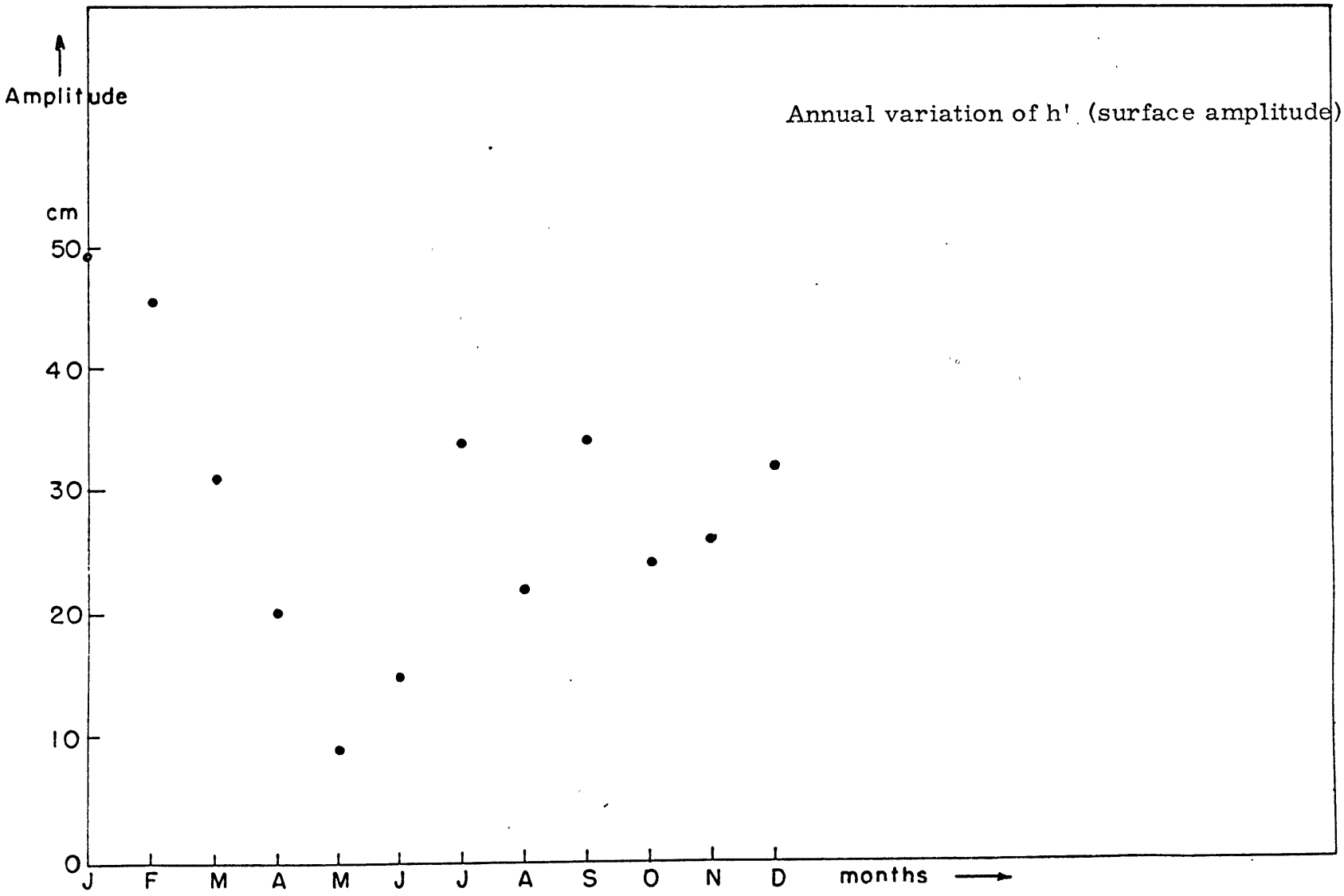

Figure IV A-16

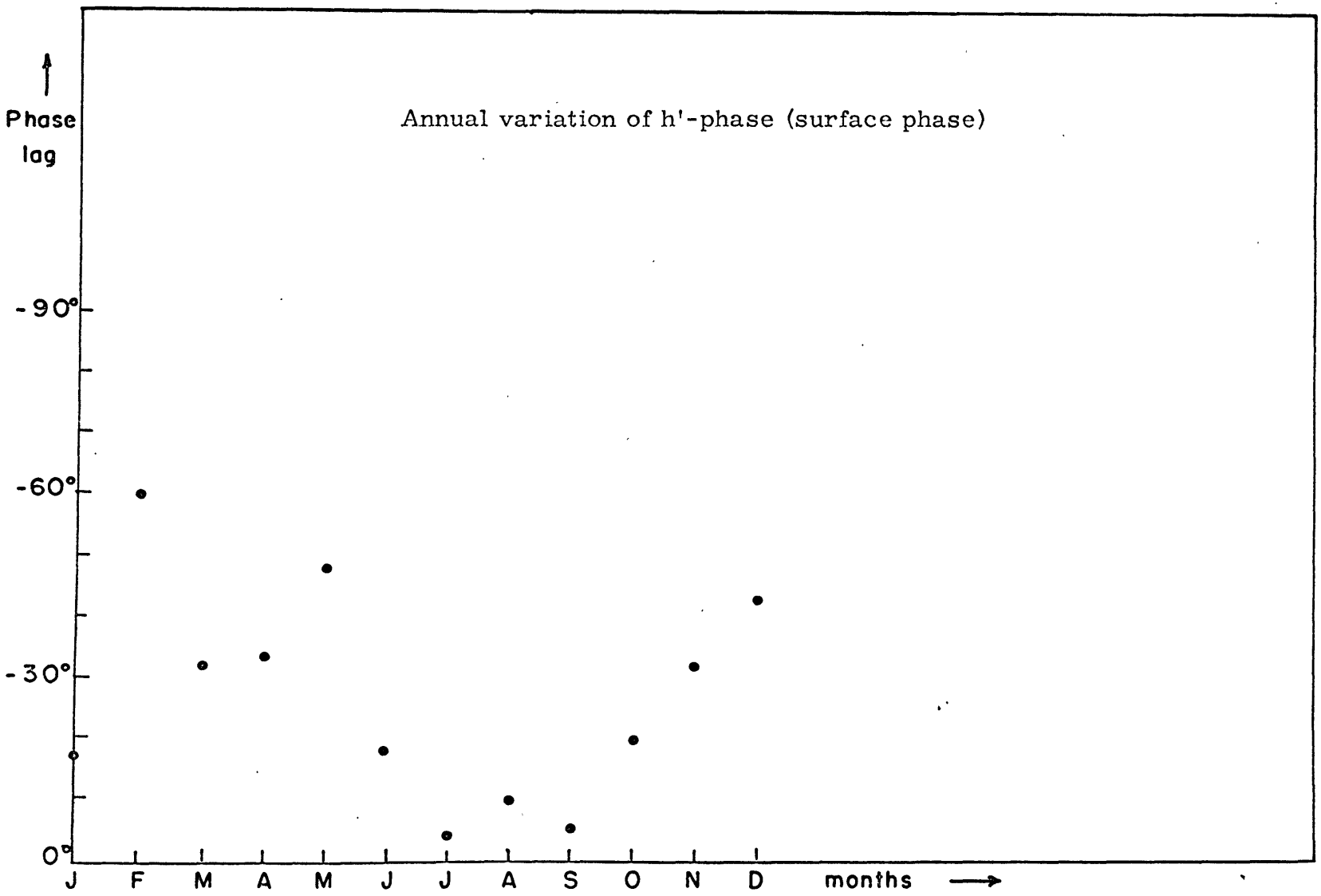

Figure IV A-17

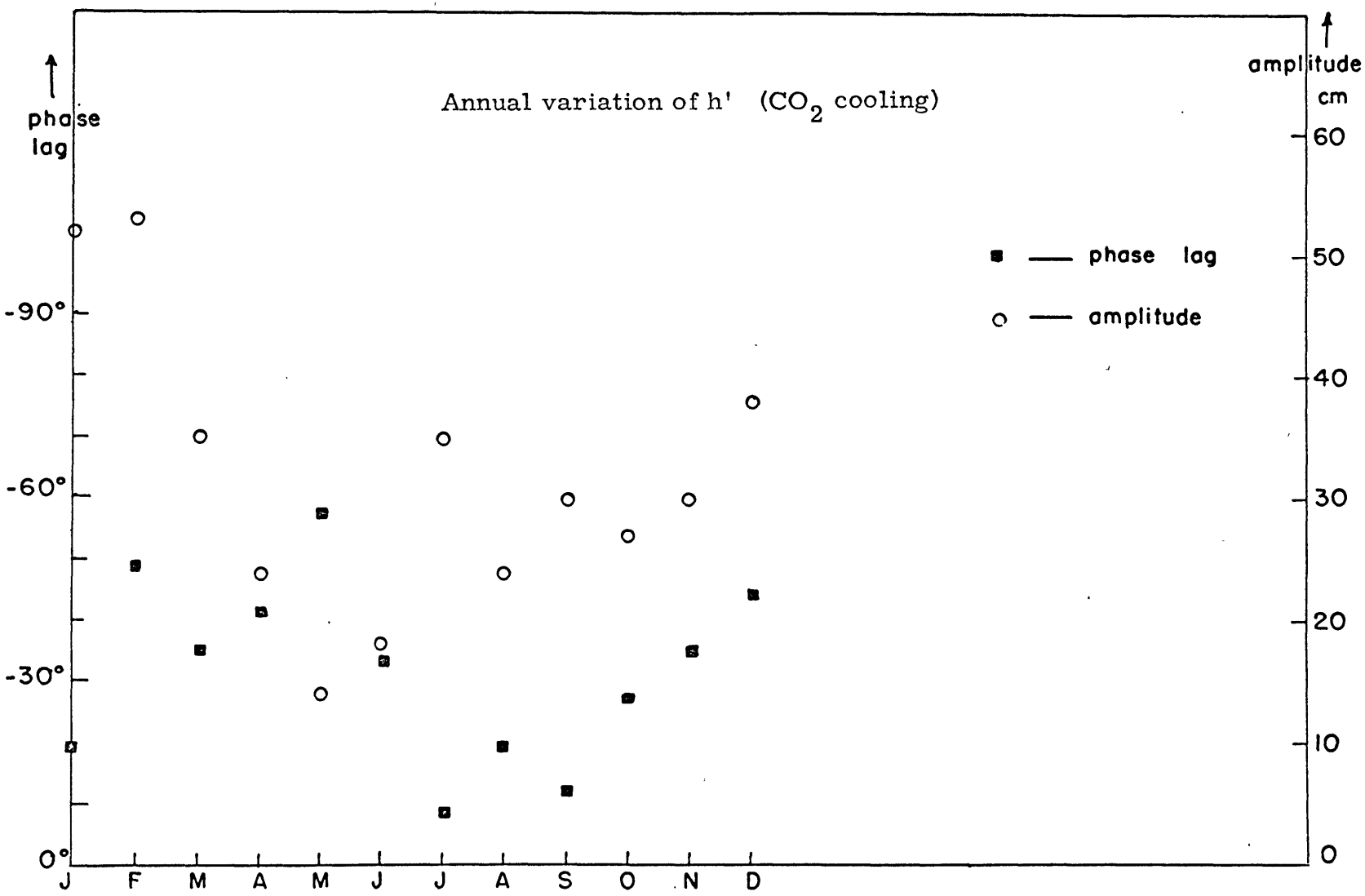
Annual variation of h' (CO_2 cooling)
phase lag
amplitude
cm
-90°
-60°
-30°
0°
60
50
40
30
20
10
0
J F M A M J J A S O N D
phase lag
amplitude

Figure IV B-1

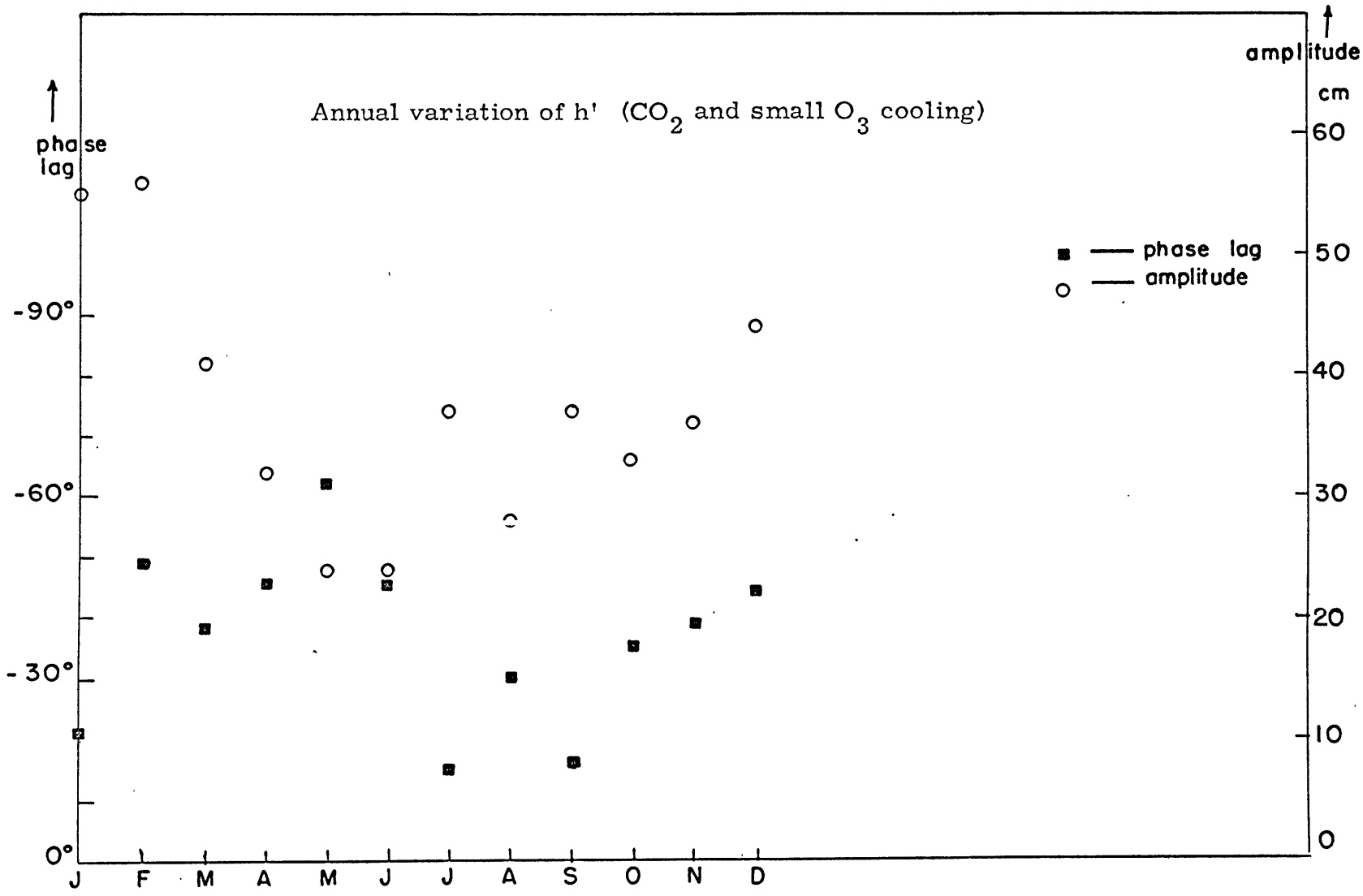
Annual variation of h' (CO_2 and small O_3 cooling)
phase lag
amplitude
cm
-90°
-60°
-30°
0°
60
50
40
30
20
10
0
J F M A M J J A S O N D
phase lag
amplitude

Figure IVB-2

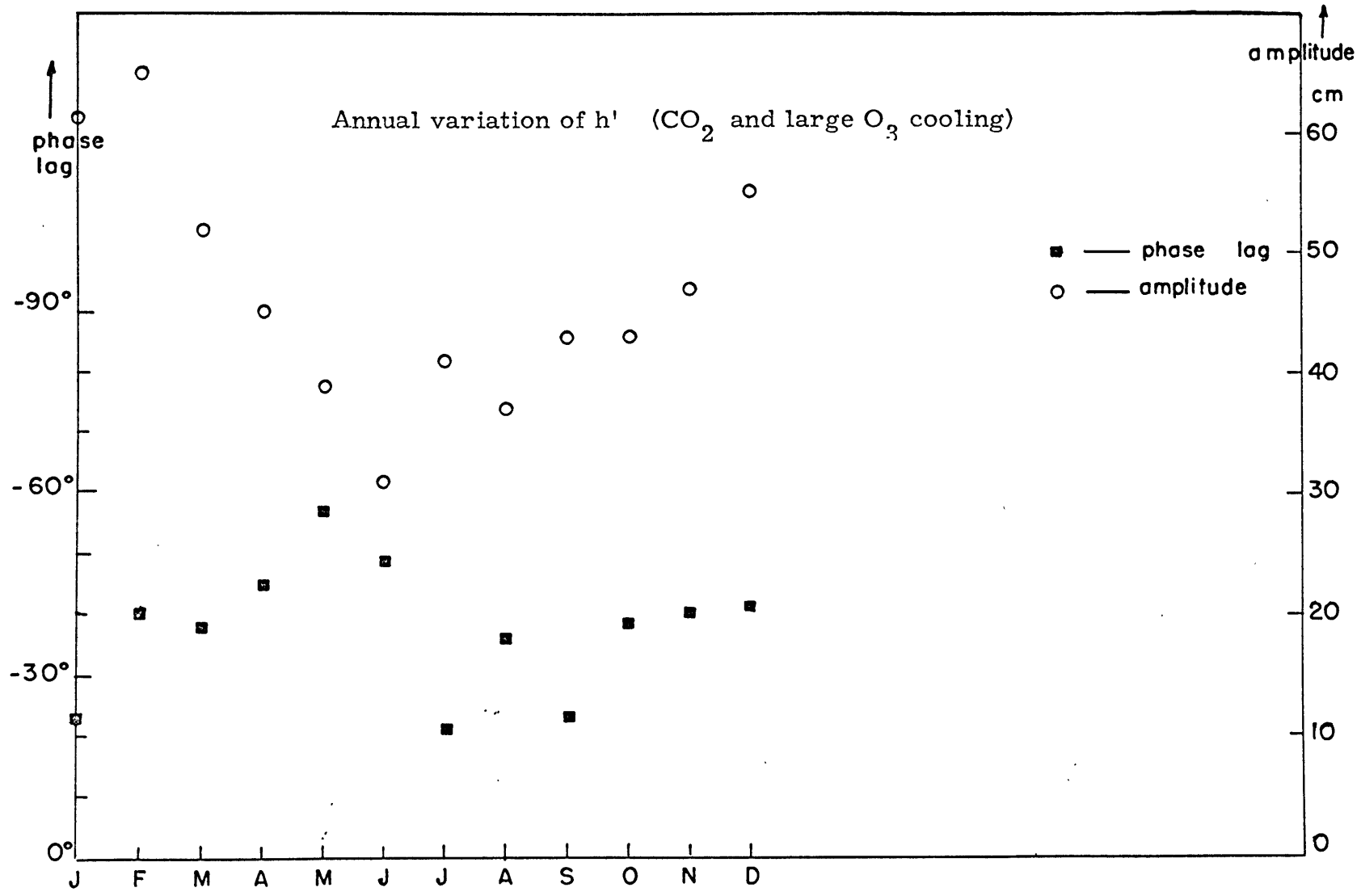
Annual variation of h' (CO_2 and large O_3 cooling)
phase lag
amplitude
cm
-90°
-60°
-30°
0°
60
50
40
30
20
10
0
J F M A M J J A S O N D
phase lag
amplitude

Figure IV B-3

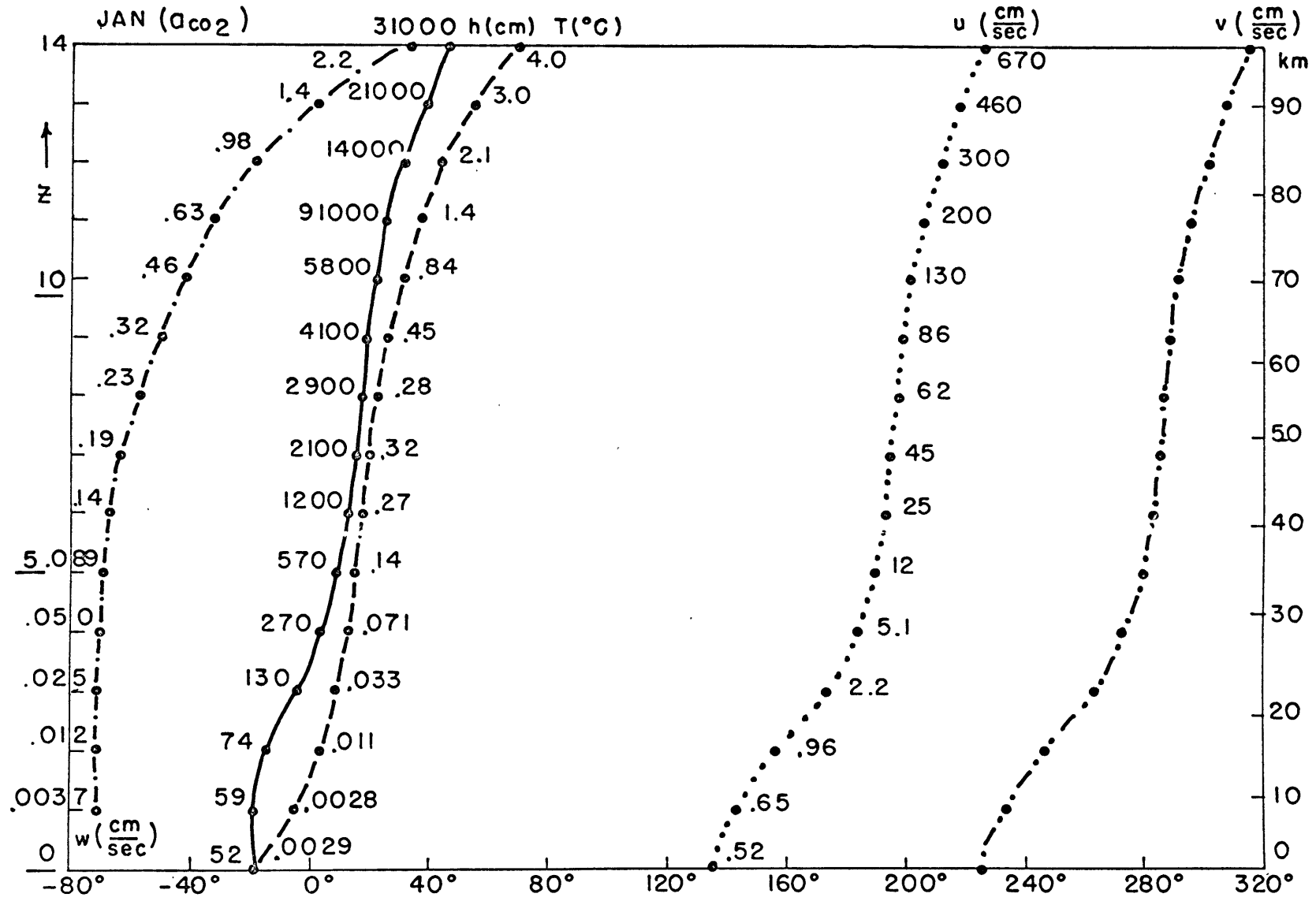
JAN (a_{CO_2})
31000 h(cm) T(°C)
u ($\frac{cm}{sec}$)
v ($\frac{cm}{sec}$)
w ($\frac{cm}{sec}$)
N
km
14
10
5.0
.05
.02
.01
.003
0
2.2
1.4
21000
4.0
3.0
.98
14000
2.1
.63
91000
1.4
.46
5800
.84
.32
4100
.45
.23
2900
.28
.19
2100
.32
.14
1200
.27
.089
570
.14
.050
270
.071
.025
130
.033
.012
74
.011
.0037
59
.0028
52
.0029
670
460
300
200
130
86
62
45
25
12
5.1
2.2
.96
.65
.52
90
80
70
60
50
40
30
20
10
0
-80°
-40°
0°
40°
80°
120°
160°
200°
240°
280°
320°

Figure IV B-4

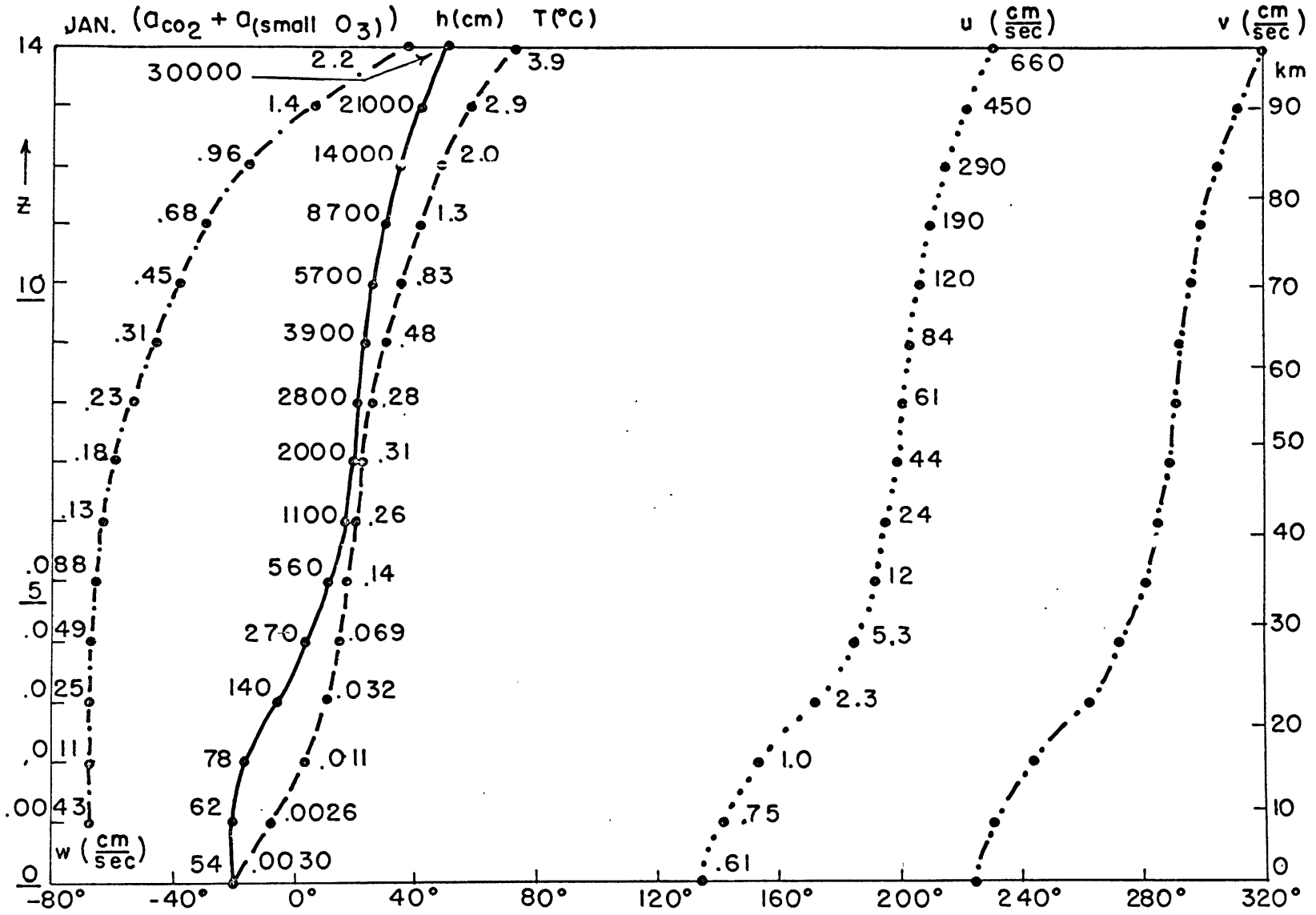
JAN. (a_{CO_2} + $a_{(small\ O_3)}$)
h(cm)
T(°C)
u ($\frac{cm}{sec}$)
v ($\frac{cm}{sec}$)
z
km
w ($\frac{cm}{sec}$)
30000
2.2
3.9
660
1.4
21000
2.9
450
.96
14000
2.0
290
.68
8700
1.3
190
.45
5700
.83
120
.31
3900
.48
84
.23
2800
.28
61
.18
2000
.31
44
.13
1100
.26
24
.088
560
.14
12
.049
270
.069
5.3
.025
140
.032
2.3
.011
78
.011
1.0
.0043
62
.0026
.75
54
.0030
.61
14
10
5
0
90
80
70
60
50
40
30
20
10
0
-80°
-40°
0°
40°
80°
120°
160°
200°
240°
280°
320°

Figure IV B-5

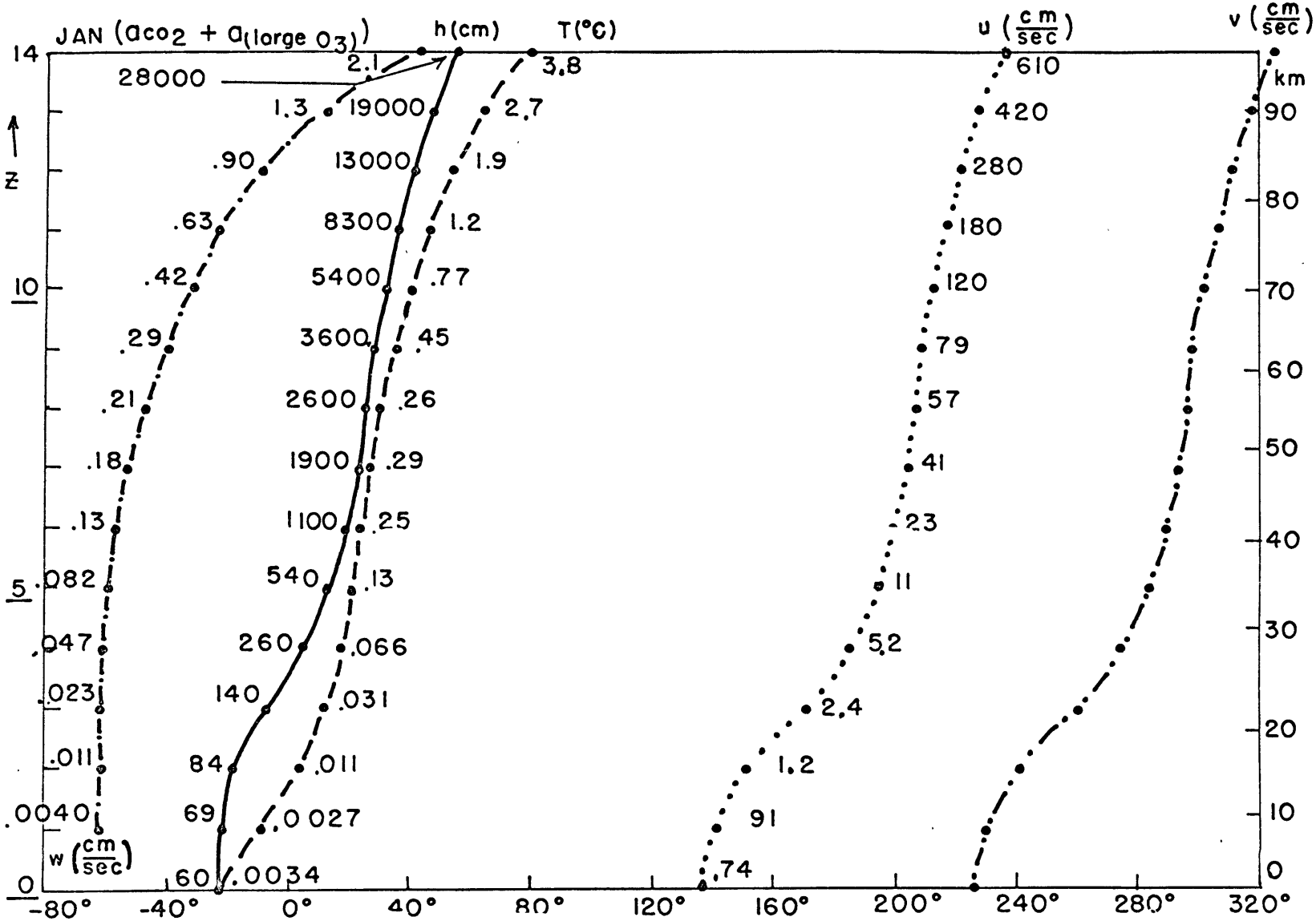
JAN (α_{CO_2} + $\alpha_{(large\ O_3)}$)
h(cm)
T(°C)
u ($\frac{cm}{sec}$)
v ($\frac{cm}{sec}$)
z
km
w ($\frac{cm}{sec}$)
28000
19000
13000
8300
5400
3600
2600
1900
1100
540
260
140
84
69
60
2.1
1.3
.90
.63
.42
.29
.21
.18
.13
.082
.047
.023
.011
.0040
3.8
2.7
1.9
1.2
.77
.45
.26
.29
.25
.13
.066
.031
.011
.0027
.0034
610
420
280
180
120
79
57
41
23
11
5.2
2.4
1.2
91
.74
14
10
5
0
90
80
70
60
50
40
30
20
10
0
-80°
-40°
0°
40°
80°
120°
160°
200°
240°
280°
320°

Figure IV B-6

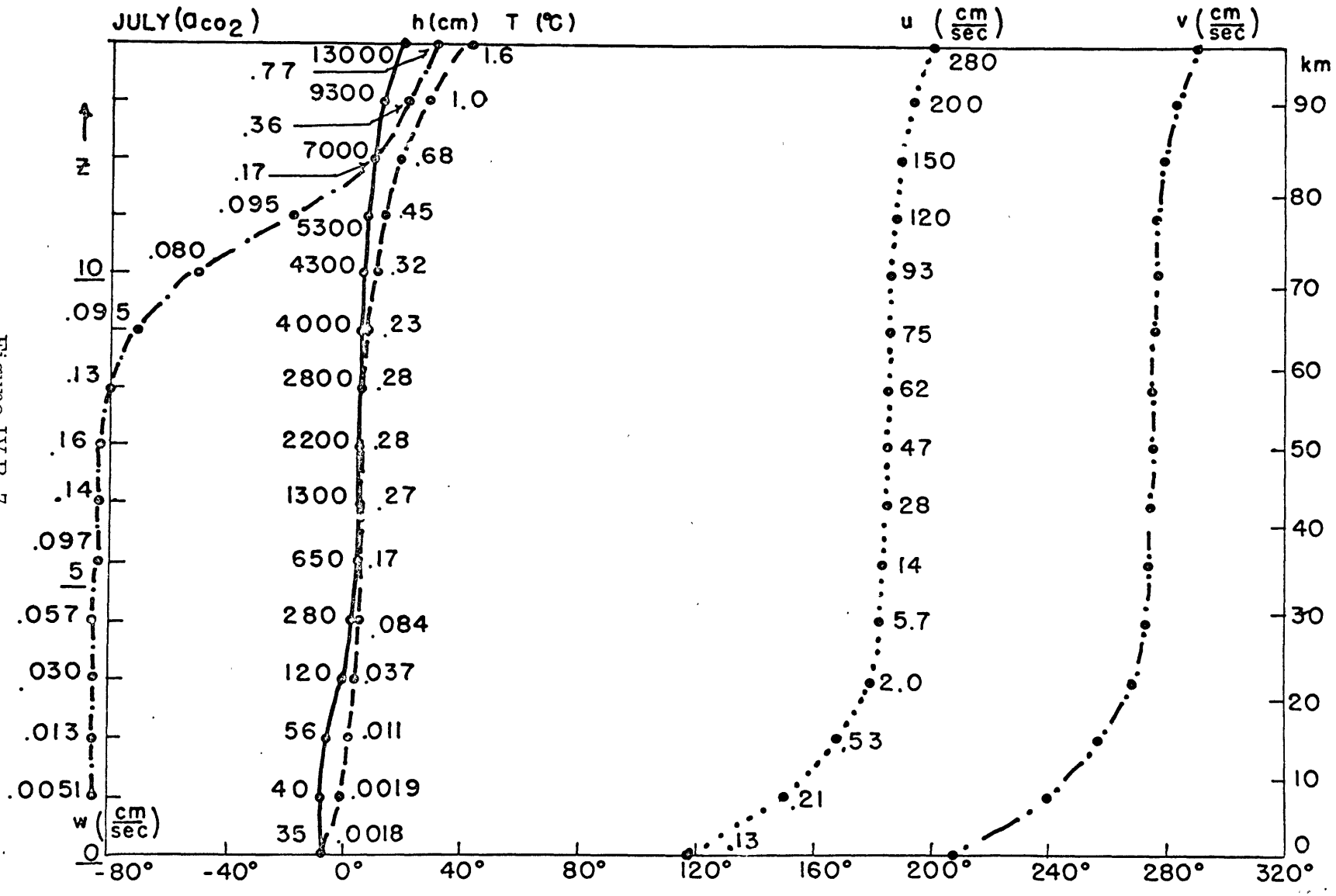
JULY (a_{CO_2})
h(cm)
T (°C)
u ($\frac{cm}{sec}$)
v ($\frac{cm}{sec}$)
z
km
w ($\frac{cm}{sec}$)
13000
9300
7000
5300
4300
4000
2800
2200
1300
650
280
120
56
40
35
.77
.36
.17
.095
.080
.09
.13
.16
.14
.097
.057
.030
.013
.0051
0
1.6
1.0
.68
.45
.32
.23
.28
.28
.27
.17
.084
.037
.011
.0019
.0018
280
200
150
120
93
75
62
47
28
14
5.7
2.0
.53
.21
.13
90
80
70
60
50
40
30
20
10
0
-80°
-40°
0°
40°
80°
120°
160°
200°
240°
280°
320°

Figure IV B-7

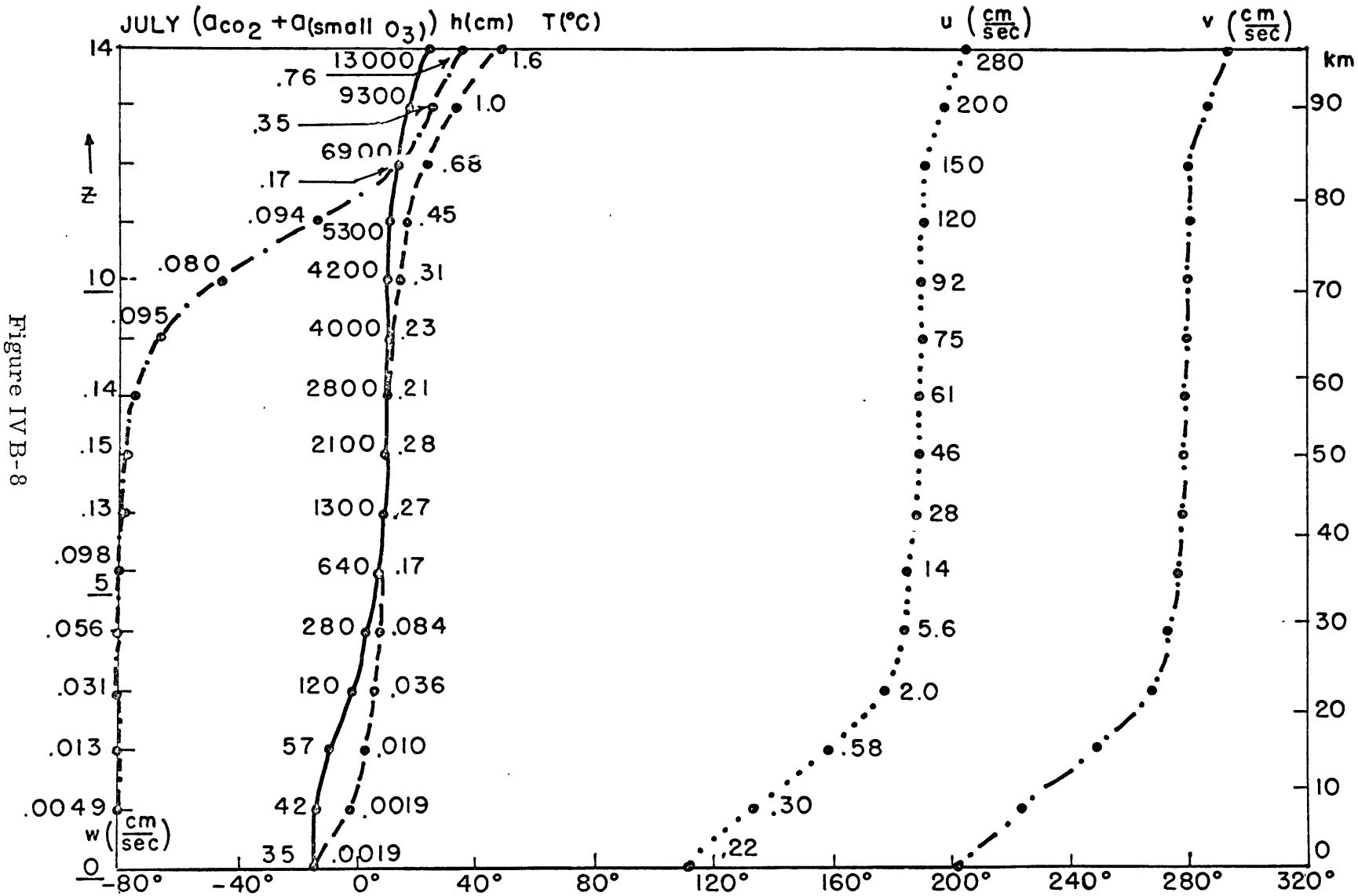
JULY (a_{CO_2} + $a_{(small\ O_3)}$) h(cm) T(°C)
u ($\frac{cm}{sec}$)
v ($\frac{cm}{sec}$)
km
z
w ($\frac{cm}{sec}$)
14
10
5
0
.76
.35
.17
.094
.080
.095
.14
.15
.13
.098
.056
.031
.013
.0049
13000
9300
6900
5300
4200
4000
2800
2100
1300
640
280
120
57
42
35
1.6
1.0
.68
.45
.31
.23
.21
.28
.27
.17
.084
.036
.010
.0019
.0019
280
200
150
120
92
75
61
46
28
14
5.6
2.0
.58
.30
.22
90
80
70
60
50
40
30
20
10
0
-80°
-40°
0°
40°
80°
120°
160°
200°
240°
280°
320°

Figure IV B-8

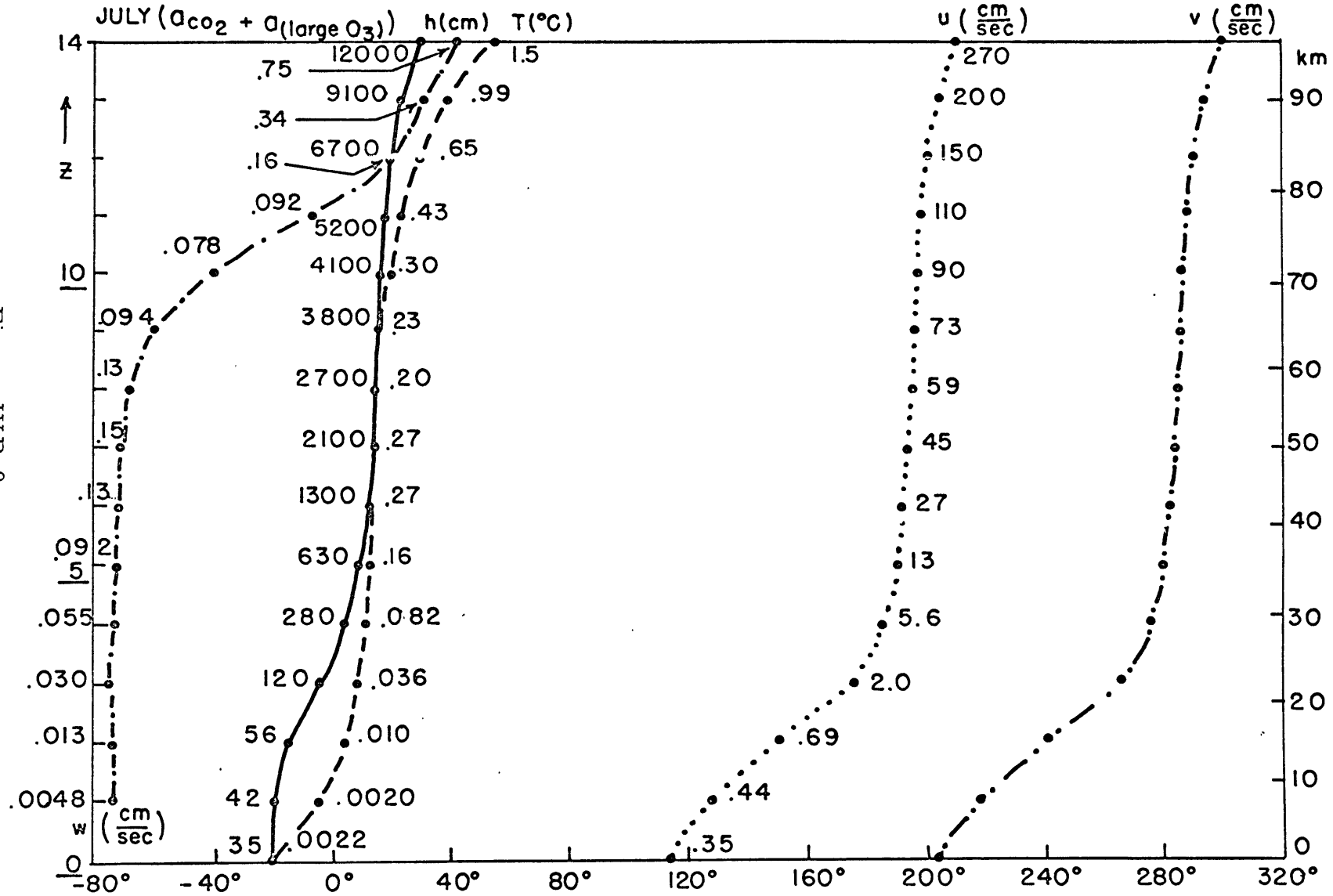
JULY (a_{CO_2} + $a_{(large\ O_3)}$)
h(cm)
T(°C)
u (cm/sec)
v (cm/sec)
km
z
w (cm/sec)
12000
9100
6700
5200
4100
3800
2700
2100
1300
630
280
120
56
42
35
.75
.34
.16
.092
.078
.094
.13
.15
.3
.2
.5
.055
.030
.013
.0048
1.5
.99
.65
.43
.30
.23
.20
.27
.27
.16
.082
.036
.010
.0020
.0022
270
200
150
110
90
73
59
45
27
13
5.6
2.0
.69
.44
.35
14
10
0
90
80
70
60
50
40
30
20
10
0
-80°
-40°
0°
40°
80°
120°
160°
200°
240°
280°
320°

Figure IVB-9

CHAPTER V

ENERGETICS

Section A: Energetics Formulation

It is of interest to look at the energetics of the lunar tidal problem both to investigate the effectiveness of the "mesospheric barrier" and to look at the distribution and amount of energy depletion due to Newtonian Cooling.

A convenient starting point for looking at energetics is the set of linearized primitive equations from which the tidal equations were derived. These are as follows:

$$\frac{\partial u}{\partial t} - (2\Omega \sin\varphi)v + \frac{1}{a\cos\varphi}\frac{\partial \phi'}{\partial \lambda} = 0 \qquad \text{VA-1}$$

$$\frac{\partial v}{\partial t} + (2\Omega \sin\varphi)u + \frac{1}{a}\frac{\partial \phi'}{\partial \varphi} = 0 \qquad \text{VA-2}$$

$$\frac{1}{a\cos\varphi}\frac{\partial u}{\partial \lambda} + \frac{1}{a\cos\varphi}\frac{\partial}{\partial \varphi}(v\cos\varphi) + \frac{\partial w}{\partial z} - w = 0 \qquad \text{VA-3}$$

$$\frac{\partial T'}{\partial t} + w(\bar{T}_z + \gamma\bar{T}) = \frac{J}{c_p} - a_0 T' \qquad \text{VA-4}$$

$$\frac{\partial \phi'}{\partial z} = RT'. \qquad \text{VA-5}$$

These equations hold for any linearized hydrostatic motions, neglecting viscous effects, with the Newtonian Cooling approximation.

Multiplying equation V A-1 by U and equation V A-2 by V gives the following equation:

$$\frac{\partial}{\partial t}\left[\tfrac{1}{2}(u^2+v^2)\right] + (a\cos\varphi)^{-1} u \frac{\partial \phi'}{\partial \lambda} + a^{-1} v \frac{\partial \phi'}{\partial \varphi} = 0 , \qquad \text{V A-6}$$

which may be written as

$$\frac{\partial}{\partial t}\left[\tfrac{1}{2}(u^2+v^2)\right] + (a\cos\varphi)^{-1} \frac{\partial}{\partial \lambda}(u\phi') + (a\cos\varphi)^{-1} \frac{\partial}{\partial \varphi}(v\phi'\cos\varphi) \qquad \text{V A-7}$$

$$- \phi'\left[(a\cos\varphi)^{-1} \frac{\partial u}{\partial \lambda} + (a\cos\varphi)^{-1} \frac{\partial}{\partial \varphi}(v\cos\varphi)\right] = 0$$

The continuity equation V A-3 is now used to rewrite equation V A-7 as

$$\frac{\partial}{\partial t}\left[\tfrac{1}{2}(u^2+v^2)\right] + (a\cos\varphi)^{-1} \frac{\partial}{\partial \lambda}(u\phi') + (a\cos\varphi)^{-1} \frac{\partial}{\partial \varphi}(v\phi'\cos\varphi) \qquad \text{V A-8}$$

$$+ \phi'\left[\frac{\partial w}{\partial z} - w\right] = 0 .$$

Now $\frac{\partial w}{\partial z} - w = \frac{\partial w}{\partial p}$, so equation V A-8 becomes

V A-9

$$\frac{\partial}{\partial t}\left[\tfrac{1}{2}(u^2+v^2)\right] + (a\cos\varphi)^{-1} \frac{\partial}{\partial \lambda}(u\phi') + (a\cos\varphi)^{-1} \frac{\partial}{\partial \varphi}(v\phi'\cos\varphi)$$

$$+ \frac{\partial}{\partial p}(w\phi') - w\frac{\partial \phi'}{\partial p} = 0 .$$

Solving equation VA-4 for $w = -\frac{1}{\rho}\omega$ implies

$$\omega = \frac{\frac{\partial T'}{\partial t} + a_0 T' - \frac{J}{c_p}}{\frac{1}{\rho}\left(\bar{T}_2 + \gamma\bar{T}\right)} \qquad \text{VA-10}$$

With equation VA-10 and the hydrostatic equation, $\frac{\partial \phi'}{\partial p} = -\frac{RT'}{p}$, the following equation is finally obtained from equation VA-9:

$$\frac{\partial}{\partial t}\left[\tfrac{1}{2}(u^2+v^2) + \frac{\frac{1}{2}\gamma T'^2}{\frac{1}{R}(\bar{T}_2+\gamma\bar{T})}\right] + (a\cos\varphi)^{-1}\frac{\partial}{\partial\lambda}(u\phi') + \qquad \text{VA-11}$$

$$a^{-1}\frac{\partial}{\partial\varphi}(v\phi') + \frac{\partial}{\partial p}(\omega\phi') = \frac{\gamma J T'}{(\bar{T}_2+\gamma\bar{T})} - \frac{a_0 T'^2}{\frac{1}{R}(\bar{T}_2+\gamma\bar{T})}$$

Equation VA-11 may be expressed in words in the following manner. The time derivative of the kinetic plus "available potential energy" is balanced by: 1. the convergence of the energy flux, 2. the creation of energy by heating, and 3. the loss of energy due to cooling-to-space.

If equation VA-11 is integrated over a sphere and over a tidal period for the lunar tide (J = 0), it becomes

$$\frac{\partial}{\partial p}\overline{(\omega\phi')} = -\frac{a_0\overline{T'^2}}{\frac{1}{R}(\bar{T}_2+\gamma\bar{T})} \qquad \text{VA-12}$$

($\overline{(\ )}$ = average value of ( ) over a period); thus, the divergence

of the vertical energy flux must balance the loss of energy due to infrared cooling.

In order to obtain results with this tidal energy formulation, it is convenient to express $\overline{\omega\phi'}$ in the tidal variable Y^m_n.

Recalling the definition of $Y^m_n (= e^{z/2} w^m_n)$, it is seen that $\omega^m_n = -\rho_0 e^{-z/2} Y^m_n$ or

$$\mathcal{R}\ell\, \omega^m_n = -\rho_0 e^{-z/2} H^m_n(\varphi)\left[Y_r^{(m,n)} \cos(\nu t + m\lambda) - Y_i^{(m,n)} \sin(\nu t + m\lambda)\right] . \qquad \text{VA-13}$$

It was also seen that

$$\phi'^m_n = \frac{(2\Omega a)^2}{\nu\gamma^m_n} e^{z/2} i \left[\frac{1}{2} Y^m_n - \frac{dY^m_n}{dz}\right] , \text{ (equation II B-3)}$$

so

$$\mathcal{R}\ell\, \phi'^m_n = \frac{g D^m_n}{\nu} e^{z/2} H^m_n(\varphi)\left\{\left(-\frac{1}{2} Y_i^{(m,n)} + \frac{dY_i^{(m,n)}}{dz}\right)\cos[\nu t + m\lambda] + \left(-\frac{1}{2} Y_r^{(m,n)} + \frac{dY_r^{(m,n)}}{dz}\right)\sin[\nu t + m\lambda]\right\} . \qquad \text{VA-14}$$

Multiplying equation VA-13 by equation VA-14 gives

$$\omega\phi' = -\rho_0 \frac{g D^m_n}{\nu} [H^m_n]^2 \Big[-Y_r^{(m,n)} \Big(\frac{dY_i^{(m,n)}}{dz} - \frac{1}{2} Y_i^{(m,n)} \Big) \cos^2[\nu\tau + m\lambda]$$

$$+ Y_i^{(m,n)} \Big(\frac{dY_r^{(m,n)}}{dz} - \frac{1}{2} Y_r^{(m,n)} \Big) \sin^2[\nu t + m\lambda]$$

$$- Y_r^{(m,n)} \Big(\frac{dY_r^{(m,n)}}{dz} - \frac{1}{2} Y_r^{(m,n)} \Big) \sin[\nu\tau + m\lambda] \cos[\nu\tau + m\lambda]$$

$$+ Y_i^{(m,n)} \Big(\frac{dY_i^{(m,n)}}{dz} - \frac{1}{2} Y_i^{(m,n)} \Big) \sin[\nu\tau + m\lambda] \cos[\nu\tau + m\lambda] \Big] . \qquad \text{VA-15}$$

Now $\overline{\omega\phi'} = \frac{1}{2\pi} \int_{-\pi}^{\pi} \omega\phi' \, d[\nu\tau + m\lambda]$, so performing the indicated averaging on equation VA-15 and using the well-known relations

$$\int_{-\pi}^{\pi} \cos^2 x \, dx = \int_{-\pi}^{\pi} \sin^2 x \, dx = \pi$$

$$\int_{-\pi}^{\pi} \sin x \cos x \, dx = 0$$

implies that

$$\overline{\omega\phi'} = \rho_0 \frac{g D^m_n}{\nu} \big(H^m_n(z)\big)^2 \Big[\frac{1}{2} \Big(Y_r^{(m,n)} \frac{dY_i^{(m,n)}}{dz} - Y_i^{(m,n)} \frac{dY_r^{(m,n)}}{dz} \Big) \Big] \qquad \text{VA-16}$$

As is usual in these wave propagation problems, the energy flux proves to be proportional to the Wronskian of Y^m_n.

Section B: Energetics Results

Having formulated the energetics of the lunar tide in the last section, some energy calculations will be presented in this section. More specifically calculations of the averaged vertical energy flux, $\overline{\omega\phi'}$, will be given.

At this point, it should be recalled that the lunar tidal problem is being treated in a pressure coordinate system; thus, the energy flux is in units appropriate to such a coordinate system. It should also be noted that the following results are shown in CGS units ($\omega\phi' \sim$ gm cm sec^{-5}).

It has been mentioned throughout that the enhanced "mesospheric barrier" in summer is of great importance in dealing with annual changes in the lunar semidiurnal tide in the atmosphere. The monthly values of the vertical energy flux, with no Newtonian Cooling, is shown in figure V B-1. It is evident that there is much less vertical energy flux in summer than winter.[1] This result fits nicely into the idea of there being an increased barrier to wave propagation in the summer. Since there is no dissipation in this calculation, the vertical energy flux must be constant with height which, along with assuming a steady state tidal oscillation, would

1. Irregularities such as that in January and February are probably due to arbitrary differences in the analysis of the stability function.

imply such an annual variation in the vertical energy flux. Because this energy flux is smaller in summer, the lunar tidal wave more closely resembles a standing wave in summer than in winter, thus leading to the smaller summer phase lag in the surface pressure oscillation both in the observed and calculated tide.

The effects of Newtonian Cooling on the energy flux are shown in figures VB-2 and VB-3. These figures show the vertical energy flux calculations for January and July with 1. no Newtonian Cooling, 2. CO_2 Newtonian Cooling, 3. CO_2 and small O_3 Newtonian Cooling, and 4. CO_2 and large O_3 Newtonian Cooling. As expected, it is seen that more energy is lost when there is a greater amount of cooling present, but there are also other things to be seen. The addition of Newtonian Cooling has the effect of increasing the flux at lower levels and decreasing the flux at higher levels relative to the results with no cooling. It is also seen that approximately the same amount of energy is dissipated in July as in January giving a much greater fraction of energy lost in July.

It thus becomes clear why the seasonal variation in phase lags were lost with the addition of large Newtonian Cooling. The proposed explanation for the annual variation in the phase lag was the variation in trapping due to the changing "mesospheric barrier". This explanation becomes largely irrelevant if most of

the tidal energy is dissipated before it even reaches this "barrier". This is the case if the energy is dissipated in the ozonosphere as shown in figures VB-2 and VB-3.

This disappearance of the seasonal behavior does not negate the validity of the explanation of the phase lag variations in terms of the "mesospheric barrier". The annual behavior was only seen to vanish with the addition of the O_3 Newtonian Cooling and not with CO_2[1]. The cooling due to ozone is suspect not only because of uncertainties in O_3 amounts but also to even greater uncertainties in O_3 photochemistry. It is even possible to view the present work as contributing some small evidence in favor of the modified O_3 photochemistry as the energy losses with O_3 present seem a bit excessive.

---

1. The use of an annual average for α_{CO_2} might also tend to mask such a seasonal variation.

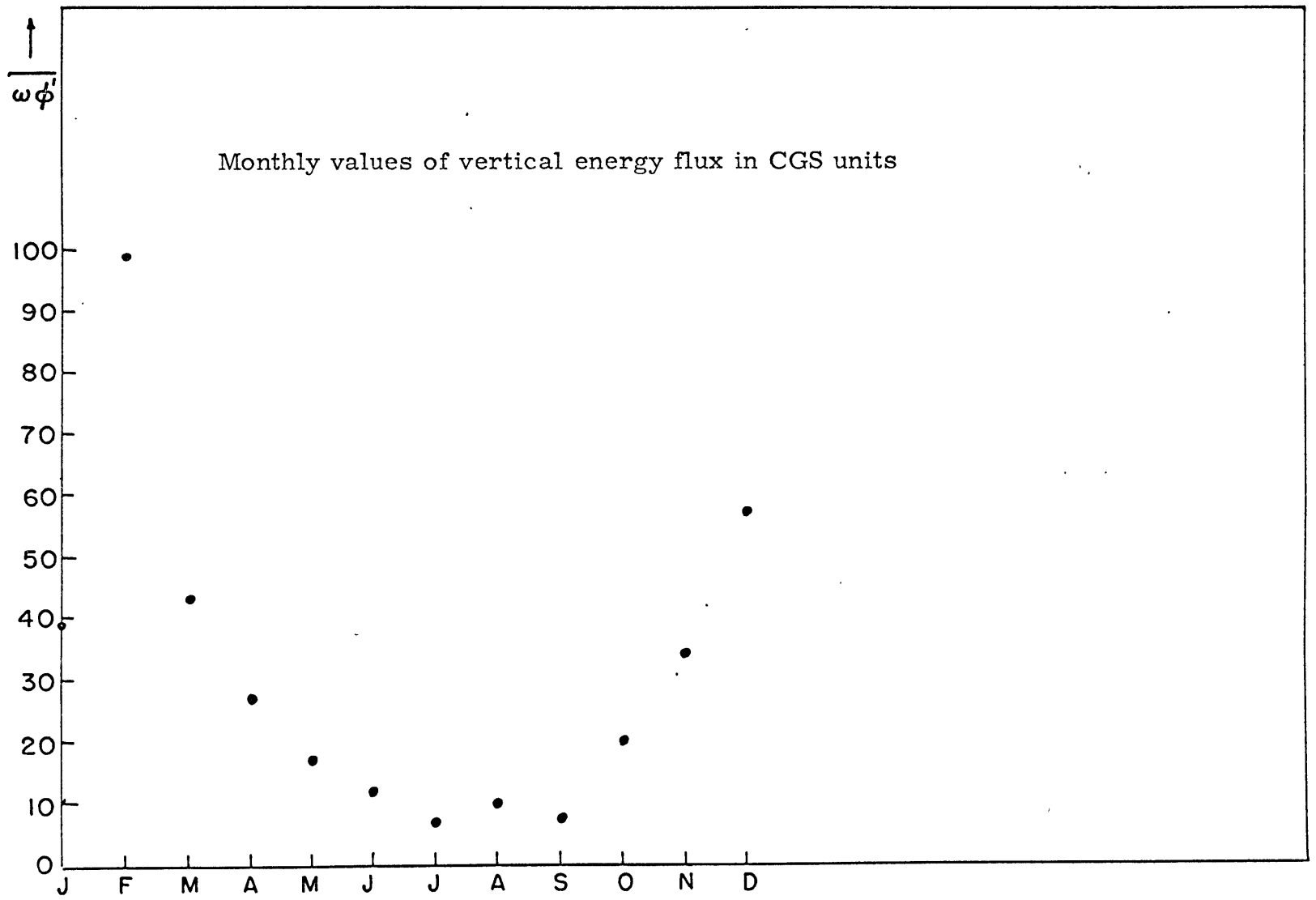
$\overline{\omega\phi'}$
Monthly values of vertical energy flux in CGS units
100
90
80
70
60
50
40
30
20
10
0
J
F
M
A
M
J
J
A
S
O
N
D

Figure V B-1

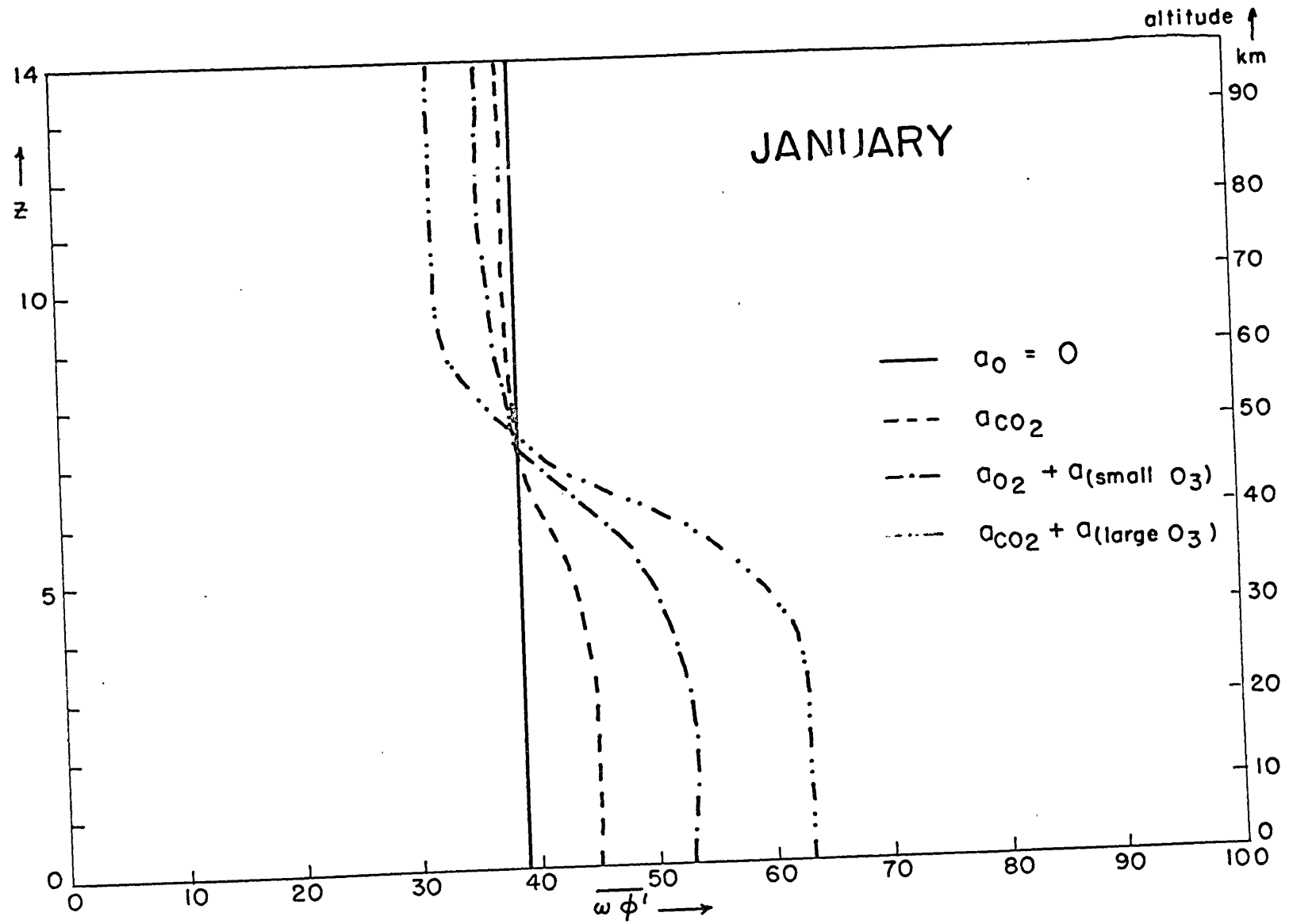
altitude
km
JANUARY
z
$\overline{\omega \phi'}$
$a_0 = 0$
a_{CO_2}
$a_{O_2} + a_{(small\ O_3)}$
$a_{CO_2} + a_{(large\ O_3)}$
0
5
10
14
0
10
20
30
40
50
60
70
80
90
100

Figure V B-2

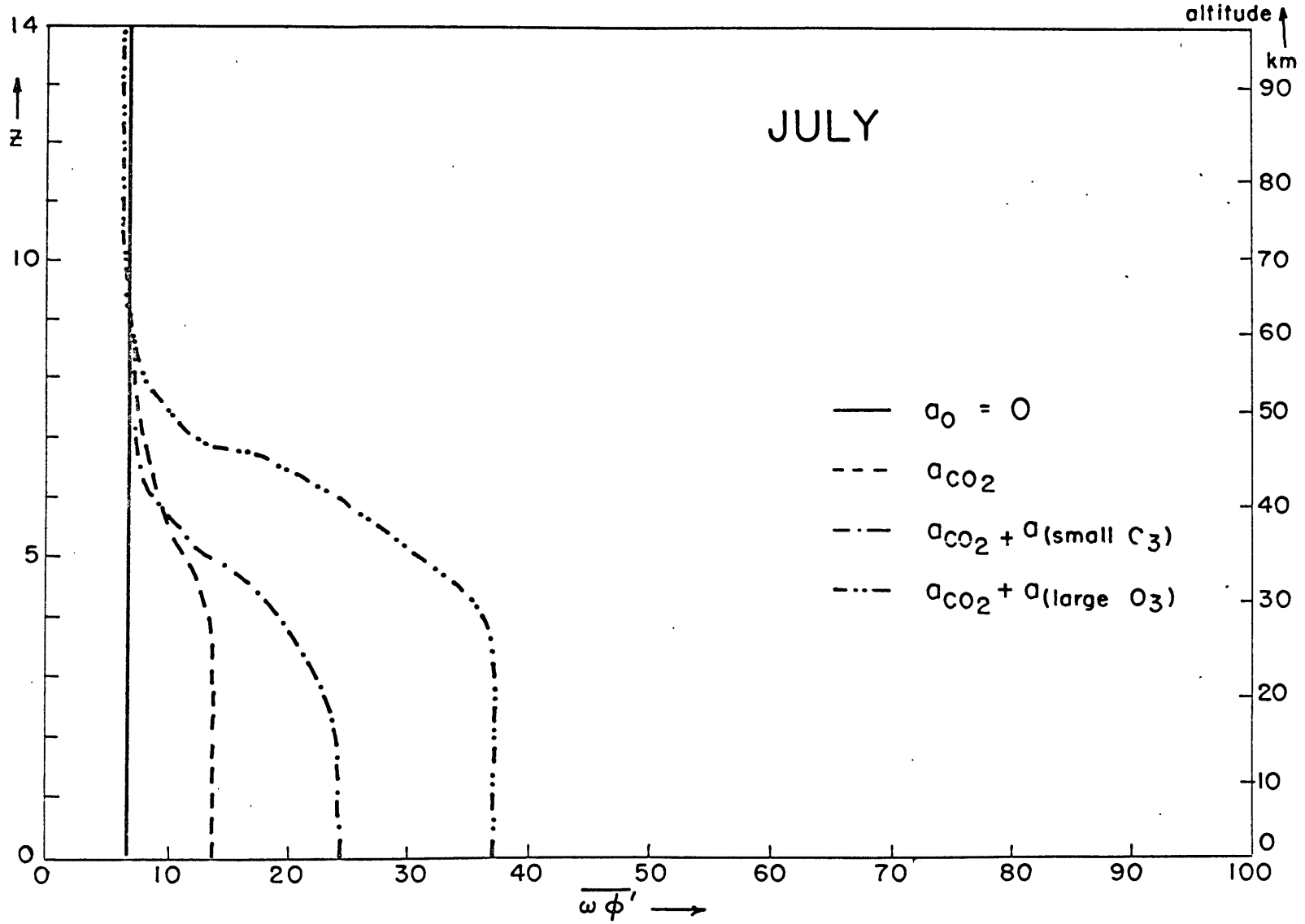
JULY
altitude
km
z
$a_0 = 0$
a_{CO_2}
$a_{CO_2} + a_{(small\ O_3)}$
$a_{CO_2} + a_{(large\ O_3)}$
$\overline{\omega \phi'}$
0
5
10
14
0
10
20
30
40
50
60
70
80
90
100
0
10
20
30
40
50
60
70
80
90

Figure V B-3

CHAPTER VI

SIMPLE STUDIES

Section A: Numerical Studies

In the two previous chapters, calculations of the semidiurnal lunar tide performed with the monthly stability profiles gave a seasonal variation in the tide that was correlated with changes in these stability profiles. The writer attributes these changes in the calculated tide to the seasonal variation in the strength of the "mesospheric barrier". This interpretation would be clearer if this "mesospheric barrier" ~~was~~ were the only portion of the stability curve that changed with season. This is not the case. Although the most marked changes in the stability curve do occur in the mesosphere, there are also changes in the "tropospheric barrier" and "stratospheric cavity". There is also a seasonal variation in the surface temperature which affects the lower boundary condition.

The purpose of this section is to isolate these varying "parameters" and see what happens to the tidal calculations as these "parameters" are changed, keeping everything else constant.

The complete tidal calculations will not be presented in this section, since the author believes that the number of pages required to give the complete results would not only be excessive but

also be confusing to the reader. For this reason, only the calculated amplitude and phase of the surface variation in geopotential height along with the vertical energy flux are shown.

The stability curves that were used in making the mesospheric test are shown in figure VI A-1. It was the author's intention to progress smoothly from a mid-winter mesosphere (# 1) to a mid-summer mesosphere (# 6). The solid curve (# 7) is the annual average stability curve. The results of the mesospheric test are shown in table VI A-1[1]. These results show both the phase lag and energy flux decreasing markedly with an increasing "mesospheric barrier" while the amplitude of the surface pressure oscillation is seen to increase slightly.

The curves for the tropospheric test are shown in figure VI A-2 with the corresponding results in table VI A-2. The solid curve is again the annual average. The amplitude increases while the phase lag is seen to decrease with increasing "tropospheric barrier" strength. The energy flux first decreases slightly and then increases slightly with increasing barrier strength.

The stratospheric test was carried out using the curves shown in figure VI A-3 with the results in table VI A-3. These calcula-

---

1. Throughout this section parantheses, ( ), will denote results for the annual average curve and brackets, [ ], will denote results for the annual curve with a winter mesosphere.

tions show the amplitude decreasing with increasing "stratospheric cavity" through curve (5) with the amplitude increasing by an order of magnitude for curves (6) and (7). The phase lag shows somewhat irregular but small variations through curve (5) with large variations in curves (6) and (7). The energy flux increases with increasing "stratospheric cavity" with very large increases for curves (6) and (7). It should be kept in mind when looking at these results that stratospheres (6) and (7) appear to be quite unrealistic when compared with observations.

Taking the annual stability curve, calculations were performed for various values of the surface temperature. The results of this experiment are shown in table VI A-4. Both the amplitude and energy flux are seen to decrease slightly with increasing surface temperature while the phase lag remains constant.

Referring back to figure VI A-1 one can see that the annual stability curve is closer to the summer situation than to the winter, in the sense of there being a fairly strong "mesospheric barrier". It is of interest to ask whether with a lesser "mesospheric barrier" similar changes in the non-mesospheric portion of the stability curve might give different variations in the results. For this reason the same tropospheric curves, stratospheric curves, and changes in surface temperature as before were stu-

died with a winter mesosphere.

These tropospheric and stratospheric tests with winter mesospheres are shown in figures VI A-4 and VI A-5. The corresponding results are shown in tables VI A-5 and VI A-6 with the results of the surface temperature test being shown in table VI A-7. The results with winter mesospheres are qualitatively the same as the corresponding results with the annual mesospheres. As would be suggested by the mesospheric test, the amplitudes of the surface oscillation in geopotential height are less with the winter mesosphere while the phase lags and energy fluxes are greater. In all these tests the variations of amplitude, phase lag, and energy flux, while being qualitatively the same for the winter and annual mesospheres, are roughly in proportion to their magnitudes.

In summary, these simple numerical experiments have shown that the seasonal changes in strength of the "mesospheric barrier" dominate the seasonal variations of the lunar tide. This is concluded since the observed changes in the mesospheric portion of the stability curve cause greater variations in the results than would the observed variations in the troposphere, stratosphere, or in surface temperature.

Finally it will be remembered that a standard thermosphere has been assumed for all months. This standard thermosphere

has been used in formulating the "radiation condition". In the following numerical experiment the slope of the thermosphere is varied and results are presented for these thermospheres with an annual mesosphere and a winter mesosphere. The curves and results for this thermospheric test are shown in figures VI A-6 and VI A-7 and tables VI A-8 and VI A-9. It is seen that in the case of the annual mesosphere the amplitude of the surface oscillation in geopotential height is rather constant while the phase lag and energy flux decrease for an increasing slope of the thermosphere. In the case of the winter mesosphere the amplitude is seen to decrease substantially while the phase lag and energy flux vary a bit irregularly by comparison. While the variation in the slope of the thermosphere causes some variation in the results, the assumption of a standard thermosphere for all seasons should not affect the qualitative results in this study of the atmospheric lunar tide.

Section B: Analytic Studies

subsection a: Isothermal calculation

Analytical solutions to the lunar tidal problem may be obtained for certain model atmospheres. The simplest of these is the isothermal atmosphere, since it is specified by only one parameter, the temperature. It is quite worthwhile to see this

isothermal solution for the lunar tide because, in this case, the details of calculation do not pose such a barrier to understanding as in the general case.

There are two distinct solutions to be considered for the lunar tide in an isothermal atmosphere. The first of these is the situation in which energy is propagating upwards, and the second is where energy is being prevented from leaving the system (trapping). Due to its greater physical significance, the first situation will be treated first.

Since the atmosphere is isothermal, the stability function is given by a constant

$$S = \frac{g}{(2\Omega a)^2} \chi^3 \bar{H} \qquad \left(\gamma_n^m S = \chi^3 \frac{\bar{H}}{D_n^m}\right) . \qquad \text{VIBa-1}$$

The vertical tidal equation is $(a_0 = 0)$

$$\frac{d^2 Y_n^m}{dz^2} + \left(-\frac{1}{4} + \gamma_n^m S\right) Y_n^m = 0 \ ^1 . \qquad \text{VIBa-2}$$

If $K^2 = -\frac{1}{4} + \gamma S$ ($K^2 > 0$ for the propagating case), the solution to equation VIBa-2 may be written

$$Y = Ae^{iKz} + Be^{-iKz} \qquad \text{VIBa-3}$$

where A and B are complex constants. The "radiation con-

---

1. In the remainder of this and the next section the super and subscripts $()_n^m$ will be dropped.

dition" requires that the phase velocity of the wave be directed downwards, since in a gravity wave the group velocity (velocity of energy propagation) is directed opposite to the phase velocity; hence,

$$Y = Ae^{iKz} \qquad \text{VI Ba-4}$$

The constant A may be obtained by using the lower boundary condition

$$\frac{dY}{dz} - \left(\frac{1}{2} - \frac{\bar{H}}{D}\right)Y = \frac{i\nu}{gD}\Omega \quad \text{at} \quad z=0, \qquad \text{VI Ba-5}$$

giving

$$A = \frac{\frac{\nu}{gD}\Omega\left[K - i\left(\frac{1}{2} - \frac{\bar{H}}{D}\right)\right]}{K^2 + \left(\frac{1}{2} - \frac{\bar{H}}{D}\right)^2} \; ; \qquad \text{VI Ba-6}$$

thus, for the propagating case

$$Y = \frac{\frac{\nu}{gD}\Omega\left[K - i\left(\frac{1}{2} - \frac{\bar{H}}{D}\right)\right]}{K^2 + \left(\frac{1}{2} - \frac{\bar{H}}{D}\right)^2} e^{iKz} \; . \qquad \text{VI Ba-7}$$

For the trapped case ($K^2 < 0$) the solution to equation VI Ba-2 is

$$Y = Ae^{Kz} + Be^{-Kz} \; . \qquad \text{VI Ba-8}$$

Instead of the "radiation condition", it is required in this case that the vertical energy flux remain finite at ∞ so that the so-

lution becomes

$$Y = Be^{-Kz} . \qquad \text{VI Ba-9}$$

Putting equation VI Ba-9 into the lower boundary condition VI Ba-5 gives the solution in the trapped case as

$$Y = \frac{-\frac{i\nu}{gD}\Omega}{K + (\frac{1}{2} - \frac{\bar{H}}{D})} e^{-Kz} . \qquad \text{VI Ba-10}$$

According to the form of equation VI Ba-7, it is easily seen that resonances are not possible in the propagating case since the denominator is always positive. In the trapped case, equation VI Ba-10, the denominator becomes zero when $K = \frac{\bar{H}}{D} - \frac{1}{2}$ or, solving for $\bar{H}$, when $\bar{H} = \frac{5}{7}D$ (assuming $\mathcal{R} = \frac{2}{7}$ as in the case of a predominantly diatomic gas such as air). This is as it should be, since resonances in forced oscillations should only occur when the energy being put into the system, through the forcing, is trapped in the system.

In previous sections, it was seen that a phase lag of the surface pressure oscillation was a feature of both the observations and the calculated results. It is of interest to compare the surface pressure oscillation in the propagating isothermal case with that in the trapped case. The geopotential height oscillation is given by

$$h' = H_n^m(\rho)\frac{D_n^m}{\nu}e^{z/2}\left\{\left(-\tfrac{1}{2}Y_i^{(m,n)} + \frac{dY_i^{(m,n)}}{dz} - \frac{\nu e^{-z/2}}{g D_n^m}\Omega_n^m\right)\cos[\nu\tau + m\lambda]\right.$$

$$\left. + \left(-\tfrac{1}{2}Y_r^{(m,n)} + \frac{dY_r^{(m,n)}}{dz}\right)\sin[\nu\tau + m\lambda]\right\} \qquad \text{VI Ba-11}$$

but may be rewritten as

$$h' = H_n^m(\rho)\frac{D_n^m}{\nu}e^{z/2}\zeta\cos[\nu t + m\lambda + \phi(z)], \qquad \text{VI Ba-12}$$

where

$$\left(-\tfrac{1}{2}Y_i^{(m,n)} + \frac{dY_i^{(m,n)}}{dz} - \frac{\nu e^{-z/2}}{g D_n^m}\Omega_n^m\right) = \zeta\cos\phi(z) \qquad \text{VI Ba-13}$$

and

$$\left(-\tfrac{1}{2}Y_r^{(m,n)} + \frac{dY_r^{(m,n)}}{dz}\right) = -\zeta\sin\phi(z)\ . \qquad \text{VI Ba-14}$$

Since

$$\kappa^2 = -\tfrac{1}{4} + \gamma\beta' = -\tfrac{1}{4} + \gamma\beta\frac{\bar{H}}{D}\ , \qquad \text{VI Ba-15}$$

it is easily seen that the propagating and trapped regimes are given by the following inequalities:

$$D\left\{\begin{matrix}<\\>\end{matrix}\right\}\frac{8}{7}\bar{H} \quad \text{implies} \quad \left\{\begin{matrix}\text{propagating}\\ \text{trapped}\end{matrix}\right\} \qquad \text{VI Ba-16}$$

It is easily verified from equations VI Ba-6 and VI Ba-10 that the decomposition of $Y|_{z=0}$ into real and imaginary parts for the

1. In the remainder of this section it is assumed that $\gamma\beta = \frac{2}{7}$.

two regimes are given by

Propagating	Trapped
$Y_r\|_{z=0} = \frac{\frac{\nu\chi}{gD}\Omega}{K^2+(\frac{1}{2}-\frac{\bar{H}}{D})^2}$	$Y_r\|_{z=0} = 0$
$Y_i\|_{z=0} = \frac{-\frac{\nu}{gD}\Omega(\frac{1}{2}-\frac{\bar{H}}{D})}{K^2+(\frac{1}{2}-\frac{\bar{H}}{D})^2}$	$Y_i\|_{z=0} = \frac{-\frac{\nu}{gD}\Omega}{K+(\frac{1}{2}-\frac{\bar{H}}{D})}$
$\frac{dY_r}{dz}\|_{z=0} = \frac{\frac{\nu\chi}{gD}(\frac{1}{2}-\frac{\bar{H}}{D})}{K^2+(\frac{1}{2}-\frac{\bar{H}}{D})^2}$	$\frac{dY_r}{dz}\|_{z=0} = 0$
$\frac{dY_i}{dz}\|_{z=0} = \frac{\frac{\nu K^2}{gD}\Omega}{K^2+(\frac{1}{2}-\frac{\bar{H}}{D})^2}$	$\frac{dY_i}{dz}\|_{z=0} = \frac{\frac{\nu K}{gD}\Omega}{K+(\frac{1}{2}-\frac{\bar{H}}{D})}$.

VI Ba-17

Putting VI Ba-17 into equations VI Ba-13 and VI Ba-14 gives the following:

Propagating $(D<\frac{8}{7}\bar{H})$	Trapped $(D>\frac{8}{7}\bar{H})$
$G\sin\phi\|_{z=0} = \frac{\frac{\nu K}{gD}\Omega(\frac{\bar{H}}{D})}{K^2+(\frac{1}{2}-\frac{\bar{H}}{D})^2} < 0$	$G\sin\phi\|_{z=0} = 0$
$G\cos\phi\|_{z=0} = \frac{\frac{\nu}{gD}\Omega[(\frac{\bar{H}}{D})(\frac{1}{2}-\frac{\bar{H}}{D})]}{K^2+(\frac{1}{2}-\frac{\bar{H}}{D})^2} > 0$	$G\cos\phi\|_{z=0} = \frac{\frac{\nu}{gD}\Omega(\frac{\bar{H}}{D})}{K+(\frac{1}{2}-\frac{\bar{H}}{D})} < 0$ (if $\frac{\bar{H}}{D}>\frac{5}{7}$) > 0 (if $\frac{\bar{H}}{D}<\frac{5}{7}$) .

VI Ba-18

Thus, it is shown that there is always a phase lag (with $-\frac{\pi}{2}<\phi<0$) in the propagating case with an isothermal atmosphere. In the trapped case the surface pressure oscillation is always exactly in phase or out of phase with the forcing (0^o or 180^o phase lag)

depending on whether the scale height (temperature) is greater or less than the resonance value.

This isothermal calculation does not prove, for an arbitrary atmospheric temperature structure, that a phase lag is necessary if the wave energy is being propagated to infinity. It is quite suggestive of this result, nevertheless.

subsection b: δ -FCN barrier

It was seen in the last section that a calculation of the lunar tide using an isothermal atmosphere (propagating case) reproduced some important observed features -- most notably, the phase lag of the surface pressure oscillation. In this section, a simple model atmosphere will be utilized to investigate how changes in atmospheric "barriers" affect the lunar semidiurnal tide.

This model atmosphere is shown in figure VIBb-1. It is seen that this model consists of an isothermal atmosphere with a δ -function "barrier". With this model, it is possible to look into the effects of a δ - function "barrier" varying in both strength, S_0 , and location, z_0 .

In the case of this special atmosphere, the vertical tidal equation becomes

$$\frac{d^2Y}{dz^2} + [\gamma S_1 - \gamma \Delta S_0 \delta(z - z_0)] Y = 0 \qquad \text{VI Bb-1}$$

The boundary conditions are as follows:

(1) at $z = 0$, $\frac{dY}{dz} - (\frac{1}{2} - \frac{H}{D})Y = \frac{i\nu}{gD}\Omega$

(2) at $z = \infty$, no energy is propagating downwards.

The solution to equation VI Bb-1 so long as $z \neq z_0$ is

$$Y = Ae^{iK_1 z} + Be^{-iK_1 z} \qquad \text{where } K_1^2 = \gamma S_1$$

(A and B are arbitrary complex constants).

With boundary condition (2), the situation is pictured in figure VI Bb-2. $|T|$ is the magnitude of the wave transmitted through the "barrier" while $|R|$ is the magnitude of the reflected wave.

The three constants A , R , and T may be obtained by the following three conditions:

(1) boundary condition (1)

(2) Y is continuous across z_0

(3) the "jump condition" on $\frac{dY}{dz}$ across z_0 , which is obtained by integrating equation VI Bb-1 across z_0 .

These conditions are respectively:

$$iK_1 A - iK_1 R - \left(\tfrac{1}{2} - \tfrac{\bar{H}}{D}\right)(A+R) = \frac{i\nu}{gD}\Omega \,, \qquad \text{VI Bb-2}$$

$$A e^{iK_1 z_0} + R e^{-iK_1 z_0} = T e^{iK_1 z_0} \,, \qquad \text{VI Bb-3}$$

and

$$iK_1 T e^{iK_1 z_0} - iK_1 A e^{iK_1 z_0} - iK_1 R e^{-iK_1 z_0} = \gamma S_0' T e^{iK_1 z_0} \,. \qquad \text{VI Bb-4}$$

Equations VI Bb-2, VI Bb-3, and VI Bb-4, when used to solve for A, R, and T give

$$\left.\begin{aligned} T &= \left[\frac{2iK_1}{2iK_1 - \gamma S_0'}\right] A \,, \quad R = \left[\frac{\gamma S_0' e^{2iK_1 z_0}}{2iK_1 - \gamma S_0'}\right] A, \\ A &= \frac{\frac{i\nu}{gD}\Omega}{iK_1\left[1 - \left(\frac{\gamma S_0' e^{2iK_1 z_0}}{2iK_1 - \gamma S_0'}\right)\right] - \left(\tfrac{1}{2} - \tfrac{\bar{H}}{D}\right)\left[1 + \frac{\gamma S_0' e^{2iK_1 z_0}}{2iK_1 - \gamma S_0'}\right]} \,. \end{aligned}\right\} \qquad \text{VI Bb-5}$$

It is seen from VI Bb-5 that when $S_0' = 0$, $|T| = |A|$ and $R = 0$ while if $S_0' = \infty$, $T = 0$ and $|R| = |A|$. This is as it should be, since there should be perfect transmission with no "barrier" and no transmission with an infinite "barrier".

There exists a resonance when

$$iK_1\left[1 - \left(\frac{\gamma S_0' e^{2iK_1 z_0}}{2iK_1 - \gamma S_0'}\right)\right] = \left(\tfrac{1}{2} - \tfrac{\bar{H}}{D}\right)\left[1 + \frac{\gamma S_0' e^{2iK_1 z_0}}{2iK_1 - \gamma S_0'}\right], \qquad \text{VI Bb-6}$$

or alternatively when

$$\left(\frac{\gamma S_0 e^{2iK_1 z_0}}{2iK_1 - \gamma S_0}\right) = \frac{iK_1 - (\frac{1}{2} - \frac{\bar{H}}{D})}{iK_1 + (\frac{1}{2} - \frac{\bar{H}}{D})} \quad . \qquad \text{VI Bb-7}$$

Taking the absolute value of equation VI Bb-7 implies that

$\left|\frac{\gamma S_0}{2iK_1 - \gamma S_0}\right| = 1$ which can only be true if $S_0 = \infty$;

otherwise,

$\left|\frac{\gamma S_0}{2iK_1 - \gamma S_0}\right| < 1$. As expected then, resonances can only occur with an infinite barrier. Even with $S_0 = \infty$, it is seen, going back to equation VI Bb-7, that resonances can only take place when

$$z_0 = -\frac{1}{K_1} \tan^{-1}\left\{\frac{K_1}{\frac{1}{2} - \frac{\bar{H}}{D}}\right\} \quad .$$

In order to learn about partial resonances, $S_0 < \infty$, the solution to the vertical tidal equation for various values of S_0 and z_0 were found. More specifically a δ-function "barrier" was moved from $z = 0$ to $z = 14$ and solutions for the amplitudes and phases of the surface pressure oscillation were found.

Figure VI Bb-3 shows the amplification, $\bar{A}$, of the surface pressure tide over that of an isothermal atmosphere with $\bar{H} = 7.07034$ ($S_1 = .025$) as a function of z_0 for

S_0 = .005, .010, .020, .040, .080[1]. Figure VIBb-4 shows the phase lag, ϕ, of the surface pressure oscillation as a function of z_0 for S_0 = .000, .050, .010, .020, .040, .080.

In both these figures there are seen partial resonances; that is to say, regions where there is both a rapid rise in amplitude and a rapid change in phase lag. These partial resonances become much larger for larger values of S_0. Between these resonance regions (from about $z_0 = 2$ to $z_0 = 9$) the change of amplitude with S_0 is rather irregular and small, while the phase lag seems to decrease monotonically with S_0. This behavior is quite consistent with both the observed and calculated surface pressure oscillation.

---

1. For reference, the area of the "mesospheric barrier" varies from about 0.005 in mid-winter to 0.0275 in mid-summer.

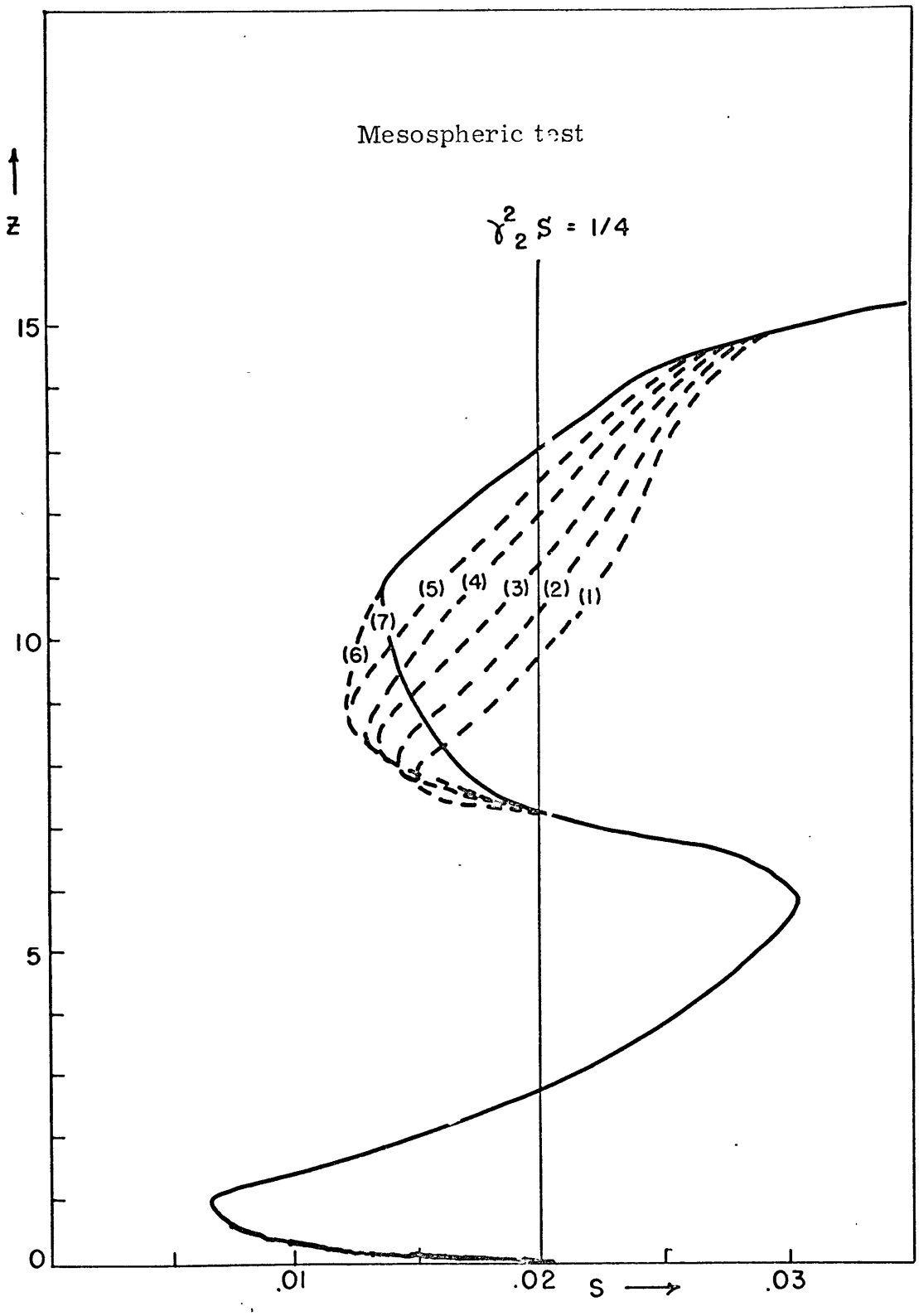

Figure VI A-1

TABLE VI A-1

MESOSPHERIC TEST

Profile	h (cm)	ϕ_0	$\overline{w\phi'}$ (CGS)
[1]	[44]	[-26°]	[53]
2	47	-12°	26
3	51	-5°	13
4	54	-3°	7.8
5	56	-2°	5.3
6	58	-1°	3.6
(7)	(52)	(-2°)	(5.7)

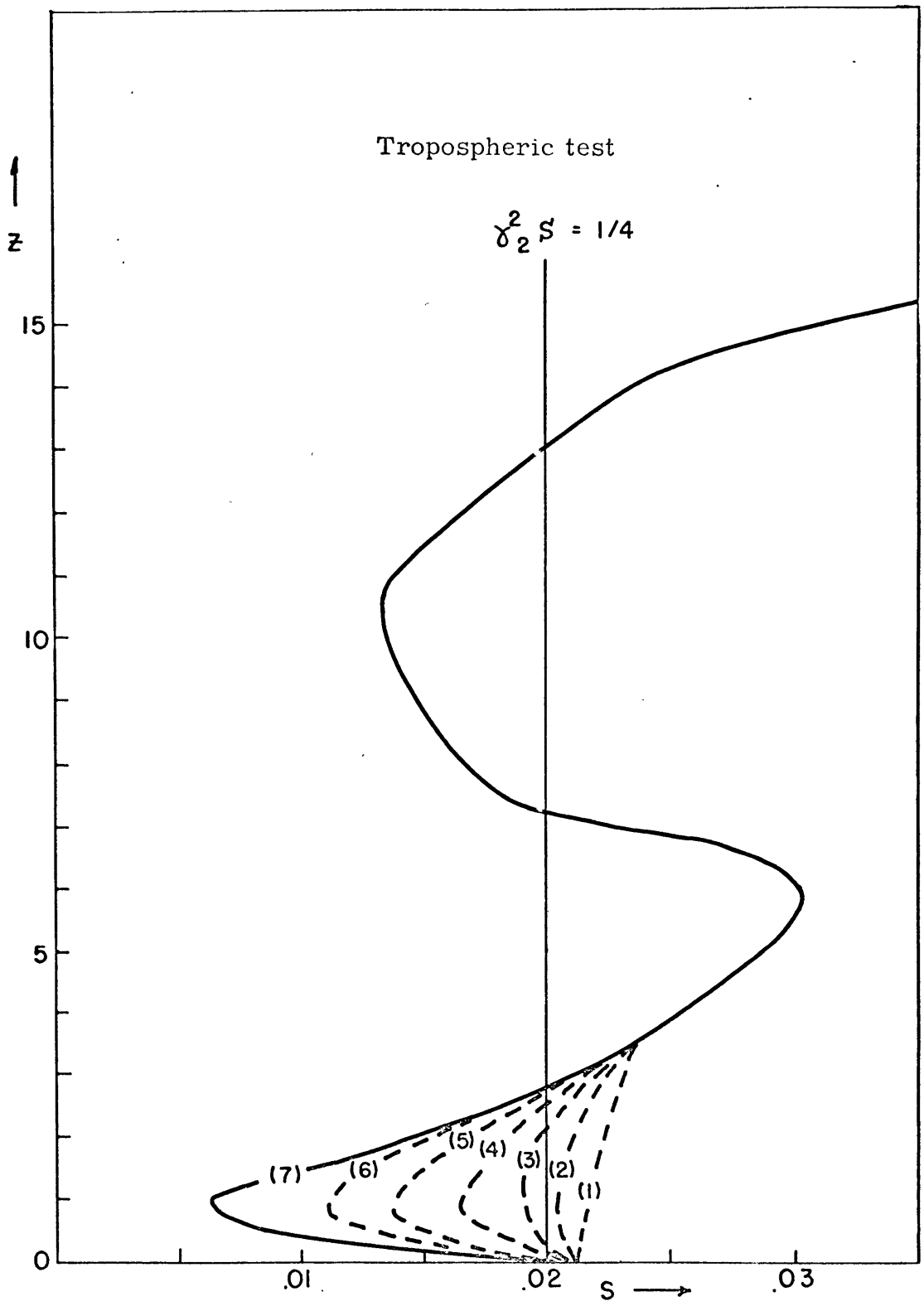

Figure VI A-2

TABLE VI A-2

TROPOSPHERIC TEST (ANNUAL MESOSPHERE)

Profile	h(cm)	ϕ_0	$\overline{\omega\phi'}$ (CGS)
1	24	-5°	5.5
2	28	-4°	5.3
3	32	-3°	5.2
4	36	-3°	5.2
5	42	-3°	5.2
6	47	-2°	5.3
(7)	52	(-2°)	(5.7)

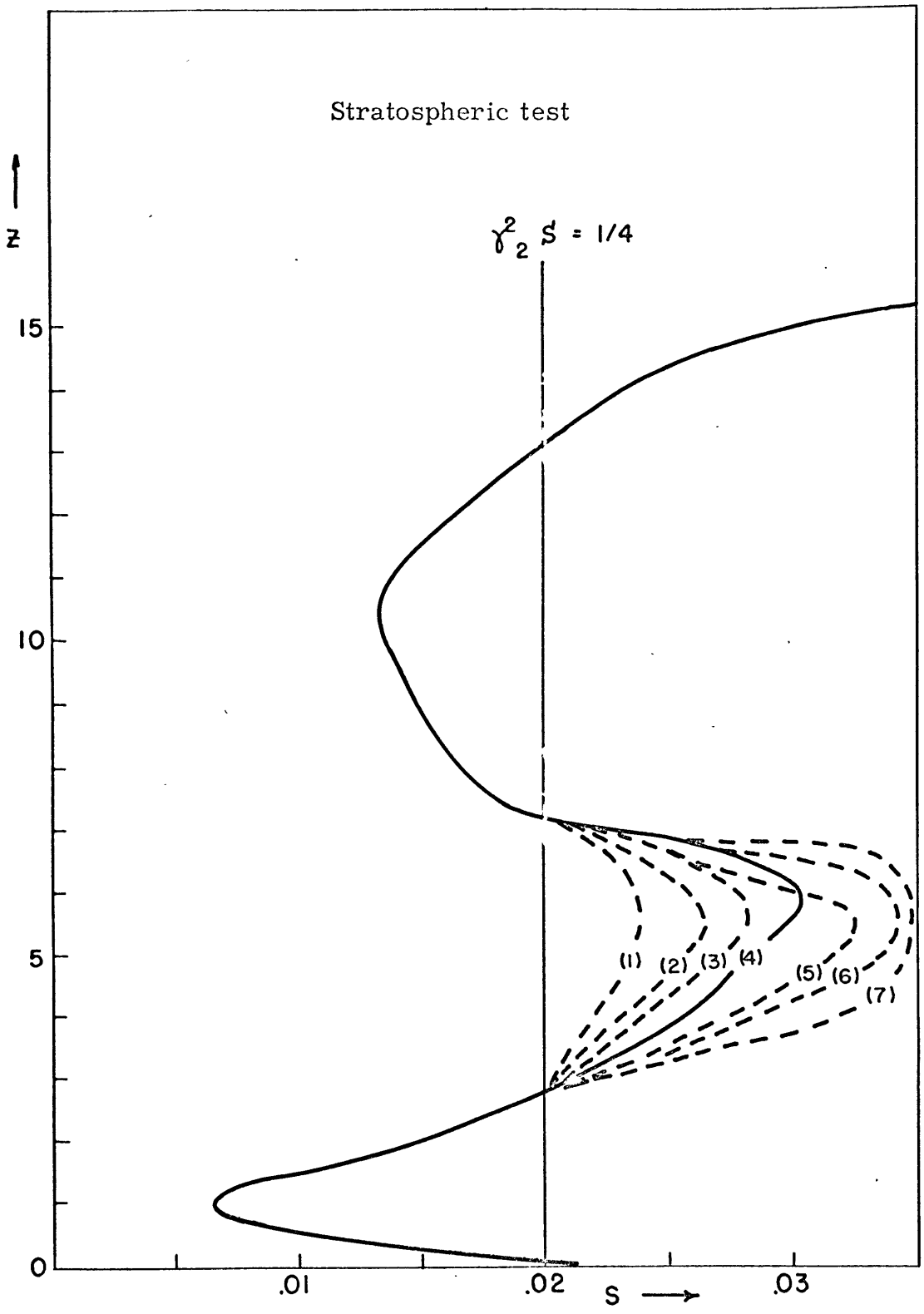

Figure VI A-3

TABLE VI A-3

STRATOSPHERIC TEST (ANNUAL MESOSPHERE)

Profile	h(cm)	ϕ_0	$\overline{\omega\phi'}$ (CGS)
1	82	$-\ 3^{o}$	1.1
2	76	$-\ 5^{o}$	1.7
3	68	$-\ 1^{o}$	2.7
(4)	(52)	$(-\ 2^{o})$	(5.7)
5	29	$-\ 8^{o}$	11
6	120	-163^{o}	100
7	200	$-\ 63^{o}$	490

TABLE VIA-4

SURFACE TEMPERATURE TEST (ANNUAL MESOSPHERE)

T_0 (^oK)	h(cm)	ϕ_o	$\overline{\omega\phi'}$ (CGS)
277^oK	54	-2^o	6.4
280^oK	53	-2^o	6.1
284^oK	53	-2^o	5.9
(287^oK)	(52)	(-2^o)	(5.7)
290^oK	52	-2^o	5.4
294^oK	52	-2^o	5.2
297^oK	51	-2^o	5.0

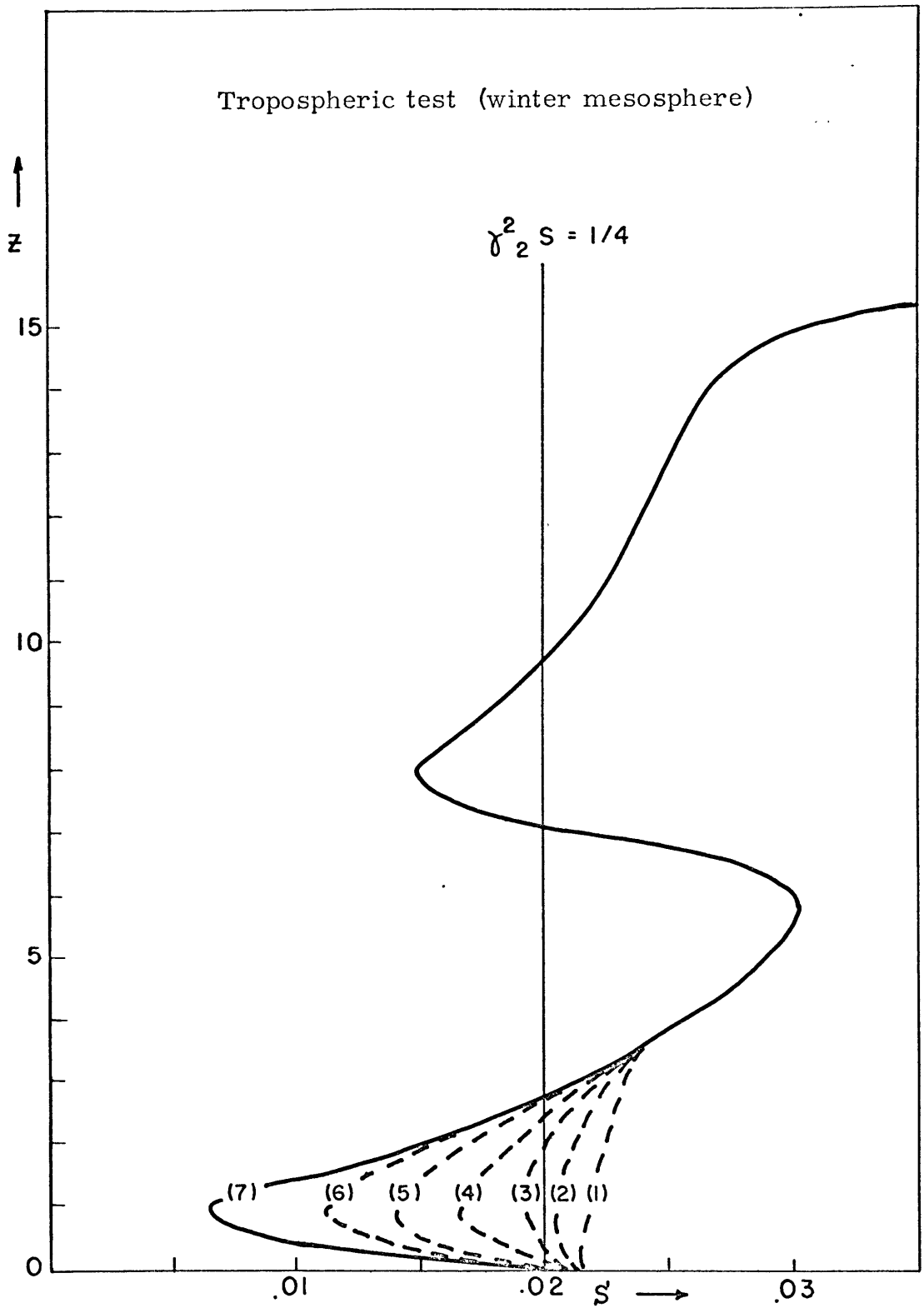
Tropospheric test (winter mesosphere)
z
γ^2_2 S = 1/4
15
10
5
0
(7)
(6)
(5)
(4)
(3)
(2)
(1)
.01
.02
S
.03

Figure VI A-4

TABLE VI A-5

TROPOSPHERIC TEST (WINTER MESOSPHERE)

Profile	h(cm)	ϕ_o	$\overline{\omega\phi'}$ (CGS)
1	23	-58^o	54
2	25	-49^o	52
3	27	-42^o	50
4	30	-36^o	50
5	35	-30^o	49
6	39	-27^o	50
[7]	[44]	-26^o	53

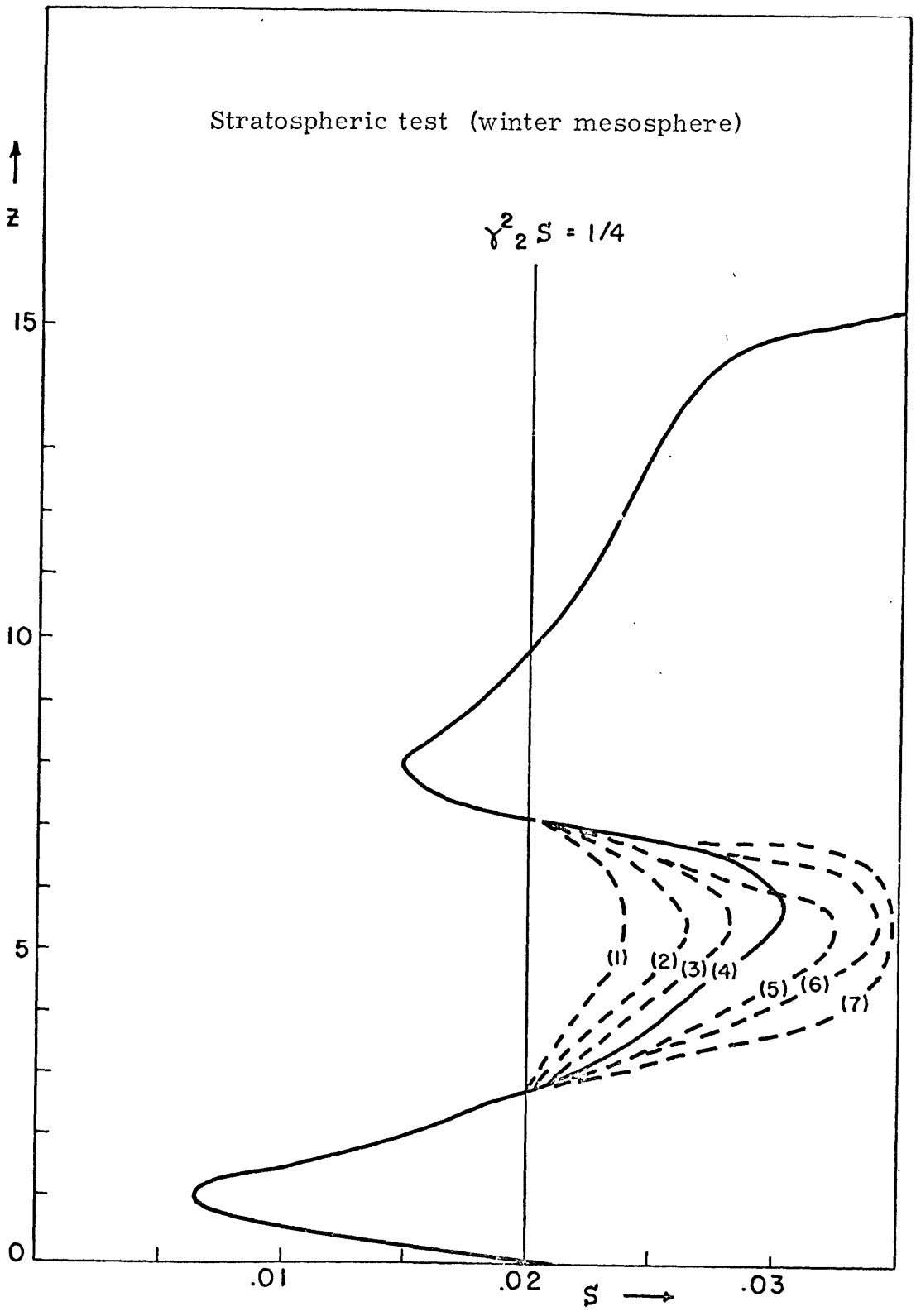
Stratospheric test (winter mesosphere)
z
$\gamma^2_2 S = 1/4$
15
10
5
0
.01
.02
.03
S
(1)
(2)
(3)
(4)
(5)
(6)
(7)

Figure VI A-5

TABLE VI A-6

STRATOSPHERIC TEST (WINTER MESOSPHERE)

Profile	h(cm)	ϕ_o	$\overline{\omega\phi'}$ (CGS)
1	79	-2^o	7.3
2	72	-4^o	12
3	62	-7^o	21
[4]	[44]	$[-26^o]$	[53]
5	40	-80^o	110
6	280	-62^o	680
7	220	-17^o	1880

TABLE VI A-7

SURFACE TEMPERATURE TEST (WINTER MESOSPHERE)

T_0 (^oK)	h (cm)	Φ_o	$\overline{\omega\Phi'}$ (CGS)
277	44	-27^o	58
280	44	-27^o	56
284	44	-26^o	55
[287]	[44]	[-26^o]	[53]
290	44	-25^o	51
294	44	-25^o	50
297	44	-25^o	48

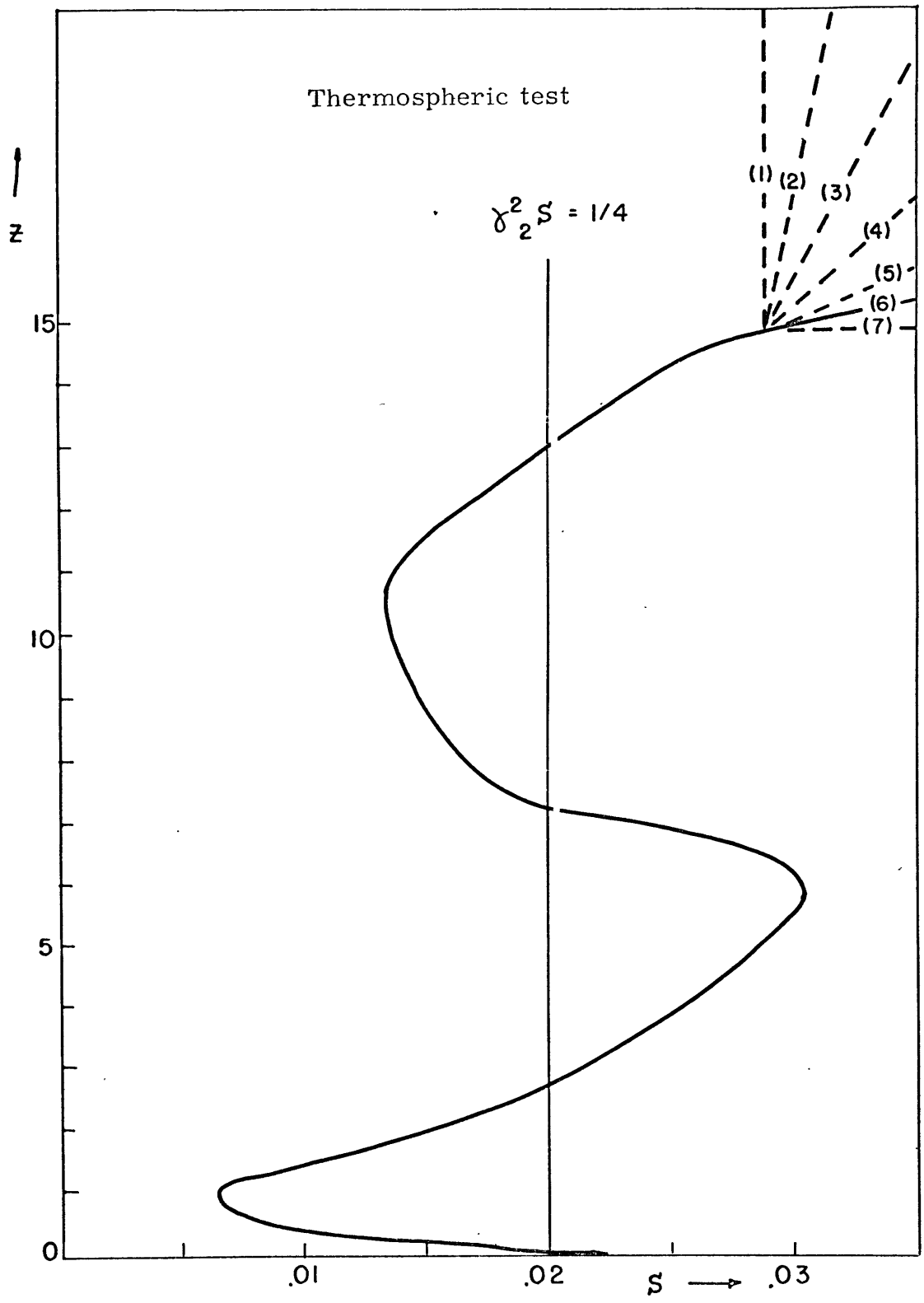

Figure VI A-6

TABLE VI A-8

THERMOSPHERIC TEST (ANNUAL MESOSPHERE)

Profile	h (cm)	ϕ_o	$\overline{\omega\phi'}$ (CGS)
1	53	-4^o	11
2	53	-4^o	11
3	52	-4^o	10
4	52	-3^o	8.3
5	52	-3^o	8.6
(6)	(52)	(-2^o)	(5.7)
7	53	-2^o	4.6

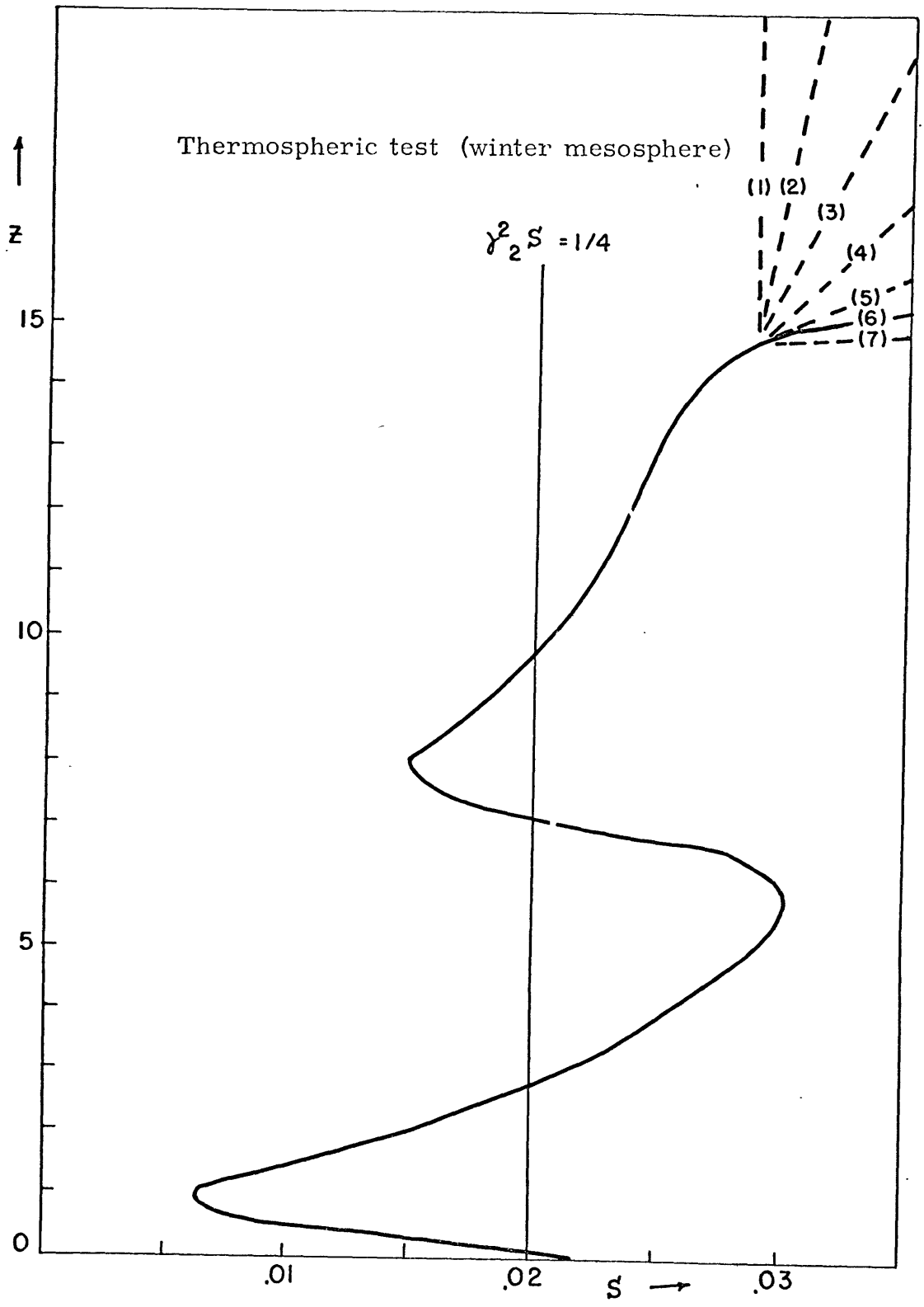
Thermospheric test (winter mesosphere)
z
15
10
5
0
$\gamma_2^2 S = 1/4$
(1) (2)
(3)
(4)
(5)
(6)
(7)
.01
.02
.03
S

Figure VI A-7

TABLE VI A-9

THERMOSPHERIC TEST (WINTER MESOSPHERE)

Profile	h (cm)	ϕ_o	$\overline{\omega \phi'}$ (CGS)
1	57	-20^o	55
2	57	-21^o	58
3	56	-23^o	60
4	51	-24^o	59
5	53	-26^o	65
[6]	[44]	[-26^o]	[53]
7	40	-23^o	43

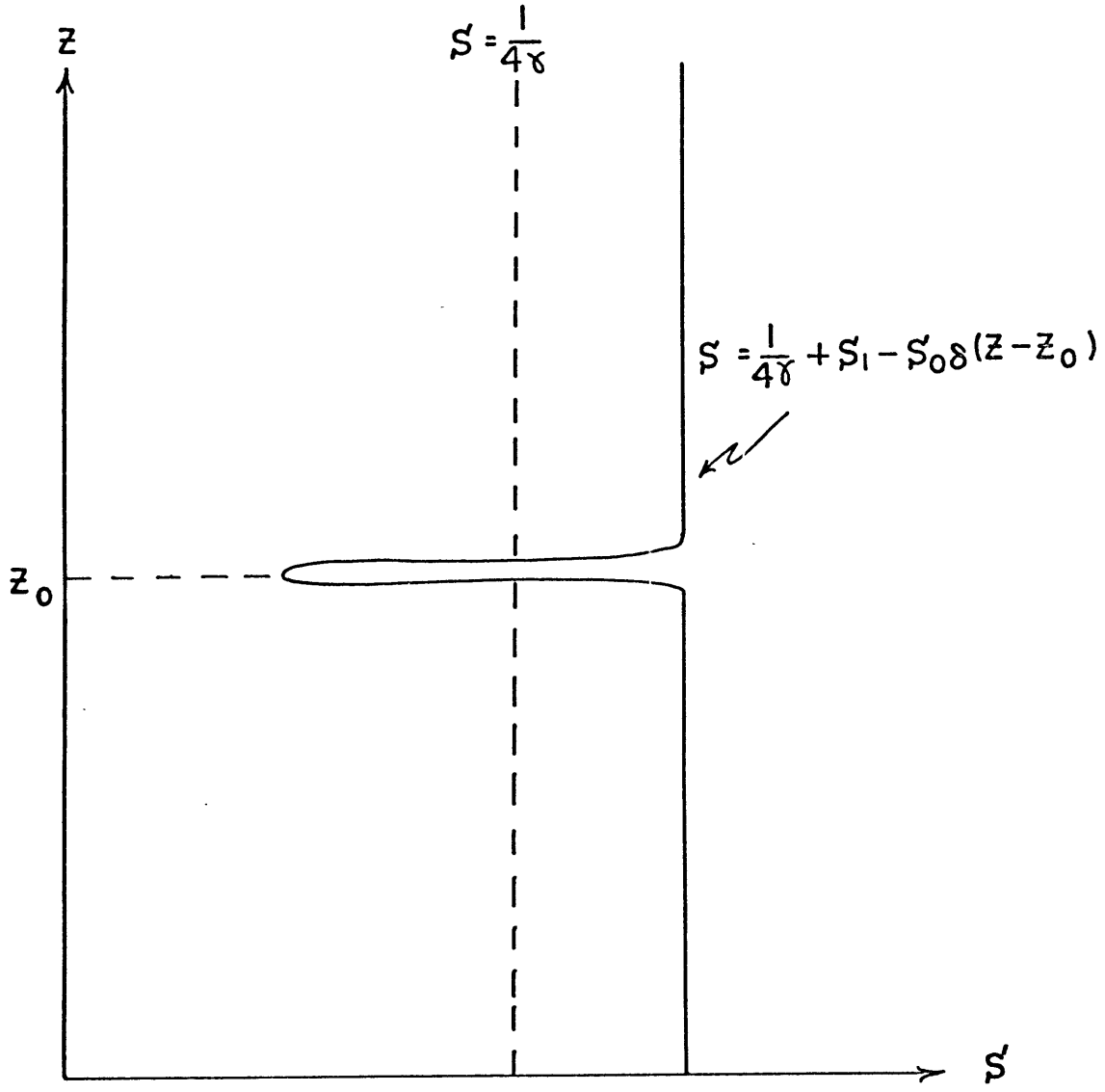

Figure VI Bb-1 "δ-function barrier" model atmosphere

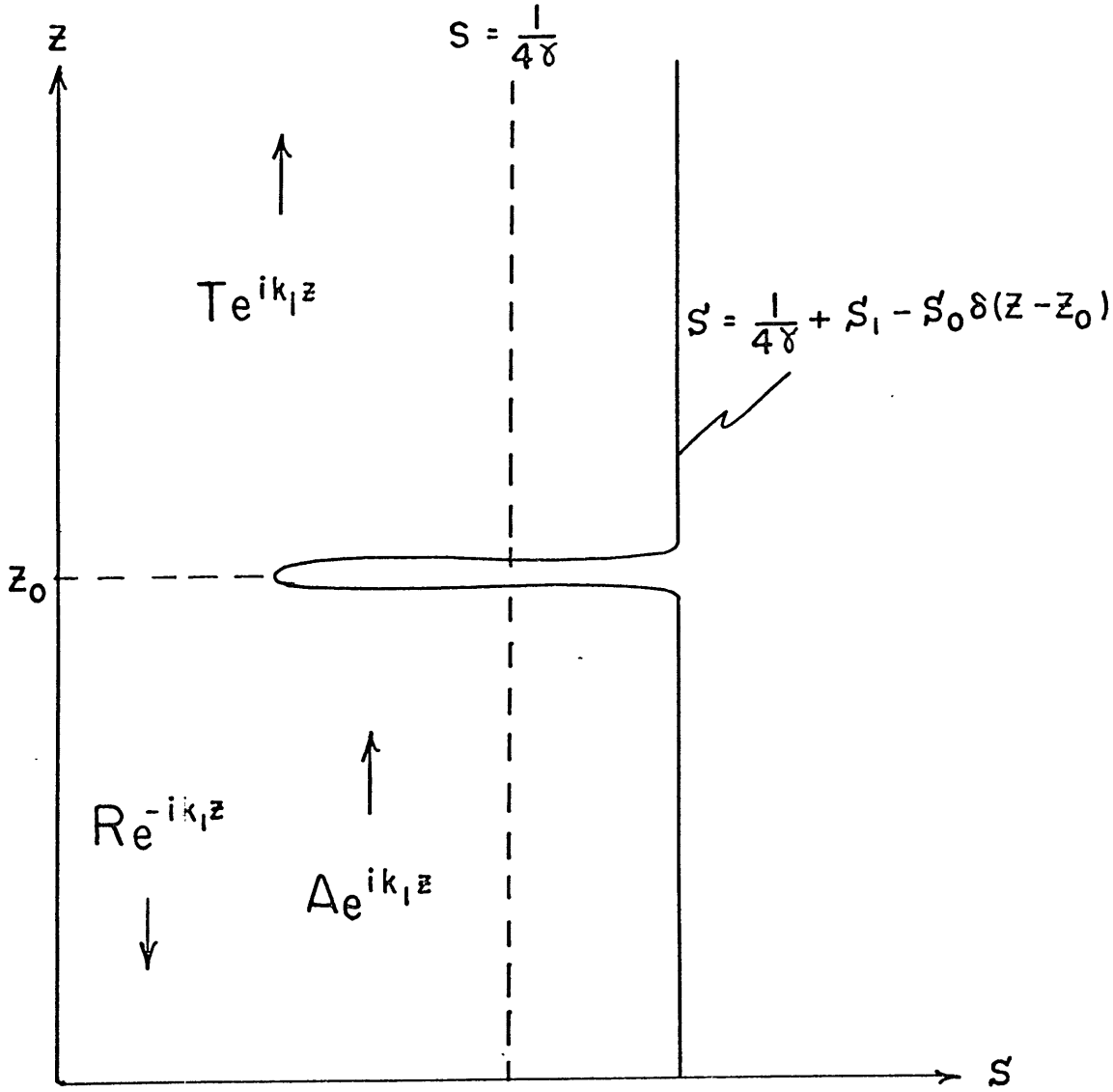

Figure VIBb-2

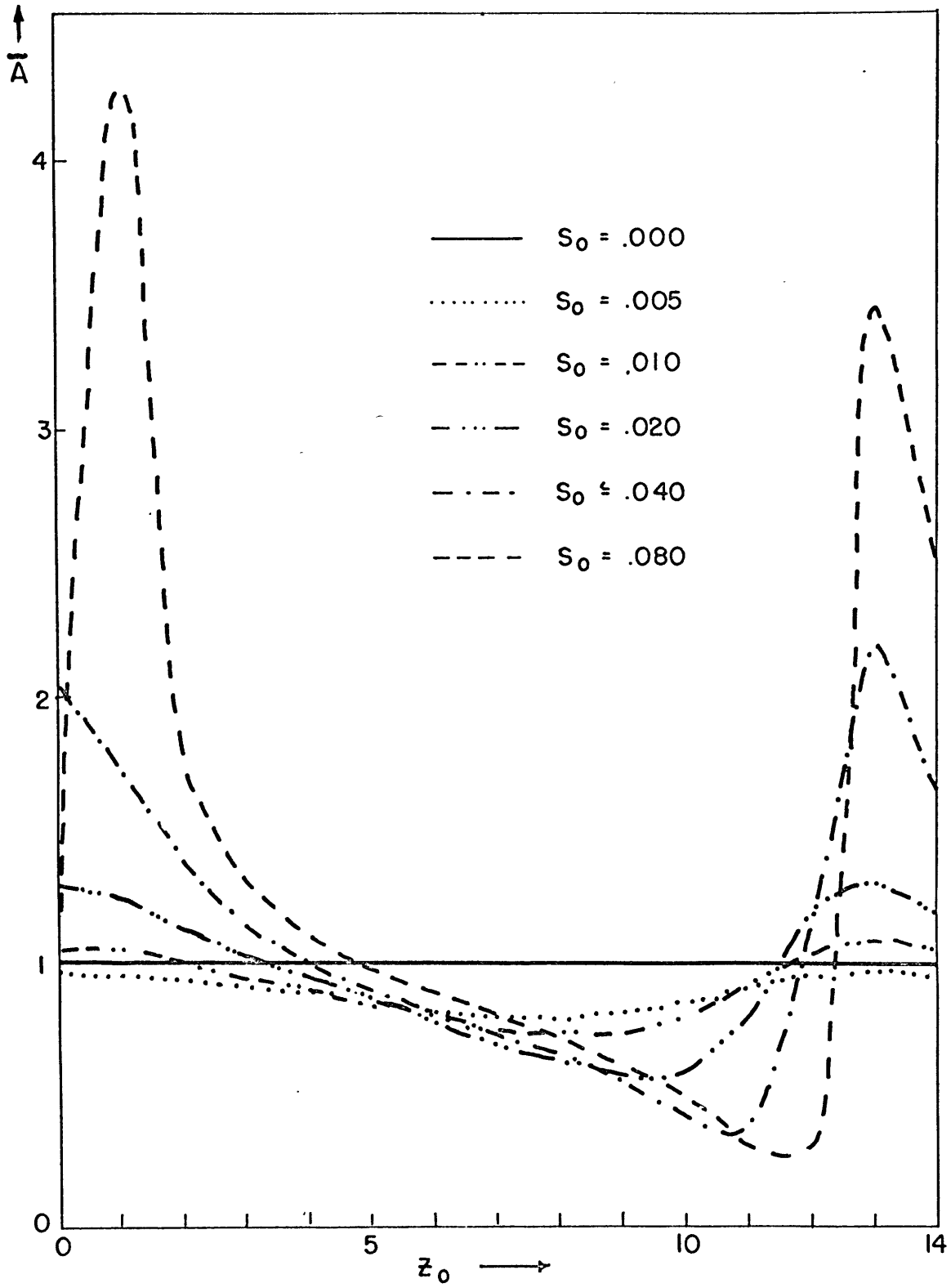

Figure VI Bb-3

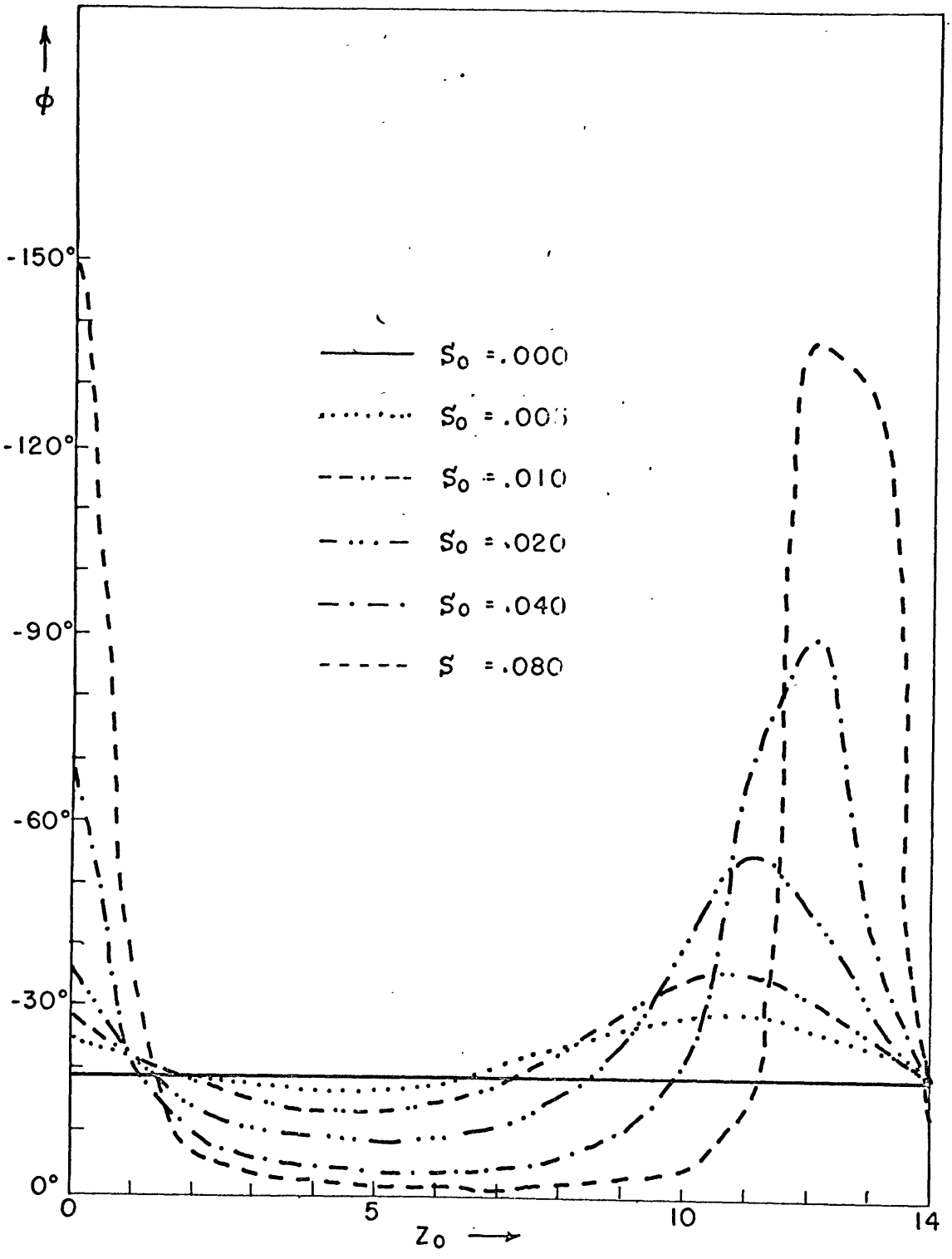

Figure VI Bb-4

CHAPTER VII

CONCLUSION

Section A: Discussion of Results

In the previous sections a simple model of the lunar semidiurnal tide in the atmosphere was presented. It was thus possible to account, quite well, for the observed features of the annually averaged lunar tide. Moreover, it gave results that resemble the observed annual variations in the surface pressure tide. The best feature of this model is its simplicity. This simplicity allows one to look more easily through the mathematics into the basic physics of the lunar tide.

In particular, the simplicity of the model allows for a very straightforward explanation of the annual changes in the surface pressure oscillation. As stated previously the monthly stability profiles were analyzed at the beginning of this study, before any calculations of the lunar tide were attempted. The calculated annual variation in amplitude and phase of the surface pressure oscillation (with no Newtonian Cooling) are thus assumed to be free of any bias resulting from the author's analysis of the stability profiles. In fact, the annual variation of phase lag is shown to be a consequence of the annual variation in the "mesospheric barrier".

This point is demonstrated by the monthly calculations, simple numerical calculations, and simple analytical work.

This effect is also easily explained physically. An increase in the "mesospheric barrier" will tend to make the tide assume the character of a standing wave in the vertical (zero vertical energy flux). A standing wave will be in phase with the forcing and thus will have a zero phase lag. This annual variation from a propagating tidal structure in the winter months to a standing tidal structure in the summer months, is graphically demonstrated in the annual variation of the vertical energy flux.

The addition of Newtonian Cooling effects upsets not only the annual variation in the tidal oscillation of surface pressure, but also the previous line of reasoning. The calculation of vertical energy flux with Newtonian Cooling showed that a substantial amount of tidal energy was being lost before it reached the "mesospheric barrier". For this reason, the changing characteristics of the tidal structure with variations in the "mesospheric barrier" become largely irrelevant. The greater the proportion of energy lost, the more irrelevant this line of reasoning becomes.

The Newtonian Cooling results should not be taken as being wholly negative, however. The treatment of Newtonian Cooling in this study is to be questioned since a Newtonian Cooling coefficient that is based on the annually averaged state of the atmosphere

is used in the monthly calculations. This might have the effect of smearing out month-to-month variations. The uncertainty in the value of the O_3 Newtonian Cooling coefficient is still more significant. The value of the Newtonian Cooling coefficient depends crucially on the assumed O_3 photochemistry, and this photochemistry is still undetermined. It was mentioned earlier that calculations in this study suggest that the classical O_3 photochemistry is not correct. Perhaps the weight of evidence from similar theoretical calculations with O_3 Newtonian Cooling will serve to settle the question of O_3 photochemistry to some extent.

Just as the simplicity of this theory of the lunar tide leads to many advantages, it also is responsible for some shortcomings. To derive the tidal equations the mean state of the atmosphere was assumed to be free of any mean wind and horizontal temperature gradients. The addition of these effects to the present theory is not an easy task, since the added terms in the "primitive equations" would prevent the separation of variables. By ignoring these effects, the author does not mean to imply that they are unimportant. It is his view, however, that when trying to model an observed phenomenon one must include physical effects in an orderly fashion so that the influence of each physical effect can be seen.

Some comment on the neglect of horizontal temperature gradients in the mean state is in order, however. In the present investigation only Northern Hemisphere data was used, since only Northern Hemisphere data was available. This gave rise to a seasonal variation in the surface pressure oscillation; whereas, an annual variation is observed. The present theory would yield an annual variation if the behavior of the temperature in the Southern Hemisphere is other than exactly equal and opposite to the behavior in the Northern Hemisphere. This would lead to an annual variation in the globally-averaged mesospheric temperature which would then lead to an annual variation in the lunar tide, as is observed. In fact, the present theory might be taken to suggest such a hemispheric asymmetry in mesospheric temperature behavior.

Section B. Suggestions For Further Research

There is much to be done in atmospheric tidal theory of both an observational and theoretical nature. The author intends to investigate the solar tides in the spirit of the present research, that is to say, he will try to model the observations of the solar tides using empirical parameters as inputs into a simple theory.

More upper atmospheric observations in the Southern Hemisphere are required for tidal calculations. These observations are needed for all studies of the upper atmosphere, of course, but are especially needed for studies of global scale phenomena such as tides.

Theoretical studies of tides including effects such as winds and horizontal temperature gradients should be attempted. These studies will, no doubt, have to be carried out numerically due to their great mathematical complexity. One such study has already been carried out by Hunt and Manabe (1968).

Of course, there is also room for many more observational studies of the lunar and solar tides. It would be very good to have more information on the yearly variations and vertical structure of these tides.

Finally, a very fertile field for study is the interaction of tidal wind fields with the electromagnetic fields in the ionosphere. Such studies would not only advance the theoretical work on tides, but also would help in interpreting data on oscillations in ionospheric parameters.

Acknowledgements

I wish to thank Prof. Victor P. Starr for being, what I consider, the ideal thesis advisor. His advice and encouragement were invaluable to me.

The basic idea for this research had its beginning in many discussions with my colleague and friend Dr. Robert E. Dickinson.

I also appreciated having the opportunity to engage in many helpful discussions with Professors Norman Phillips and Reginald Newell.

Most of the computational work was performed at the M.I.T. Computation Center with other parts being carried out by Mr. Howard Frazier at Travelers Research Center in Hartford, Connecticut.

The manuscript was typed by Mrs. Cynthia Webster while the figures were drafted by Miss Isabelle Kole and photographed by Mr. John Cook.

Financial support during my tenure as a graduate student at M.I.T. came from NASA, in the form of a NASA traineeship, and from the National Science Foundation, Grant (GA - 1310 X).

References

Abramowitz, M. and I. A. Stegun, Handbook of Mathematical Functions, Dover, 1965, 1046pp.

Appleton, E. V. and K. Weekes, 1939: "On lunar tides in the upper atmosphere," Proc. Roy. Soc. (A), 171, p. 171-187.

Butler, S. J. and K. A. Small, 1963: "The excitation of atmospheric oscillations," Proc. Roy. Soc. (A), 274, p. 91-121.

Chapman, S., 1951: "Atmospheric tides and oscillations," Compendium of Meteorology, Waverly Press Inc., p. 510-530.

Chapman, S. and K. C. Westfold, 1956: "A comparison of the annual mean solar and lunar atmospheric tides in barometric pressure, as regards their worldwide distribution of amplitude and phase," J. Atmos. Terr. Phys., 8, p. 1-23.

CIRA 1965 (COSPAR Intern. Reference Atmosphere), North-Holland Publishing Comp., 313pp.

Dickinson, R. E., 1966: "Propagators of atmospheric motions," Sci. Rept. No. 18, Planetary Circulations Project, Dept. of Meteor., M.I.T., 243pp.

Dickinson, R. E. and M. A. Geller, 1963: "A generalization of 'Tidal theory with Newtonian Cooling'," J. Atmos. Sci., 25, p. 932-933.

Flattery, T. W., 1967: "Hough functions," Tech. Rept. 21, Dept. of Geoph. Sci., U. of Chicago, 175pp.

Hildebrand, F. B., Introduction to Numerical Analysis, McGraw-Hill, 1956, 511pp.

Hunt, B. G., 1966a: "The need for a modified photochemical theory of the ozonosphere," J. Atmos. Sci., 23, p. 88-95.

Hunt, B. G., 1966b: "Photochemistry of ozone in a moist atmosphere," J. G. R., 71, p. 1385-1398.

Hunt, B. G. and S. Manabe, 1968: "An investigation of thermal tidal oscillations in the earth's atmosphere using a general circulation model," Mon. Wea. Rev., 96, p. 753-766.

IBM System 360 Scientific Subroutine Package, (C360A-CM-03X) Version II, Programmers Manual, 329 pp.

Kato, S. and S. Matsushita, 1968: "Tidal theory in the ionosphere," Trans. A. G. U., 49, p. 145.

Kertz, W., 1957: "Atmospharische Gezeiten," in Handbuch der Physik, (S. Flugge ed.), 48, p. 928-981.

Lamb, H., Hydrodynamics, Dover, 1945, 738 pp.

Laplace, P. S. (later Marquis de LaPlace), Mecanique Celeste, 2(iv), 1799, p. 294-298.

Leovy, C., 1964: "Simple models of thermally driven mesospheric circulation," J. Atmos. Sci., 21, p. 327-341.

Leovy, C., 1967: "Energetics of the middle atmosphere," The RAND Corporation, P-3679, 30 pp.

Lindzen, R. S., 1967: "Thermally driven diurnal tide in the atmosphere," Quar. J. Roy. Met. Soc., 93, p. 18-42.

Lindzen, R. S., 1968: "The application of classical atmospheric tidal theory," Proc. Roy. Soc. (A), 303, p. 299-316.

Lindzen, R. S. and R. Goody, 1965: "Radiative and photochemical processes in mesospheric dynamics: Part I, Models for radiative and photochemical processes," J. Atmos. Sci., 22, p. 341-348.

Lindzen, R. S. and D. McKenzie, 1967: "Tidal theory with Newtonian Cooling," Pure Appl. Geophys., 66, p. 90-96.

Matsushita, S., 1967: "Lunar tides in the ionosphere," In Handbuch der Physik (S. Flugge, ed.), 49/2, p. 547-602.

Morse, P. M. and H. Feshbach, Methods of Theoretical Physics, McGraw-Hill Book Company, Inc., 1953, 1978 pp.

Newton, I., Philosophiae Naturalis Principia Mathematica, London, 1687, Bk. 1, Prop. 66, Cor. 19, 20; Bk. 3, Prop. 24, 36, 37.

Rayleigh, Lord (Strutt, J.W.), 1890: "On the Vibrations of an Atmosphere," Phil. Mag., 5th Ser., 29, p. 173-180.

Rodgers, C.D., 1967: "The use of emissivity in atmospheric radiation calculations," Quart. J. Roy. Met. Soc., 93, p. 43-54.

Rodgers, C.D., and C.D. Walshaw, 1966: "The computation of infrared cooling rate in planetary atmospheres," Quart. J. Roy. Met. Soc., 92, p. 67-92.

Sawada, R., 1954: "The atmospheric lunar tides," Meteor. Papers, New York Univ., 2, no. 3, 31 pp.

Sawada, R., 1956: "The atmospheric lunar tides and the temperature profile in the upper atmosphere," Geophys. Mag., 27, p. 213-236.

Sawada, R., 1965: "The possible effect of oceans on the atmospheric lunar tide," J. Atmos. Sci., 22, p. 636-643.

Siebert, M., 1961: "The atmospheric tides," Advances in Geophysics, 7, p. 105-187.

Thompson, P.D., Numerical Weather Analysis and Prediction, The MacMillan Company, 1961, 170 pp.

Thompson, W., (later Lord Kelvin), 1882: "On the thermodynamic acceleration of the Earth's rotation," Proc. Roy. Soc. Edinb., 11, p. 396-405.

Wilkes, M.V., Oscillations of the Earth's Atmosphere, Cambridge, University Press, 1949, 74 pp.

Biography

Marvin Alan Geller was born on March 19, 1943 to Mr. James Geller and Mrs. Saide Geller in Boston, Massachusetts. During his childhood years his family lived in Brockton, Massachusetts. He graduated from Brockton High School in 1960, receiving the Rensselaer Medal, and subsequently enrolled at the Massachusetts Institute of Technology receiving his Bachelor of Science degree in Mathematics in June, 1964.

He enrolled at M.I.T. in meteorology in September, 1964. While in graduate school at M.I.T. he married the former Lynda Louise Grafinger. A daughter, Stephanie Lynn, was born from this union.

Mr. Geller was supported during his first and last years as a graduate student by a research assistantship under Prof. V. P. Starr and during the middle three years was a NASA trainee.

Mr. Geller was elected to full membership in the Society of Sigma Xi in 1968.

His publications to date are as follows:

(1) "The effect of seasonal changes in atmospheric temperature structure on the lunar tide," Trans. A.G.U., vol. 49, no. 1, March 1968, p. 179 (abstract of talk delivered at 1968 A.G.U. meeting in Washington, D.C.).

(2) "The effect of changes in atmospheric temperature

structure on the lunar tide," Bull. A. M. S., vol. 49, no. 8, Aug. 1968, p. 847 (abstract of talk delivered at 1968 Conference on Composition and Dynamics of the Upper Atmosphere in El Paso, Texas).

(3) "A generalization of 'Tidal theory with Newtonian Cooling'," J. Atmos. Sci., vol. 25, no. 5, Sept. 1968, pp. 932-933 (with R. E. Dickinson).